Task 2 - Earthquake Hazard Assessment

Regionally consistent risk assessment for earthquakes and floods and selective landslide scenario analysis for strengthening financial resilience and accelerating risk reduction in Central Asia (SFRARR Central Asia disaster risk assessment)

FINAL VERSION

15 October 2021

RED – Risk Engineering + Development – Pavia, Italy

Revision History

Version	Date	State	Initials	Changes
r1d1	23/08/2021	Draft	OGS: VP	
r1d2	27/08/2021	Draft	RED: PB; OGS: SP	General review, copyediting
r1	09/09/2021	Approved	OGS: VP, SP; RED: PB	Changes based on reviewers' comments

Executive Summary

With the goal of improving financial resilience and risk-informed investment planning, the European Union, in collaboration with the World Bank and the GFDRR, has started a program for "*Strengthening Financial Resilience and Accelerating Risk Reduction in Central Asia*" (SFRARR), aiming to advance disaster and climate resilience in Central Asia countries, which includes Kazakhstan, Kyrgyz Republic, Tajikistan, Turkmenistan and Uzbekistan. The program includes several operational components, all contributing to the development of a comprehensive probabilistic risk assessment, consistent across multiple hazards and asset types of the target countries.

Central Asia is an area characterized by complex tectonic and active deformation. The related seismic activity controls the earthquake hazard level that, due to the occurrence of secondary and tertiary effects, has also direct implications on the hazard related to mass movements (e.g., landslides and naturally dammed lake outbursts). Note that in Central Asia landslides, mudslides and debris flows are causing an extensive number of casualties every year. Climatically, this region is characterized by strong rainfall gradient contrasts, due to the diversity of climate and vegetation zones. The region is drained by large, partly snow- and glacier-fed mountain rivers, that cross or terminate in arid forelands. Central Asian countries are therefore affected by a significant river flood hazard, mainly in spring and summer seasons. The challenge posed by this combination of different hazards can only be tackled considering a multi-hazard approach harmonized among the different countries, in agreement with the requirements of the Sendai Framework for Disaster Risk Reduction, approved at the third UN World Conference on Disaster Risk Reduction in 2015.

In this report we describe the development of a new probabilistic earthquake hazard model for Central Asia, as a part of the proposed multi-hazard approach. With respect to previous regional models (e.g., the project EMCA, recently included in the global probabilistic earthquake hazard map of the Global Earthquake Model – GEM foundation), the proposed model is innovative in the following aspects:

- Earthquake recurrence is calibrated on an ad-hoc developed regional earthquake catalogue, harmonized between countries, and homogenized in moment magnitude (Mw) using the most up-to-date information from global and local sources.
- A new seismogenic source zonation is developed in cooperation with the scientific representatives of the five target countries; the source model, different for shallow, intermediate, and deep seismicity, includes a standard homogenous area source zonation and an innovative distributed seismicity model based on a rate-preserving smoothing kernel.
- Mapped active faults from regional datasets are used for the direct creation of finite fault source model, whose occurrence model is calibrated on slip rate information, to complement observed seismicity.
- A new regionalized selection of ground motion model is proposed in a new logic tree structure.

All hazard calculations were carried using the OpenQuake engine, and open-source application widely considered nowadays as state-of-art software for the calculation and assessment of seismic hazard and risk.

Index

Index of Figures

Index of Tables

1 Introduction

Due to the ongoing collision between India and Arabia with Eurasia, which induces significant stress accumulation in the earth crust around the main tectonic suture zones and up to hundreds of kilometers away (Tunini et al., 2017), Central Asia countries are naturally subject to high level of seismicity. Several damaging earthquakes have been reported in recent and historical times, while the seismic risk is exacerbated by the high vulnerability of the local building stock and infrastructures. A reliable risk assessment is, therefore, an essential step for devising an effective risk mitigation strategy, and it is the base for the formulation and enforcement of national seismic codes.

Any reliable risk assessment, however, must be based on an updated and reliable seismic hazard model for the region. Although several hazard studies have been performed locally and at national level, the last comprehensive published regional model for the whole Central Asia was developed within the frame of the EMCA project ("Earthquake Model of Central Asia"), which is almost ten years old. Nowadays, the availability of new data, local and regional seismotectonic studies and recently developed methods and tools prompt the development of a new probabilistic seismic hazard model summarizing the current state of knowledge in Central Asia.

The development of a regional model cannot be done without the contribution of experts from the local scientific community. Partnership with local governmental institutions and authorities is also an essential step to facilitate model acceptance and for potential integration with national seismic codes. Following this concept, the consortium has engaged with the local communities for building and extending awareness of seismic hazard and for enhancing the technical capacity of local experts in the use of open tools and resources (see Table 1 for the complete list of involved scientific institutions from each partner country).

In the report, we describe the implementation of a probabilistic seismic hazard model for the Central Asia, developed with the contribution and resources from local scientists primarily involved in the initiative promoted by the World Bank.

Table 1. List of partner countries of the consortium and associated scientific institutions involved in the development of the new earthquake hazard model for Central Asia.

Country	Main Scientific Institution	Local Representative
Kazakhstan	IS - Institute of Seismology	Dr. Natalya Silacheva
Kyrgyz Republic	ISNASKR - Institute of Seismology of Kyrgyz Republic	Prof. Kanatbek Abdrakhmatov
Tajikistan	IWPHE - Institute of Water Problems, Hydropower Engineering and Ecology	Prof. Zainalobudin Kobuliev
Uzbekistan	ISASUz - Institute of Seismology Uzbekistan	Prof. Vakhitkhan Ismailov
Turkmenistan	Various individual consultants	Dr. Japar Karaev

2 Seismotectonic overview

Except for the stable continental part of Kazakhstan, Central Asia is classified as a highly seismically active region. Large historical earthquake events have occurred, mostly caused by thrust and reverse-faults generated by the collision of the Eurasian and Indian plates (Ullah et al., 2015). Such compressional regime was responsible for the development of the Cenozoic belts of Tien Shan and Pamir, which accommodate a great part of the regional deformation (e.g., Abdrakhmatov et al., 1996; Zubovich et al., 2010) and where most of the seismicity occurs, often with earthquakes of magnitude larger than 7. Notable examples are the Verny (Ms = 7.3, 1887), Chilik (Ms = 8.3, 1889), Kemin (Ms = 8.2, 1911), Chatkal (Ms = 7.5, 1946) and Suusamyr (Ms = 7.3, 1992) earthquakes (Abdrakhmatov et al., 2003). The Kyrgyz Republic alone has been hit by 18 destructive earthquakes in the last 50 years, with up to 6.4 billion USD of potential economic losses estimated to be exceeded on residential buildings with a 10% probability in the next 50 years (Free et al., 2018). This seismically active region formally separates the more stable regions of the Tarim basin to the south and the Kazakh platform to the north, where a more moderate intraplate seismicity is observed but still capable of generating significant earthquakes.

On the territory of Turkmenistan, four seismically active regions can be identified: Turkmen-Khorasan, Balkhano-Caspian, Elbursky and Gaurdak-Kugitang. Strong destructive earthquakes took place, such as: Krasnovodsk catastrophic earthquake on July 8, 1895 (M=8.2); Germab earthquake on May 1, 1929 (M=7.2); Kazanjik earthquake on November 5, 1946 (M=7.0); Ashgabat catastrophic earthquake on the night of October 5-6, 1948 (M=7.3), Balkhan earthquake on December 06, 2000 G. (M=7.3). The larger seismicity is observed in the Turkmen-Khorasan and Balkhano-Caspian regions, with Ashgabat as the most seismically active area of the Turkmen-Khorasan region. Tajikistan is a seismically active region as well. Few destructive earthquakes are known, such as the Karatag earthquake in 1907 with MLH=7.4, the Sarez earthquake in 1911 with MLH=7.4, the Khain earthquake in 1949 with MLH=7.4, and recent second Sarez earthquake in 2015 with Mw=7.2.

While most of the regional seismicity occurs within the first 40km of the crust, deep earthquakes have also been observed down to 300km depth in the Pamirs-Hindukush area (King et al., 1999). Although reverse and thrust source mechanisms are dominant due to the local tectonic regime, strike-slip and -to a lower extent- normal mechanisms (or a combination of them) are also present.

3 Regional hazard studies

Earthquake hazard in Central Asia has been assessed comprehensively in several national and international studies. A first attempt of regional homogenization came from the Global Seismic Hazard Assessment Program (GSHAP) (Giardini et al., 1999), which aimed at establishing a common framework for the homogeneous evaluation of the seismic hazard at global scale. In this frame, a new seismic zonation was proposed for the Central Asia (Ulomov et al., 1999) and from that effort a first probabilistic seismic hazard model in macroseismic intensity was produced. In 2012 the project EMCA ("Earthquake Model of Central Asia") aimed at the development of a new comprehensive seismic hazard and risk model for Central Asia, as part of the global earthquake hazard and risk model under development at the GEM Foundation. Several datasets were assembled and released, including a homogenized seismic catalogue and a new earthquake source

zonation model. Outcome of the projects have been documented in several publications, such as Bindi et al. (2011, 2012) and Ullah et al. (2015).

Several studies at national level followed the aforementioned regional project EMCA, as presented in Ischuk et al. (2014, 2018) for Kyrgyzstan, Tajikistan and Eastern Uzbekistan, Silacheva et al. (2018) and Mosca et al. (2019) for Kazakhstan. A probabilistic earthquake hazard analysis of Kyrgyzstan was carried out by Abdrakhmatov et al. (2003), in terms of both peak ground acceleration and Arias Intensity, followed by a more comprehensive model developed within the Central Asia Seismic Risk Initiative (CASRI) (Abdrakhmatov, 2009) also including fault traces. Seismic hazard studies of Uzbekistan have been done within the framework of national programs, such as in Abdullabekov et al. (2002, 2012), Artikov et al. (2018, 2020). Additionally, research on seismic hazard in Turkmenistan has been conducted by the Institute of Seismology and Atmospheric Physics of the Academy of Sciences in the frame of regulatory acts (see Ministry of construction of Turkmenistan, 2017). In 2013 the Ministry of Education and Science of the Republic of Kazakhstan requested the development of probabilistic maps of the general seismic zoning of the Republic of Kazakhstan and seismic microzoning of Almaty city. The maps have been developed by the Institute of Seismology of Kazakhstan with participation of other relevant institutions and are at the stage of implementation in the building codes that will guide future construction practice. A package of maps of general seismic zoning is then included in the national Code of Rules No 2.03-30-2017 "Construction in seismic zones". The development of regulatory documents based on the package of maps of microzonation of Almaty was launched in 2020 by the Kazakh Research Institute for Construction and Architecture.

Institute of Geology, Earthquake Engineering, and Seismology of the National Academy of Sciences of Tajikistan, according to the request of the Government of Tajikistan and with technical support of the World Bank, developed in 2020 the new probabilistic seismic hazard map of the territory of Tajikistan. Results are now under examination by the Committee of Construction and Architecture by the Government of Tajikistan for inclusion in the National Building Code.

The Institute of Seismology (IS), the Seismological Experimental and Methodological Expedition (SEME), the Kazakh National Data Center (KNDC) and the Institute of Geology, Earthquake Engineering, and Seismology under the Academy of Sciences of the Republic of Tajikistan are currently participating to the ongoing ISTC Project "Central Asia Seismic Hazard Assessment and Bulletin Unification" (CASHA-BU).

Recently, the president of Uzbekistan has signed a new law on "On ensuring the seismic safety of the population and the territory of the Republic of Uzbekistan", which enforces the use of modern approaches for assessing seismic hazard with the goal of reducing the associated risk on structures and population.

4 PSHA Methodology

In this study, the seismic hazard of five Central Asian countries (Kazakhstan, Kyrgyzstan, Tajikistan, Turkmenistan, and Uzbekistan) is assessed using a probabilistic approach (e.g., Cornell 1968; McGuire 2004) as formalized in Field et al. (2003).

The Probabilistic Seismic Hazard Assessment (PSHA) allows the estimation of the annual chance of exceeding levels of ground motion at a site due to the events that may be caused by different earthquake sources, each with defined characteristics and seismogenic potential. More specifically, at any arbitrary observation site of the study region, the assessment is thus done by evaluating the ground motion level (for a set of different ground motion intensity measures) that is expected to be exceeded with given probability within a fixed observation time (e.g., 50 years). In its simplest representation, each source is considered independent from any other and the earthquake rupture process is assumed to follow a Poisson process. Each source is fully described by the geometrical properties (size, location, orientation) of all possible ruptures, and by the definition of their corresponding temporal occurrence behavior. While the former requirements can be directly obtained by analyzing available earthquake recordings (e.g., moment tensor solutions) and from geological and tectonic considerations, the latter must be calibrated on the evidence of past observed seismicity and using a sufficiently extended earthquake catalogue.

The methodology adopted for the construction of the earthquake source model for Central Asian countries follows a classical approach, which extensively relies on the analysis of the most recent and up to date geological and tectonic information from the scientific literature and on the available earthquake record log from global bulletins and local earthquake catalogue compilations.

The developed seismic source model consists of a combination of distributed seismicity (homogenous area sources and gridded smoothed rates) and finite faults, the former calibrated on occurrence analysis of a regionally harmonized earthquake catalogue, homogenized in moment magnitude (Mw) scale, while the latter was derived from a thorough evaluation of direct geological information from active fault databases and scientific literature. The advantage of such a hybrid source model is a more realistic representation of the spatial pattern of seismicity, which is hardly replicable just using standard (homogenous) source zones.

In the following we describe in detail the different components of the Central Asian hazard model, including the creation of a homogenized earthquake catalogue for the region, the active fault database, the seismicity analysis (occurrence rate estimation, maximum magnitude, definition of dominant faulting style, etc.) and the implementation of the earthquake source model. Separate sections are then dedicated to the regional selection of most suitable ground motion prediction models and to the treatment of the epistemic uncertainties using a logic-tree approach.

Calculation of seismic hazard was made using the OpenQuake engine (Pagani et al., 2014), an open-source seismic hazard and risk calculation software developed, maintained, and distributed by the Global Earthquake Model (GEM) Foundation. In the next sections we will review the most important results and products of the Central Asian model.

5 Harmonized earthquake catalogue

The creation of a state-of-art earthquake catalogue with homogenous magnitude representation (e.g., Mw) is nowadays an essential step for the development of any probabilistic earthquake hazard model, as it provides base information for the evaluation of the location, size, and occurrence of potentially damaging future earthquake events.

The main notable examples of compilation and unification of earthquake catalogues in Central Asia were carried out within the framework of the international projects CASRI (from historical time up to 2005) and EMCA (up to 2009, Mikhailova et al., 2015). Subsequently, the available information was supplemented with new data from SEME (Seismological Experimental and Methodical Expedition) and KNDC (Kazakhstan National Data Center) for Kazakhstan and adjacent territories, with the goal of supporting the development of a new national seismic zonation model and the seismic microzonation of Almaty. A revision of the EMCA catalogue (thus data before 2009) is nonetheless required. Earthquake epicenters and the magnitude conversion relations used to build the catalogue, including a description of the intensity in moment magnitude (Mw), must be verified considering the most recent information. Data after 2009 may be inconsistent across catalogues from neighboring countries in Central Asia, due to different development of the observation networks and the use of dissimilar processing techniques.

In the following, we present the processing steps, main assumptions, and subjective choices we made for the creation of a new *Harmonized Earthquake Catalogue for Central Asia* (hereinafter HECCA) in moment Magnitude (Mw) representation. The catalogue is obtained by analysis and combination of publicly available worldwide earthquake information (e.g., ISC-Reviewed, ISC-GEM, GCMT, NEIC compilations) with information from past regional projects and local agencies of the state members of the project.

Although the catalogue provides the best current snapshot of available earthquake information for the region, we nonetheless envisage future extensions of the presented compilation by progressively including new data from local agencies, temporary networks, and regional projects as soon as they will be made publicly available. For the compilation, we have used a set of freely available and open-source Python tools originally developed within the Global Earthquake Model foundation, which makes easy and feasible the process of future extensions (see the OQCatk-Lite library, https://github.com/klunk386/CatalogueTool-Lite, last accessed 23 August 2021).

5.1 Method

To produce a homogenous dataset, information from different sources must be usually collected and merged. However, harmonization of data coming from different neighboring regions and homogenization of the earthquake parameters (e.g., location solutions, reported time, intensity scale, avoiding duplications) is a rather complex process, which requires the definition of a set of objective criteria for selection, duplicate identification, merging and conversion. This is often the case when different seismological agencies are reporting the same events but with different magnitude types (e.g., Ml, Md, Ms). The same issue affects source location solutions, for instance when different earthquake phases, processing algorithms or modelling assumptions (e.g., earth velocity structure) are used by the different networks.

For the compilation of the HECCA catalogue we followed a two-step approach. First, information from global sources and past regional projects has been collected, reviewed, and merged into a unique base compilation (the Backbone HECCA earthquake catalogue), which is subsequently complemented by the local/national datasets provided by the partners of the consortium. It must be stressed that the focus of this work is particularly on the improvement of the catalogue during the "instrumental period" (roughly after 1900, but particularly after 1950 when modern analogue

and then digital recordings became available). On the contrary, historical events have been imported directly from the EMCA compilation, assumed to be an authoritative source for the period range, without further modifications.

5.2 Input datasets

Authoritative global sources of information for the creation of the backbone part of the catalogue are the ISC-GEM catalogue, the ISC-Reviewed bulletin, the Harvard-GCMT bulletin, the USGS NEIC and the GEM Historical Catalogue, plus the regional events from the surface wave magnitude, Mlh, homogenized EMCA catalogue (Table 2). All datasets have been preliminary processed by filtering out events with magnitude (any reported type) lower than 2 and with epicenter location outside a buffer region of roughly 300km from the five target states (Figure 1), as these events would not contribute significantly to the hazard. The national earthquake catalogues from the five local partners of the consortium have then been reviewed to supplement the backbone compilation (see Table 4).

Table 2. Summary of the catalogue sources used to compile the HECCA backbone catalogue (events selected within the buffer region surrounding the study area).

Source	N. of Events	Mag. Range	Mag. Type	Year Range	Depth Range
ISC-GEM	1525	4.96 - 8.02	Mw	1906 - 2016	5.0 - 274.1
ISV-Rev	51093	2.0 - 8.4	Various types	1906 - 2018	0.0 - 441.4
GCMT	814	4.64 - 7.61	Mw	1976 - 2017	2.7 - 400.6
USGS-NEIC	15804	2.9 - 7.8	Mw, Ms, mb	1902 - 2020	0.0 - 400.57
GEM-GEHC	24	7.0 - 8.3	Mw, Ms	1052 - 1902	20.0 - 200.0
EMCA – Hist.	173	3.5 - 8.3	Mlh	-2000 - 1898	3.0 - 180.0
EMCA – Inst.	30700	2.0 - 8.2	Mlh	1901 - 2009	0.0 - 404.0

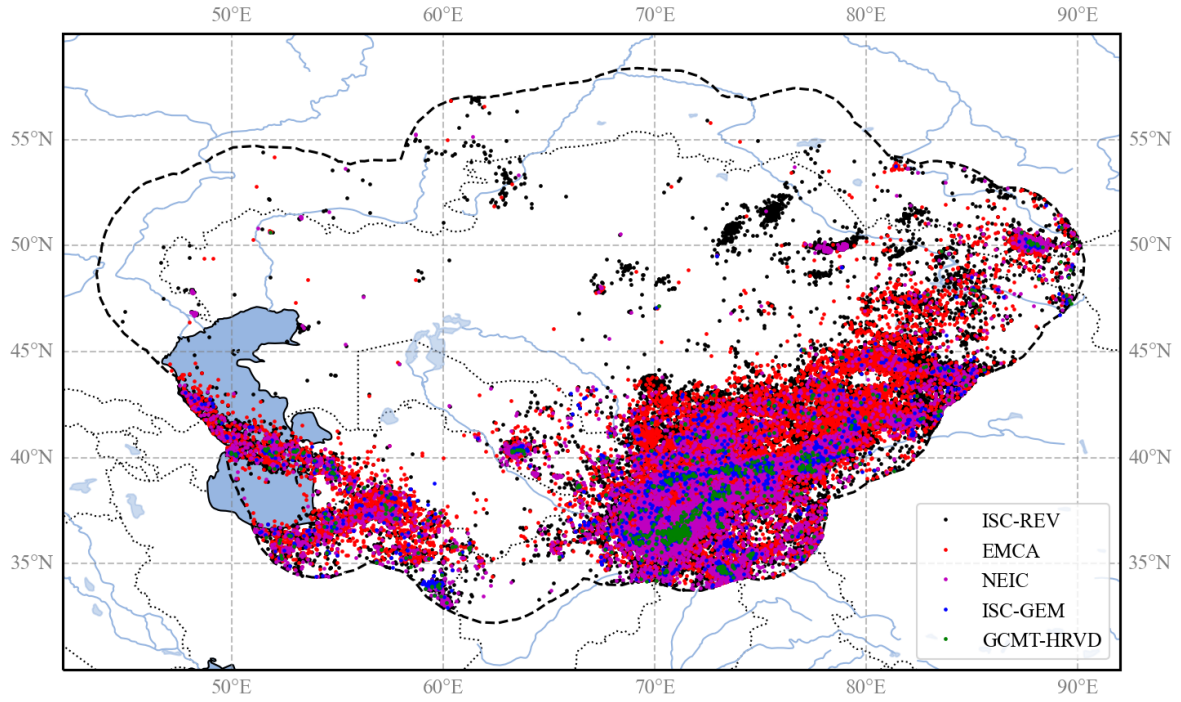

Figure 1. Distributions of the epicenters of the earthquake events from the main sources used to assemble the backbone compilation. The investigated area includes the five central Asia countries, plus a buffer region of about 300km around the national borders (black dashed line).

5.2.1 ISC-GEM homogenized catalogue

The ISC-GEM global instrumental catalogue is an improved version of the bulletin of the International Seismological Centre (ISC, Storchak et al. 2013, 2015; Di Giacomo et al. 2018). Its current version (Version 7, released on 2020-04-09) presently spans the period range 1904-2016. The compilation benefits from an accurate relocation of earthquake events made using a single location technique and uniform velocity model (Bondar et al. 2015), while magnitudes have been homogenized in Mw scale according to the rules defined in Di Giacomo et al. (2015). On a global scale, the catalogue presently covers the magnitude range from about 5 to 9.5, although the magnitude record can be considered complete above 5.5 starting from 1935.

The ISC-GEM catalogue represents the primary and most authoritative global source of the Backbone Central Asia catalogue in the instrumental period. When selecting and merging events from different sources, ISC-GEM location solutions have always the larger priority on other solutions. On the contrary, magnitude solutions have largest priority only when no direct moment magnitude (Mw) estimates are available (e.g., from the GCMT bulletin).

5.2.2 ISC Reviewed bulletin

The reviewed version of the ISC bulletin (Storchak et al. 2017; www.isc.ac.uk) is used to complement those events not captured by the ISC-GEM catalogue, particularly for magnitude below about 5.5 which are still relevant for earthquake hazard analysis.

The ISC Review bulletin provides for each event multiple location and magnitude solutions (with different magnitude types) from different reporting agencies. The Central Asia selection of the bulletin consists of 51093 events, with location solutions from 33 agencies and magnitude solutions from 108 agencies (Table 3). ISC always provide a preferred ("*prime*") location solution, which is often -but now always- the ISC own solution. For catalogue harmonization, we use the ISC prime location when available, which is derived from the same algorithm and velocity model used for the ISC-GEM catalogue, while for magnitude definition we use a selection procedure based on agency prioritization rules, which will be described more in detail in the next sections.

Table 3. Location and magnitude solutions relative to each reporting seismological agency of the ISC-Review bulletin in the study region.

Solution type	Agency (number of available solutions)
Location	ISC (41785), NNC (5646), BJI (552), IDC (478), KRNET (471), KNET (371), SOME (316), QUE (281), MOS (277), THE (241), EIDC (187), GUTE (109), NDI (77), THR (56), ASRS (53), IASBS (39), NEIC (30), ISS (26), CSEM (19), BCIS (17), DRS (15), CGS (8), OBM (6), PEK (6), MIRAS (6), MATSS (5), TIF (4), AZER (4), ISU (2), NEIS (2), MSSP (2), NORS (1), HFS1 (1)
Magnitude	IDC (92271), NNC (61850), ISC (25883), BJI (20887), NEIC (13595), MOS (13369), KRNET (9508), EIDC (4034), NEIS (2878), KNET (1376), NDI (1336), TEH (1282), QUE (1140), ASRS (1100), SOME (868), GCMT (845), CSEM (824), LDG (802), THR (762), USCGS (655), PEK (620), IASPEI (342), SZGRF (317), LAO (298), BGR (215), AZER (196), PAS (192), IASBS (116), EUROP (90), MIRAS (60), NAO (54), USGS;NEIC (51), HFS (51), ABE1 (44), GS (37), UPP (36), DRS (34), NORS (34), DSN (34), GUTE (34), OBM (31), STR (29), B&D (29), KIR (27), ZUR_RMT (27), P&S (25), BCIS (23), EVBIB (22), CGS (22), BRK (19), IPGP (18), BRK;NEIC (18), TEH;NEIC (17), COL (16), UPIES (15), ISN (14), DMN (13), MATSS (12), BRK;NEIS (12), KEW (11), MHI;NEIC (10), MAT (9), PAS;NEIC (9), KRAR (8), TIF (8), MSSP (8), UCDES (8), ROTHE (7), KISR (7), PAS;NEIS (7), NUR (6), HFS1 (6), PRA (6), AN2 (6), PSH;QUE (5), RSNC (5), MHI (4), USGS (4), OBN;NEIC (4), ZUR (4), PAL (4), SHL (3), ROM (3), LEDBW (3), STU (2), ISK (2), KLM (2), BJI;NEIC (2), GFZ (2), CNRM (2), LDSN (2), ABE3 (2), COP (2), TUL (1), KAR (1), IGS (1), CSE (1), BMO (1), PRE (1), PAL;NEIC (1), PDG (1), DNK (1), SFS (1), ISS (1), CSEM;NEIC (1), PMG (1), NDI;NEIC (1), CLL (1)

For a comprehensive list and description of reporting agency codes and magnitude types refer to:

- http://www.isc.ac.uk/iscbulletin/agencies
- https://www.usgs.gov/natural-hazards/earthquake-hazards/science/magnitude-types

5.2.3 GCMT Bulletin

The Global Centroid Moment Tensor catalogue (GCMT, Ekström et al., 2012) is a collection of moment tensor solutions for earthquakes with Mw>4.5, from 1972 to 2013. In the catalogue, while hypocenter solutions are derived from external agencies (such as the ISC) and are, therefore, generally discarded from our analysis (or marked as duplicates), Mw solutions are assumed always

as authoritative reference estimates. The Central Asia selection consists of 814 events with Mw between 4.64 and 7.61. Analysis of the moment tensor solutions for these events is also essential to constrain the rupture mechanisms of the earthquake source model (see rupture mechanism definition sections).

5.2.4 USGS - NEIC bulletin

Although the Bulletin of the International Seismological Centre is considered the final global archive of parametric earthquake data, the preliminary bulletin of the USGS National Earthquake Information Center (NEIC) can provide useful additional information, not yet reviewed by ISC. The NEIC database has generally the lowest priority with respect to the previous compilations, both in term of location and magnitude solutions.

5.2.5 GEM historical earthquake catalogue

As for the case of the ISC-GEM catalogue, the GEM historical earthquake catalogue (GEM-GHEC, Albini et al. 2014) is an authoritative global source of information for historical earthquakes. The catalogue covers events from about 1000 to 1903, compiled from macroseismic intensity data and from a review of the available literature (papers, reports, volumes) world-wide. Unfortunately, the GEM-GHEC has limited coverage in the Central Asia, with only 24 reported events of magnitude above 7, mostly captured by the EMCA catalogue.

5.2.6 The EMCA catalogue

The EMCA (Earthquake Model Central Asia) catalogue (Mikhailova et al., 2015) includes information for 33620 earthquakes that occurred in the Central Asian countries (Kazakhstan, Kyrgyzstan, Tajikistan, Uzbekistan and Turkmenistan) and represents the first important effort of harmonization of catalogue data in the region.

The EMCA catalogue covers a period from 1000 to 2009 and is homogenized in surface wave magnitude (Mlh) for the horizontal component (Rautian et al. 2007). Mlh magnitudes are not original estimates but were converted from either body wave magnitude (mb), or the energy class (K) or Mpva (regional magnitude by body waves determined by P-wave recorded by short-period instruments) using empirical regression analyses.

For the harmonization process, the catalogue was split into two main blocks, the pre-instrumental or historical (before 1900) and instrumental (after 1900) periods. Being out of the scope of the present project the review of historical information, all reported events before 1900 were considered authoritative sources for the compilation of the new harmonized catalogue. On the contrary, location solutions from the instrumental period have been deeply reviewed and, where necessary, superseded with solutions from the new catalogue entries. On the contrary, magnitude solutions were considered always authoritative over all other magnitude types (Ms, mb, Ml, Md) but not over Mw estimates from the moment tensor inversion and the ISC-GEM catalogue.

5.2.7 Local earthquake datasets

The earthquake record of the backbone compilation was then integrated with information from the local earthquake catalogues provided by the national seismological agencies. These datasets are

the result of regional earthquake monitoring performed with temporary and national permanent seismic network installations and are an essential complement to the globally available information, particularly for the low magnitudes. Main characteristics of the national datasets reviewed for inclusion in the HECCA catalogue are provided in Table 4. It must be noted that several events of the local contributions were already available from the global sources and in the EMCA catalogue. Therefore, the selection was focused on identifying and including the missing events, particularly for the most recent time interval, following the harmonization procedures described in the following sections.

Table 4. Summary of the local national sources used to complement the final HECCA catalogue (magnitude range is referred to the final conversion).

Source	N. of Events	Mag. Range	Mag. Type	Year Range	Depth Range (km)
Kazakhstan	30930	2.1 - 8.3 (Ms)	Kp, Mlh, Ms	-250 - 2020	0 - 210
Kyrgyzstan	34434	2.2 - 7.7 (Ms)	Kr, Mlh, Ms	-250 - 2020	0 - 99
Tajikistan	66602	4.0 – 16.5 (Kr)	Kr	1962-1991	0 - 350
Uzbekistan	1837	3.5 – 9.2 (Mlh)	Kr, Mlh	1955-2020	0 - 35
Turkmenistan	7416	8.6 – 14 (Kp)	Kp, Mpv	1997-2014	0 - 63

5.3 Merging catalogues

To produce a unique catalogue compilation, as a first step the same events from the different input sources must be identified and merged by means of a duplicate finding algorithm. Our approach is based on spatial and temporal matching of the reported hypocentral solutions within pre-defined windows, whose length is tuned according to the expected accuracy of the solution in a specific time range. For the current study we have identified an optimal time lag of 15s and a space distance of 60 km between solutions (see Figure 2). This combination could capture over 95% of the duplicated events in the instrumental period (after 1900). It must be noted that, being an automated process, misidentification errors are nonetheless possible. As no unique window length exists that allows capturing all duplicated events across catalogues without erroneously including a fraction of independent events, an additional conditionality of magnitude range matching was added, to decrease the probability of false match identifications. A conditionality of 1 magnitude unit was introduced as maximum allowed intensity difference between duplicated events.

Due to the limited extension of the historical record (from EMCA and GEM-GEHC), merging of historical data sources was then performed manually.

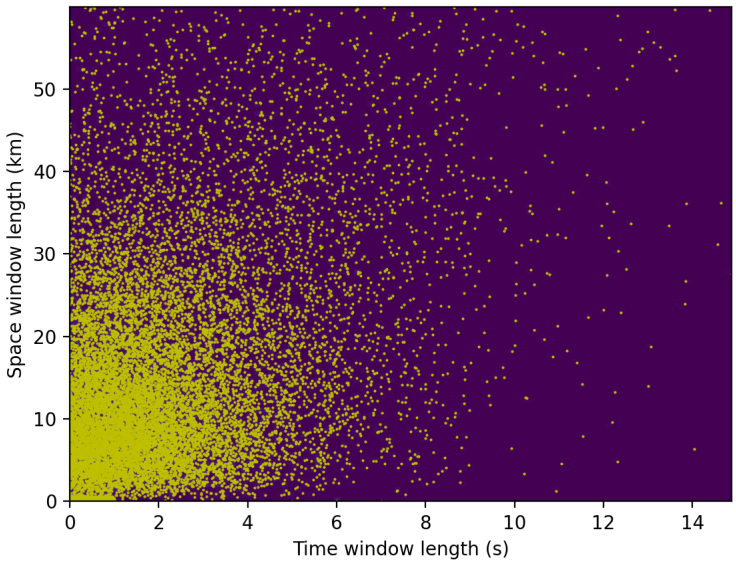

Figure 2. Time and space distance of the events identified as duplicates between the ISC bulletin and the EMCA catalogue. More than 95% of the events is captured by a 15s and 60km window, although the bulk of events is within a 5s and 25km error.

Once duplicate events between catalogues have been identified, merging is then performed by collapsing the solutions into a single event with multiple location representations. As last step, then, the preferred location solutions are selected according to ad-hoc defined priority rules (see Table 5 for the main contributors of the backbone catalogue to location solutions, sorted by priority). It is worth noting that EMCA has lower priority with respect to other reporting sources only for the location solutions. In fact, a considerable fraction of the EMCA events have shown scarce spatial resolution (producing a "gridded" pattern in the distribution of the epicentres). As indicated, reporting sources like the ISC-GEM (and more recently also ISC-rev) are now providing reprocessed solutions using more recent and better performing algorithms and regionally consistent velocity models.

Table 5. Number of events selected as preferred location solutions from the different input datasets used to assemble the backbone catalogue. Sources are sorted from highest (left) to lowest (right) priority rule.

Source	ISC-GEM	ISC-Rev (prime)	GCMT	USGS-NEIC	EMCA
Initial	1526	51093	814	15804	30700
Selection	1526	49751	0	1554	16156

5.4 Magnitude homogenization

A key point in the harmonization process is to represent all available earthquake events using a unique target magnitude. In this study, we use as reference type the moment magnitude Mw (Hanks and Kanamori 1979), due to its direct connection to earthquake size and energy, and the absence

of saturation at high magnitudes. However, events with a native estimate of Mw (e.g., directly obtained from data) are limited (e.g., after 1976 for the GMCT catalogue) and, thus, conversion from other scales is often necessary.

5.4.1 Agency Selection

For magnitude homogenization we applied a magnitude agency selection criterion analogous to what has been used for the selection of the preferred location. In a first step, we explored the availability of different magnitude types from each available agency. Subsequently, the most reliable agencies have been selected and sorted according to specific priority rules. Prioritization is made based on magnitude type (from higher to lower priority: Mw → Mlh → Ms → mpv → mb → Ml) and agency-specific selection criteria. See Table 6 for the final magnitude type and agency priority list. By applying these rules, a single magnitude estimate is then assigned to each event (Table 7).

Table 6. Magnitude priority rules applied to the HECCA backbone catalogue. Magnitude types, variants and reporting agencies are sorted from highest to lowest priority.

Group	Type	Agency
Mw	Mw* (all variants)	GCMT-NDK, GCMT, HRVD, HRVD-NEIC, NEIC, USGS, USGS-NEIC, MOS, ZUR_RMT, ISC-GEM
Mlh	Mlh	EMCA
Ms	MS, Ms, MSZ, Msz, Ms1	ISC, IDC, MOS, BJI, SOME, NEIC, EIDC, NEIS, PEK, PAS
mpv	Mpv	NNC
mb	mb, mb1, Mb	ISC, IDC, MOS, NNC, KRNET, NEIC, NEIS, USGS, BJI, QUE, EIDC, USCGS
ml	ML, Ml, mL	IDC, EIDC, BJI, CSEM, TEH, THR
others	Md and unknown types	Not represented in the final compilation

Table 7. Number of events selected as preferred magnitude solutions from the different reporting agencies for the instrumental period (after 1900). Agencies are sorted according to relative frequency of the events (from highest to lowest).

Agency	N. of Events	Magnitude (relative occurrence)
EMCA	29334	Mlh (29334)
NNC	23679	mpv (23575) mb (104)
IDC	4194	MS (3516) mb (596) mb1 (54) ML (28)
ISC	3855	mb (2732) MS (1123)
USGS	1407	mb (1353) Mww (36) Mwr (18)
ISC-GEM	1059	Mw (1059)
KRNET	906	mb (906)
GCMT-NDK	816	MW (816)

BJI	751	ML (299) mL (244) Ms (147) mb (39) MS (22)
QUE	360	mb (360)
NEIS	327	mb (293) MSZ (21) MS (13)
NEIC	302	mb (239) Mwr (43) MS (10) MW (3) MSZ (3) Mww (3) Mw (1)
TEH	254	ML (254)
MOS	246	mb (131) MS (43) Mb (38) Ms (34)
CSEM	231	ML (231)
EIDC	204	mb (141) MS (62) mL (1)
SOME	127	MS (127)
USCGS	54	mb (54)
THR	47	ML (47)
GCMT	45	MW (45)
PEK	43	MS (43)
PAS	37	MS (37)
ZUR_RMT	18	Mw (18)

5.4.2 Magnitude conversion

As last step of the catalogue homogenization procedure, all events with different magnitude types must be converted to a reference scale, in this case the moment magnitude Mw. For the conversion, we use preferentially robust, well-tested and globally calibrated magnitude conversion relations for the most common magnitude scales (Ms, mb, Ml) while ad-hoc relations have been developed using an orthogonal regression approach to convert specific scales (Mpv and Mlh) to Mw (e.g., Figure 3). For these models, to stabilize the regression result, saturation limits of each scale have been accounted as additional physical constraint of the regression model. See Table 8 for the full list of conversion rules.

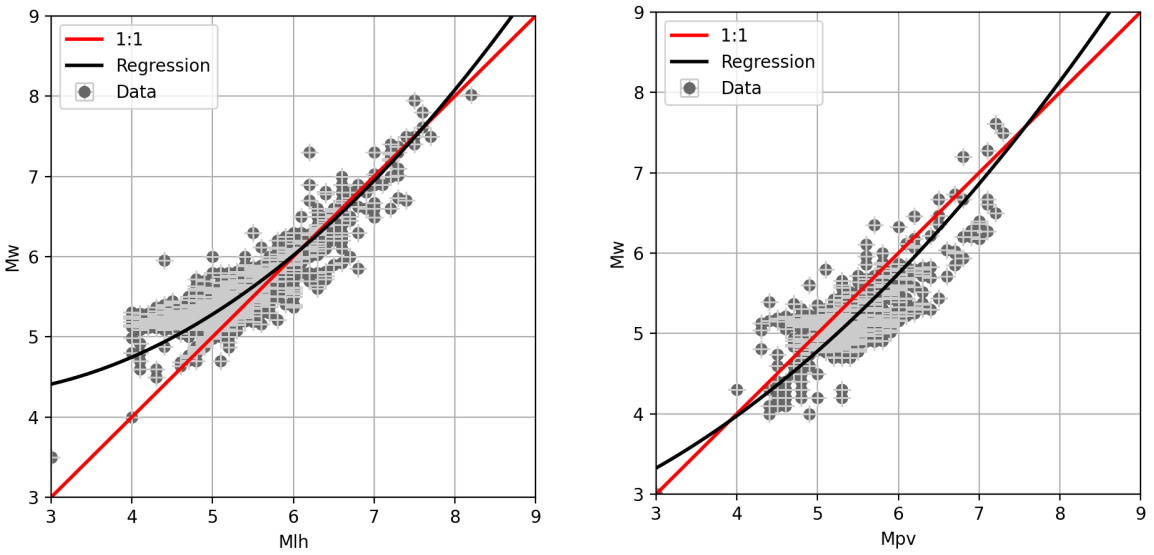

Figure 3. Magnitude conversion relations developed for Mlh and Mpv scale to Mw by fitting 2nd degree polynomial to observed magnitude pairs using the orthogonal least squares regression technique (Table 8).

Table 8. Magnitude conversion relations used for the homogenization of the HECCA catalogue in Mw.

Type	Conversion Rule
Mw	1:1
Mlh	4.594 - 0.359M + 0.099M^2 (this study)
Ms	Di Giacomo et al. (2015) – Exponential
Mpv	2.311 + 0.104M + 0.078 M^2 (this study)
mb	Weatherill et al. (2016) – Linear (NEIC calibration)
ml	Edwards et al. (2010) - Polynomial
Md and others unknown types	1:1
Kr (energy magnitude)	Bindi et al. (2011)

5.5 Integration of local data

The harmonization process (duplicate identification, location selection, magnitude conversion) was first performed on the global and regional datasets to produce the backbone part of the harmonized catalogue. The inclusion of local (national) datasets to the backbone compilation was then performed following the same integration criteria, but in a separate phase. Event merging of the different national contributions was performed individually for each country, so that each dataset was assumed authoritative on its territory and no additional priority rules for selection were then required. In addition, consistent magnitude conversion rules were used, as specified in Table 8.

5.6 Output harmonized catalogue

The harmonized backbone catalogue for Central Asia presently consists of 77376 events up to 2020 and in the range 3.0<Mw<8.5 (see, e.g., Figure 4, Figure 5 and Figure 6), although minimum regional completeness is found of about Mw 4 to 4.5. On the total number of compiled events, about 10646 are from newly included local data (roughly 13% of the total). The historical period (before 1900) is covered mostly by the EMCA catalogue, while the instrumental period has been deeply revised in this study and extended by the inclusion of new homogenous location solutions from global datasets, additional magnitude conversion relations and recent events (e.g., after 2009) from regional datasets.

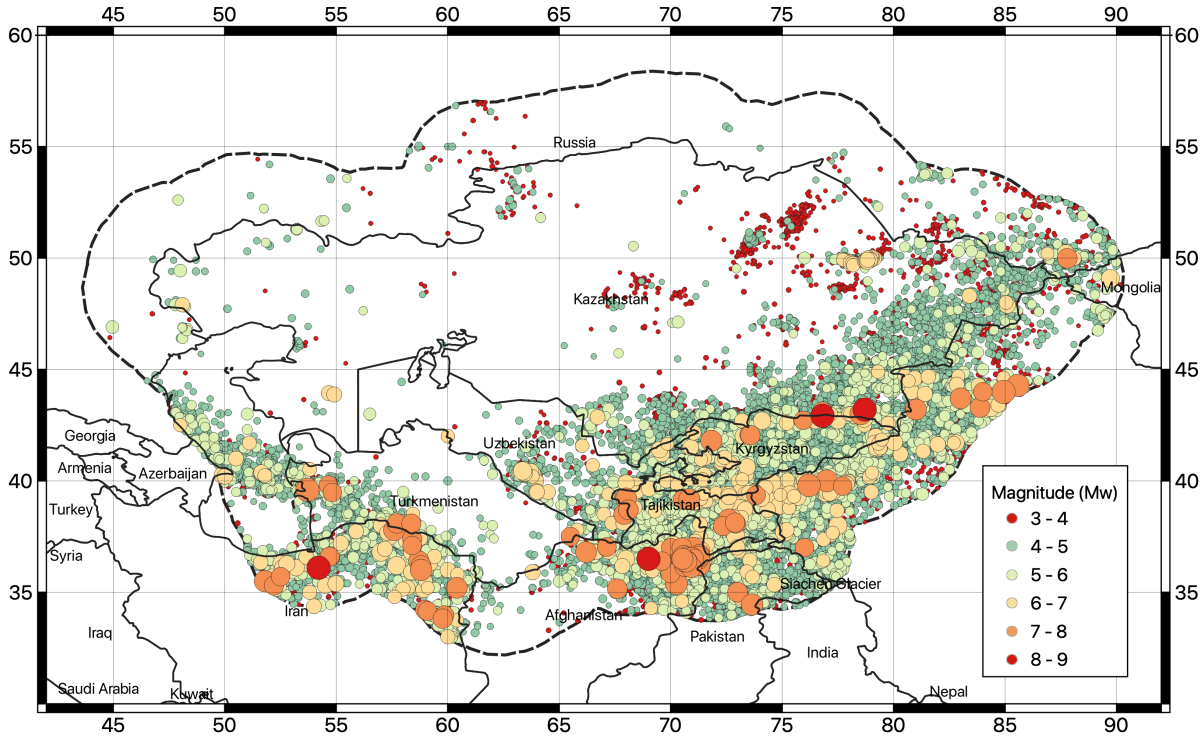

Figure 4. Geographical distribution of earthquake hypocenters (Mw>3) of the newly developed Mw harmonized catalogue for Central Asia (HECCA).

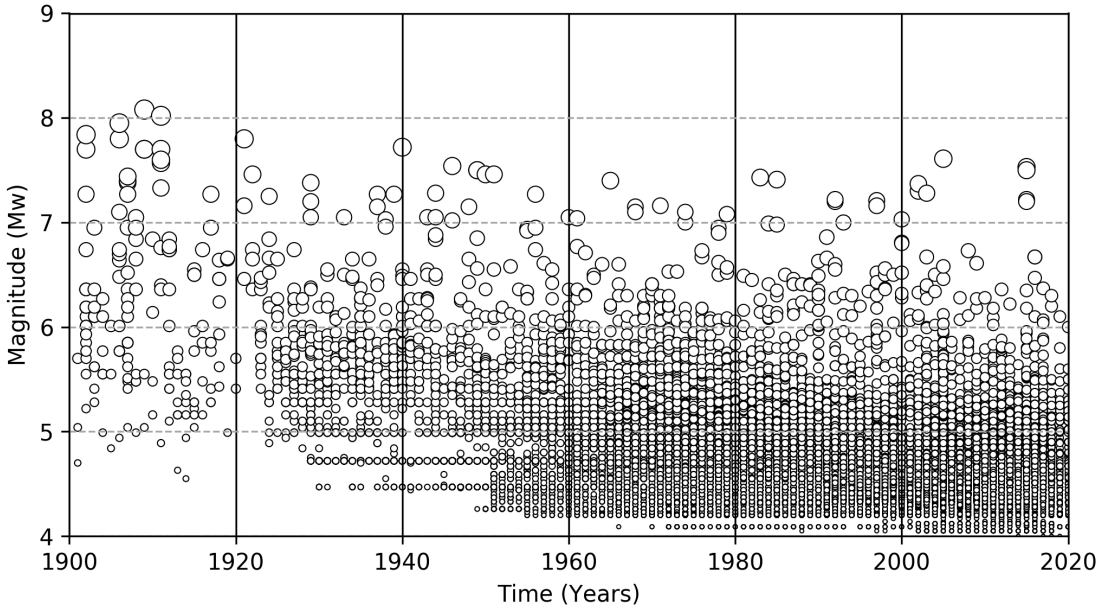

Figure 5. Time-magnitude distribution of the earthquake events of the HECCA catalogue in the instrumental period (after 1900).

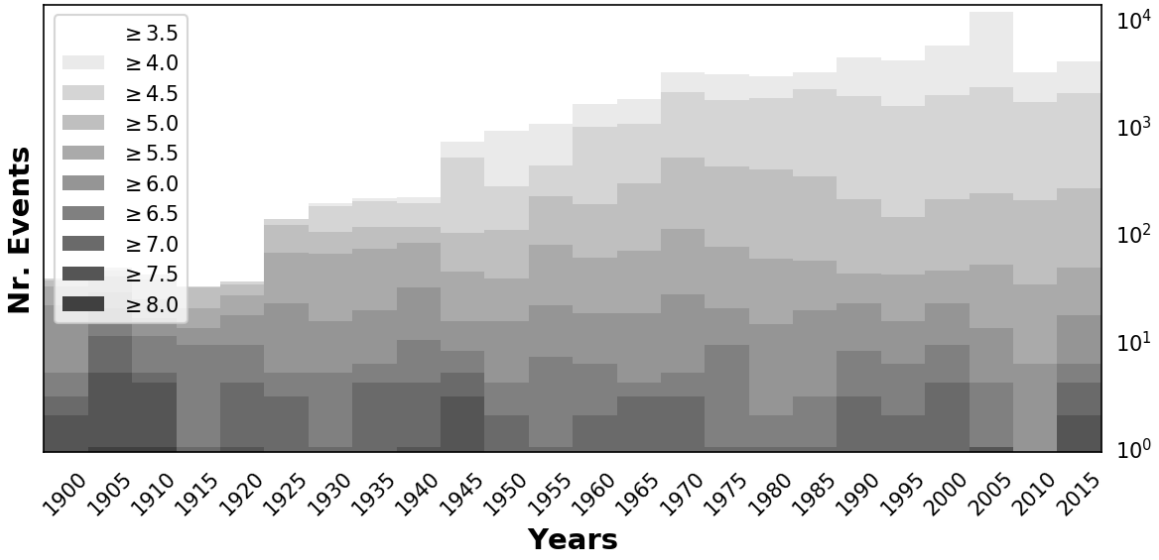

Figure 6. Number of events of the Central Asia catalog computed for five-year windows in the period 1900-2015. Shades are for bins of increasing magnitude threshold (cumulative).

6 Earthquake catalogue declustering

Probabilistic seismic hazard analysis assumes that earthquake occurrences are independent and that their probability distribution is that of a Poisson process. In reality, earthquake catalogues are affected by a fraction of correlated events, highly dependent in space and time. Cluster of correlated

events can be of natural origin (e.g., the aftershocks following a major event), induced by anthropogenic activity on the natural environment (e.g., geothermal exploitation, carbon sequestration) or purely artificial (e.g., blasts, mining explosions). In all cases, those events must be removed to force the earthquake record to represent Poisson process. To do that, declustering procedures are usually applied. What is left can be thought as a collection of independent mainshocks (i.e., events with largest magnitude in a cluster) of purely tectonic origin.

6.1 Aftershock removal

In this study, removal of earthquake aftershocks, foreshocks and triggered events in all clusters is performed using a direct search approach, where all events falling within a magnitude-dependent time-distance window from the assumed mainshock (largest event in the cluster) are considered dependent and then purged from the catalogue. Several time-distance windows have been proposed in the literature. We have tested the algorithms of Gardner and Knopoff (1974), Uhrhammer (1986) and Grunthal (1985), each providing different estimates of the relative aftershock content. By directly inspecting the performances of the three algorithms on the HECCA catalogue (e.g., Figure 7, Table 9), both in term of geographical distribution of the residual events and of variation in the occurrence rates, we have selected the Gardner and Knopoff (1974) as the approach that provides the most appropriate and balanced result for Central Asia, being not too aggressive while at the same time capable of capturing the largest fraction of dependent events.

Table 9. Number of earthquakes per magnitude bin from the non-declustered d catalog and using different declustering algorithms.

	All events	3<Mw<4	4<Mw<5	5<Mw<6	6<Mw<7	7<Mw<8
Before declustering	77376	25178	47599	4060	444	91
GardnerKnopoff	24373	7398	14878	1774	248	71
Uhrhammer	49018	17191	29146	2337	272	68
Grunthal	14283	3654	8788	1539	228	70

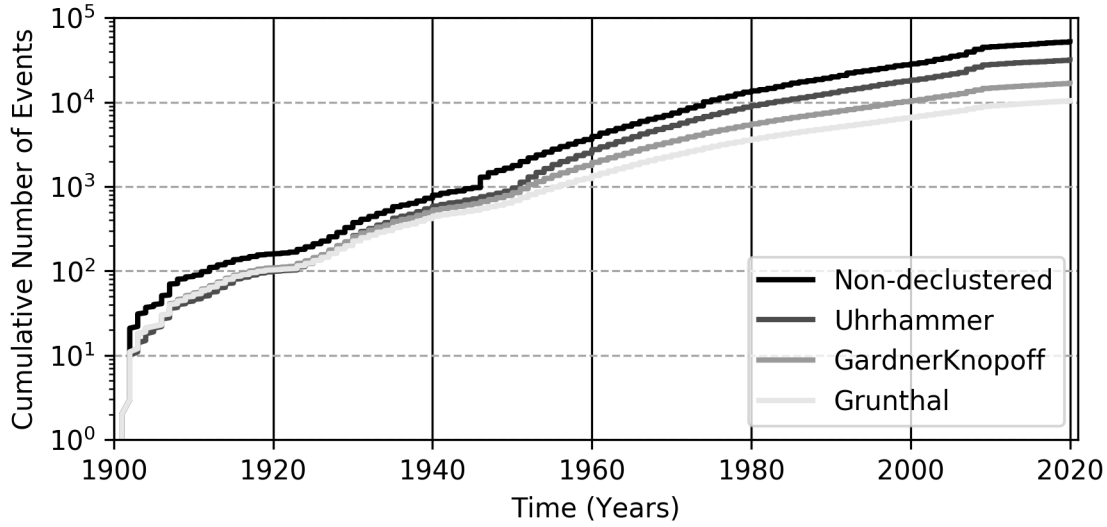

Figure 7. Cumulative number of events over time for the full (non-declustered) HECCA catalogue and for the three catalogs obtained using the three considered declustering algorithms.

6.2 Induced and artificial event removal

In principle, induced and artificial events, being man-made, should be known from the origin and, therefore, could be manually removed from the earthquake record. In case of Central Asia, however, the log of these events is fragmented and often uncomplete. Thus, an alternative (and possibly automated) removal strategy must be implemented and applied. The major issue is that these events may overlap in time and space the existing background seismicity, which should not be altered to avoid biased estimation of the local hazard.

Here, we applied a modification of the declustering algorithm used to purge natural aftershocks, under the assumption that such artificial events are also highly clustered in space and time and, at the same time, that the largest events in the cluster are likely of natural origin. Starting from a Gardner and Knopoff (1974) window, a variable scaling factor is then applied to the spatial and temporal extent of the window, till an optimal tradeoff between purged event and residual seismicity (compatible with regional background) is found. After several trials, we have identified the best scaling factor for the area as 100. To avoid altering the earthquake record in areas not affected by artificial events, the procedure is applied only on buffer regions (polygons) on known anthropogenic activity (e.g., Figure 8 for the Kazakhstan clusters).

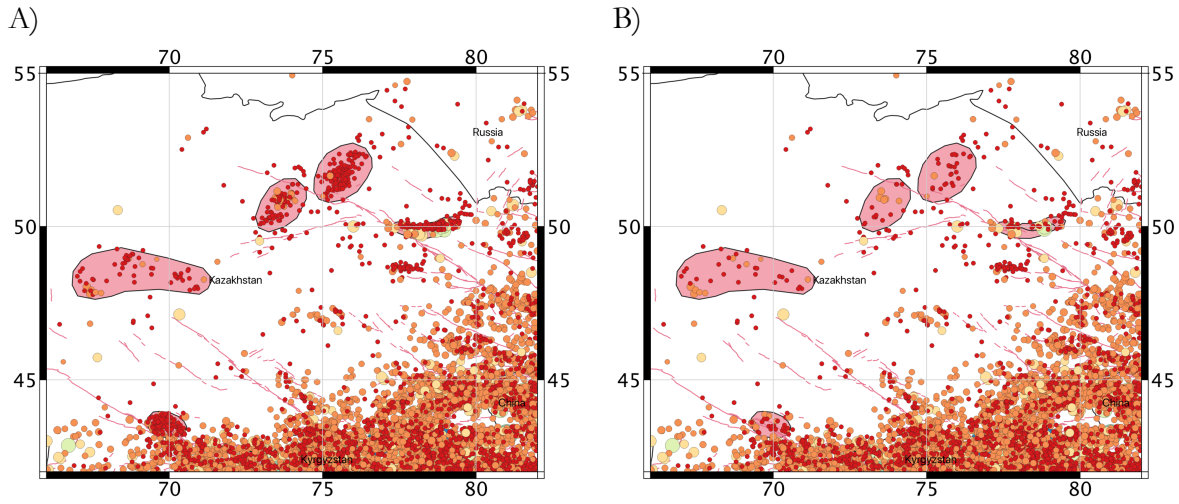

Figure 8. Example of application of the procedure to remove artificial events from the catalogue. In pink, the polygons isolating areas of known anthropogenic activity.

7 Seismic source zonation

Discretization of the study area into several zones of supposedly uniform temporal and spatial earthquake occurrence is the base of the distributed seismicity approach, where observed seismicity is not related to any known (or inferred) tectonic structure, but rather assumed to have equal probability to occur anywhere within the area. Moreover, subdivision into discrete zones is also an essential requirement for the calibration of analytical occurrence model, whose parameters must be constrained by a sufficiently large set of events to provide statistical significance.

In this study, the implementation of the homogenous area source model was primarily done on the base of the harmonized earthquake catalogue for the region (evaluation of the mean activity rate across the area, distribution of seismogenic depths), accounting also for all existing information from the scientific literature and past studies available for the target region, including geological and seismotectonic interpretations (description of fault systems, e.g. from the ACROSS database, and their relation to the local stress and deformation regimes), existing seismicity analyses and previous earthquake hazard assessments from past regional projects (e.g., GSHAP, Giardini et al, 1999, and EMCA) and published studies (e.g., Abdullabekov et al., 2012; Ischuk et al., 2018; Silacheva et al., 2018).

Geometry of the source zones were drawn following the guidelines proposed by Vilanova et al. (2014) that provide a set of objective criteria to delineate regions of supposedly homogenous seismic potential. Additional direct constraints came from the local experts of the consortium, whose feedback has been progressively integrated into the various revisions of the model during several meetings (a total of five review meetings were held, with two of them mostly focused on the source model implementation), and through individual communications. Here, the source zonation model (in geojson and shapefile format) was shared with partners and the proposed revisions collected and integrated. The current accepted revision is presently Version 6.

In the developed model, three independent layers of zonation have been implemented according to source depth: the standard zonation model for shallow seismicity (< 50km), and two additional layers of zones for intermediate (50-150km) and deep (> 150km) seismicity.

7.1 Shallow seismicity zonation

The shallow seismicity model is applied to represent earthquake source within 50 km depth. It consists of 61 homogenous source zones, grouped into 7 main tectonic groups (A to G, Figure 9) assumed to have comparable behavior in terms of earthquake productivity (particularly for the b-value of the Gutenberg-Richter relation) and rupture mechanism, both related to the different rheological behavior and stress/deformation regime of the crust. In agreement with the limits of the investigated area (see the buffer region used for the creation of the harmonized catalogue), area source zones were drawn within 300km from the target state borders.

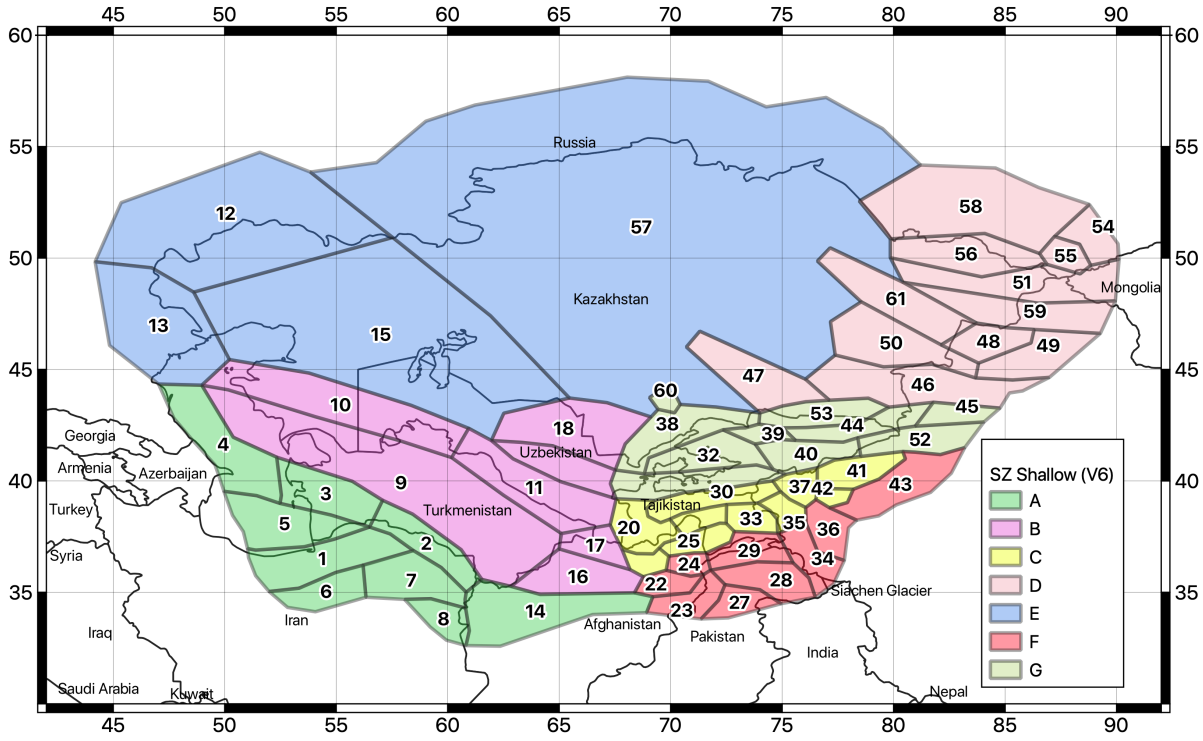

Figure 9. Earthquake source zonation model for the shallow crust (<50km). Different colors indicate the different tectonic groups (A to G).

7.2 Deep source zonation

The analysis of hypocentral depth distribution (see seismicity analysis section) revealed that a significant fraction of earthquakes is located at depth below 40-50km, considered the lowermost thickness of the continental (brittle) crust for the area. These deep events are clustered into two main regions (see Figure 10) where crustal thickening likely occurs, due to the development of deep thrusts induced by the continental collisional. Earthquake sources at these depths have different

characteristics with respect to the observed shallow seismicity and should be therefore treated separately. Because of that, two intermediate-depth (H and K) and one deep (L) source zones have been implemented separately, to represent the seismogenic range 50-150km and 150-400km.

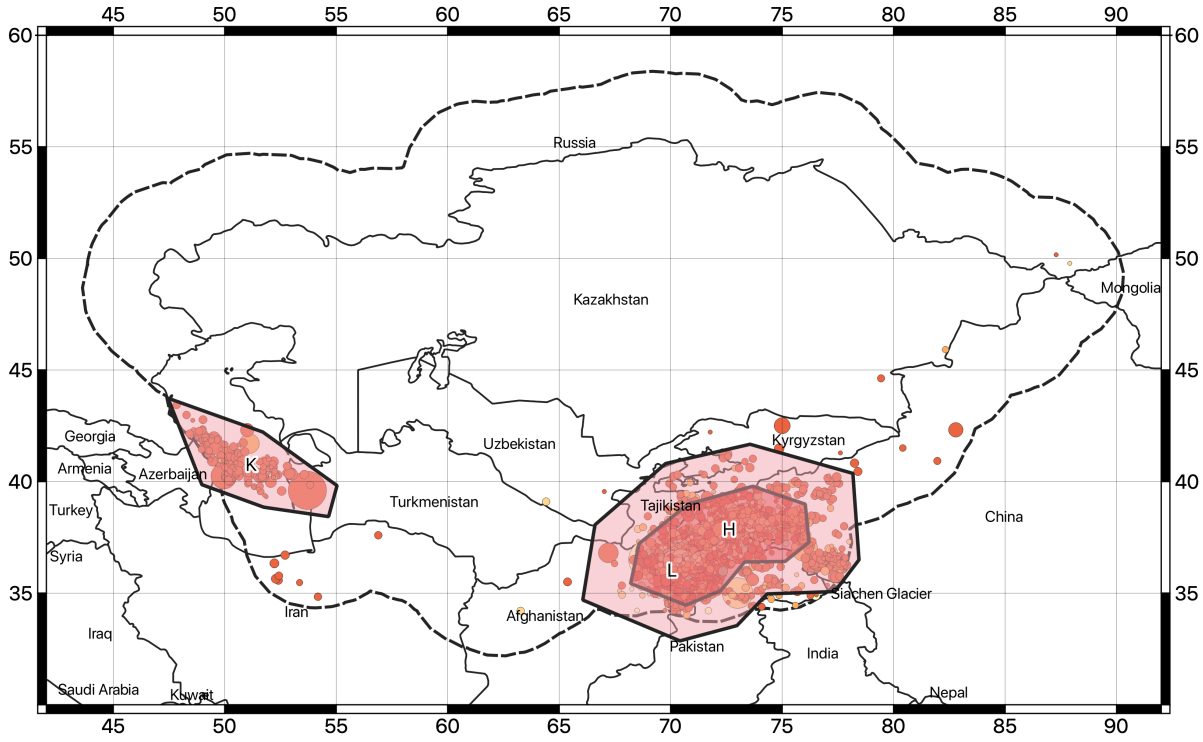

Figure 10. Earthquake source zonation model for the intermediate (H and K zones, 50-150km) and deep (L zone, >150km) earthquakes.

8 Seismicity Analysis

While seismic zonation provides a mean to distinguish between regions of different seismic behavior, the different source properties (e.g., hypocentral depth distribution, temporal occurrence model and dominant rupture mechanism) must then be defined separately for each discrete zone to create the final source model. In the following, a comprehensive description of the source model parameterization is given.

8.1 Hypocentre depth distribution

A depth probability density distribution was estimated for the different source groups from the analysis of the harmonized earthquake catalogue (Figure 11). Events with unknown depth were excluded from the analysis, as well as events with typical fixed depth solution (e.g., 0, 5, 10, 33 km etc.) to avoid biased statistic. Nonetheless, enough samples were available to perform a reasonably robust analysis on each source group, allowing the definition of discrete depth distributions compatible with the seismotectonic features expected for the area. Finally, to account for the

uncertainty of the solutions, a level or regularization was added to the data, by applying a smoothing procedure to the final probability distributions.

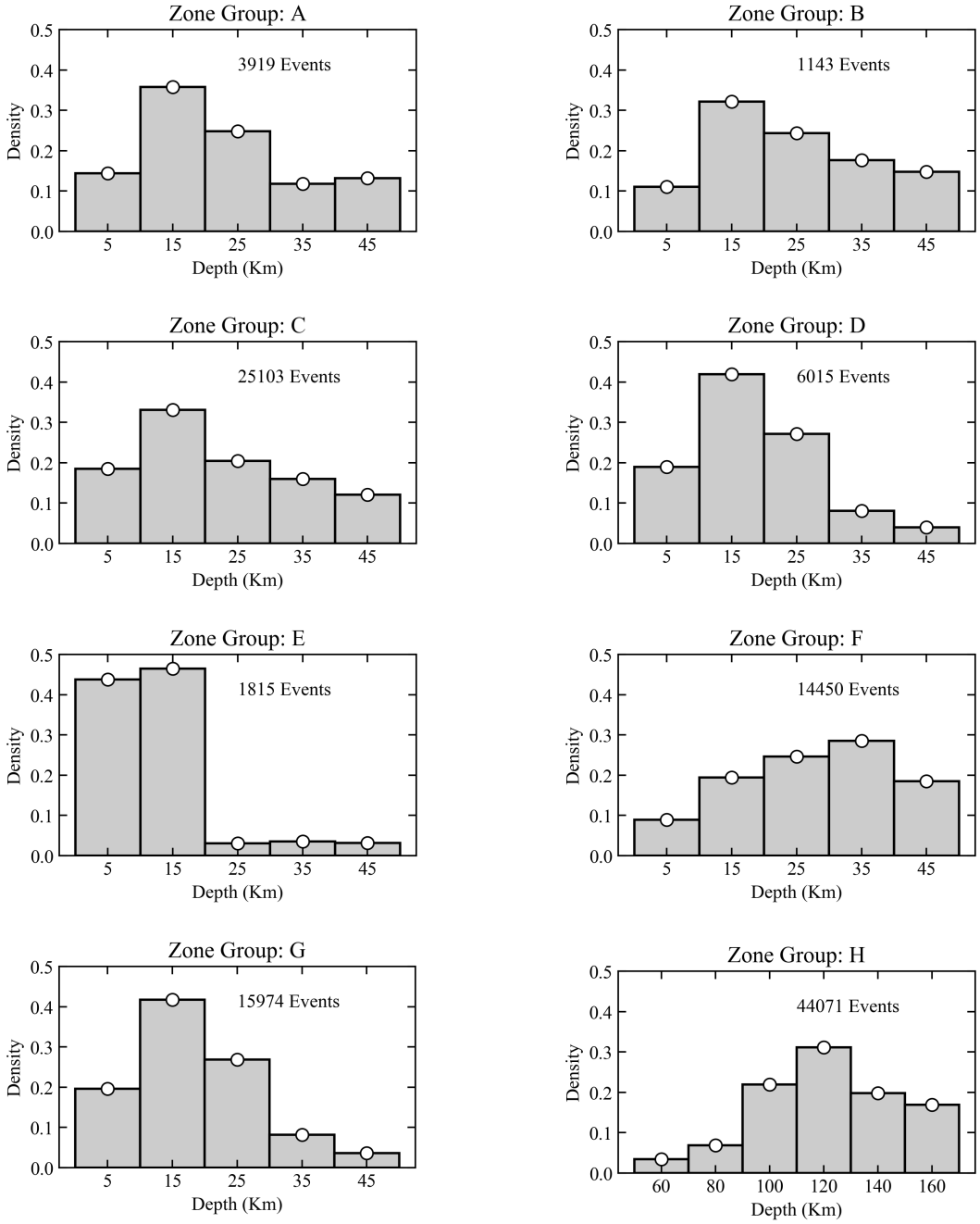

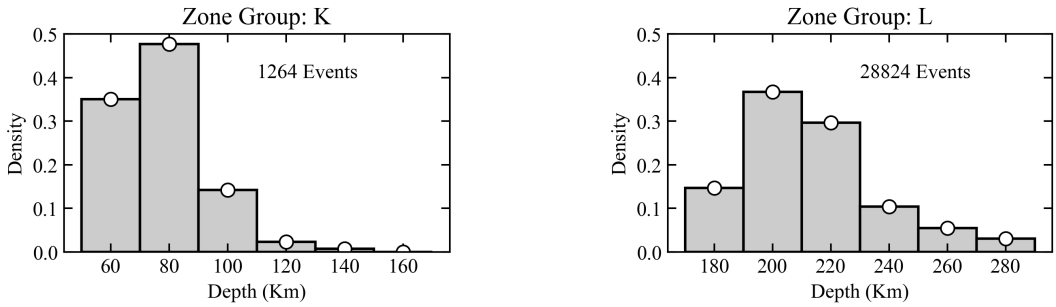

Figure 11. Normalized histograms of the earthquake hypocentral depths for the main tectonic groups of the Central Asia source model (A-G shallow depth sources, H-K intermediate depth sources, L deep sources).

8.2 Occurrence rate model

The temporal occurrence of the seismic events was assumed to follow a truncated Gutenberg-Richter (GR) model. According to this assumption, the GR parameters (a- and b-value) were estimated for each tectonic group and source zone by fitting observed annual rates from the declustered earthquake catalogue using a linear least-square approach on incremental (non-cumulative) magnitude bins. The calibration was performed following a two-step approach. First, a separate occurrence model was characterized for each of the main source groups, to establish regional b-values. Subsequently, the productivity (a-value) of each zone was individually characterized by imposing the (fixed) b-value of the corresponding group. Being b-value calibration a generally problematic task, especially in case of zones of limited extension and with limited number of earthquake events available, such a two-step procedure proved to be particularly useful to stabilize the results and, therefore, to produce more reliable productivity estimates.

Observed annual occurrence rates were obtained from the catalogue by prior definition of the completeness periods of the different magnitude ranges. Completeness analysis was performed manually for each source group, by iteratively modifying the completeness matrix while comparing the quality of the GR fit till a satisfactory solution was obtained (see Table 10 for a summary of the completeness matrix of each group). It must be additionally noted that the width of non-cumulative magnitude bins is not required to be uniform, allowing for greater flexibility in the definition of completeness periods in the different magnitude ranges.

Table 10. Completeness matrix for each source group of the area source model.

Source Group	Magnitude	Bin width	Starting year	Ending year
A	4.25	0.25	1990	2020
	4.50	0.25	1965	2020
	4.75	0.25	1965	2020
	5.00	0.50	1950	2020
	5.50	0.50	1920	2020
	6.00	0.50	1900	2020
	6.50	1.00	1850	2020

	7.50	1.00	1800	2020
B	4.25	0.25	1980	2020
	4.50	0.25	1965	2020
	4.75	0.25	1965	2020
	5.00	0.50	1950	2020
	5.50	0.50	1905	2020
	6.00	0.50	1900	2020
	6.50	1.00	1850	2020
C	4.50	0.25	1960	2020
	4.75	0.25	1960	2020
	5.00	0.50	1950	2020
	5.50	0.50	1920	2020
	6.00	0.50	1900	2020
	6.50	0.50	1900	2020
	7.00	1.00	1900	2020
D	4.50	0.25	1960	2020
	4.75	0.25	1960	2020
	5.00	0.50	1950	2020
	5.50	0.50	1920	2020
	6.00	1.00	1850	2020
	7.00	1.00	1800	2020
E	4.00	0.50	2000	2020
	4.50	0.50	1960	2020
F	4.00	0.50	1990	2020
	4.50	0.50	1970	2020
	5.00	0.50	1950	2020
	5.50	0.50	1920	2020
	6.00	0.50	1900	2020
G	4.50	0.25	1980	2020
	4.75	0.25	1960	2020
	5.00	0.50	1930	2020
	5.50	0.50	1910	2020
	6.00	1.00	1900	2020
	7.00	1.00	1850	2020
H	4.25	0.25	1990	2020
	4.50	0.25	1965	2020

	4.75	0.25	1965	2020
	5.00	0.50	1950	2020
	5.50	0.50	1920	2020
	6.00	1.00	1900	2020
	7.00	1.00	1850	2020
K	4.25	0.25	1990	2020
	4.50	0.25	1965	2020
	4.75	0.25	1965	2020
	5.00	0.50	1950	2020
	5.50	1.50	1900	2020
L	4.00	0.50	2000	2020
	4.50	0.50	1980	2020
	5.00	0.50	1950	2020
	5.50	1.00	1920	2020
	6.50	1.00	1900	2020
	7.50	1.00	1800	2020

Lower magnitude truncation (Mmin) of the GR relation was fixed to 4.5 for all sources, value generally accepted as the lowermost intensity being capable of generating significant damage to standard structures. Complementary, uppermost truncation (Mmax) is defined as the maximum potential earthquake expected to be generated from the source. Although algorithms for the objective estimation of Mmax exists (e.g., Kijko, 2004), their well-known instability led us to use a simpler, but rather conservative and, at the same time, defensible approach. In practice, Mmax was set as the maximum observed magnitude plus an increment of 0.4 units. The value of the increment was chosen subjectively as the highest value still providing physically credible earthquakes for the whole region, accounting also for standard uncertainty in the magnitude estimation, particularly for historical events. An additional variation of ±0.1units was then allowed in the hazard calculation (see logic-tree section) to account for epistemic uncertainty associated to the magnitude increment definition. It must be noted that the proper definition of Mmax is particularly critical just for ground motion levels with very-low probability of exceedance (thus rather long return periods), generally relevant for special structures and critical facilities. For those, a more critical review of Mmax operational definition might be necessary.

A summary of the derived G-R seismicity parameters calibrated for each tectonic source group is given in Figure 12.

Group A **Group B**

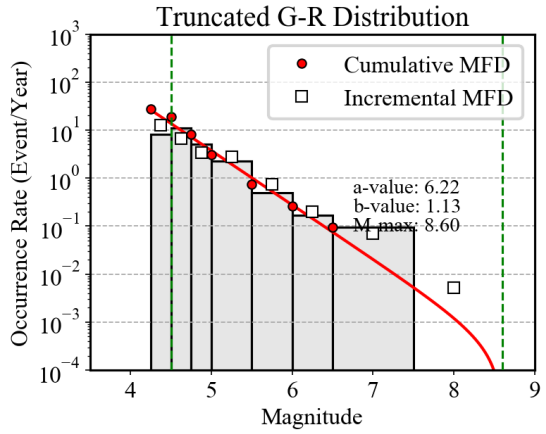

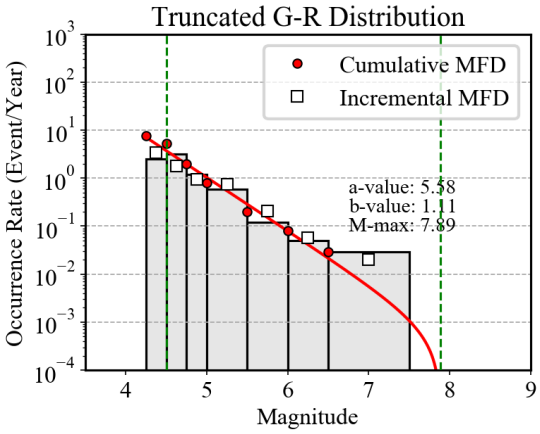

Group C

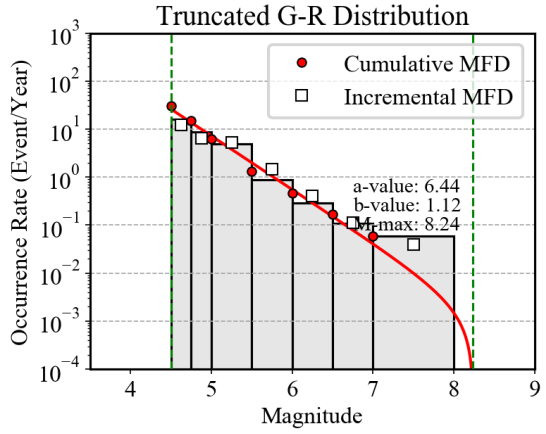

Group D

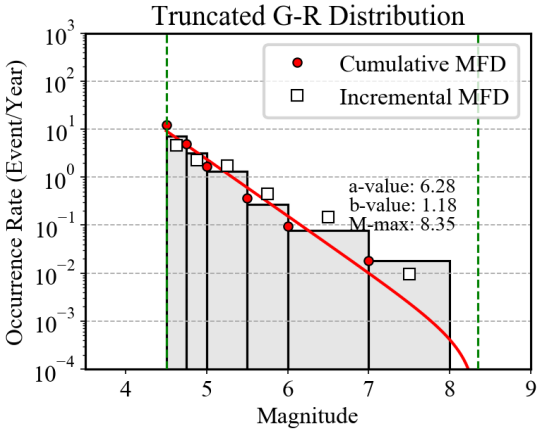

Group E

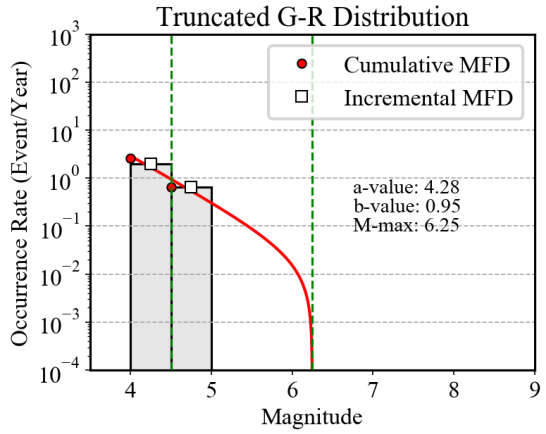

Group F

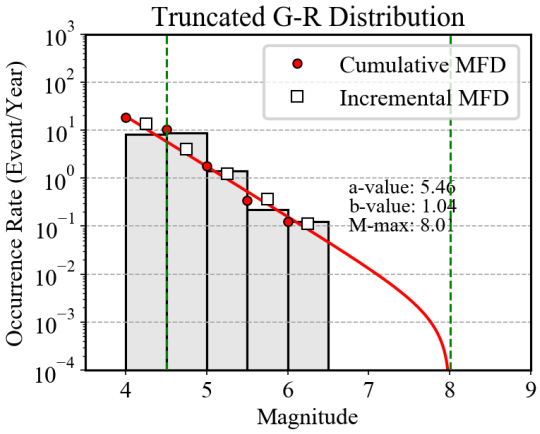

Group G

Group H

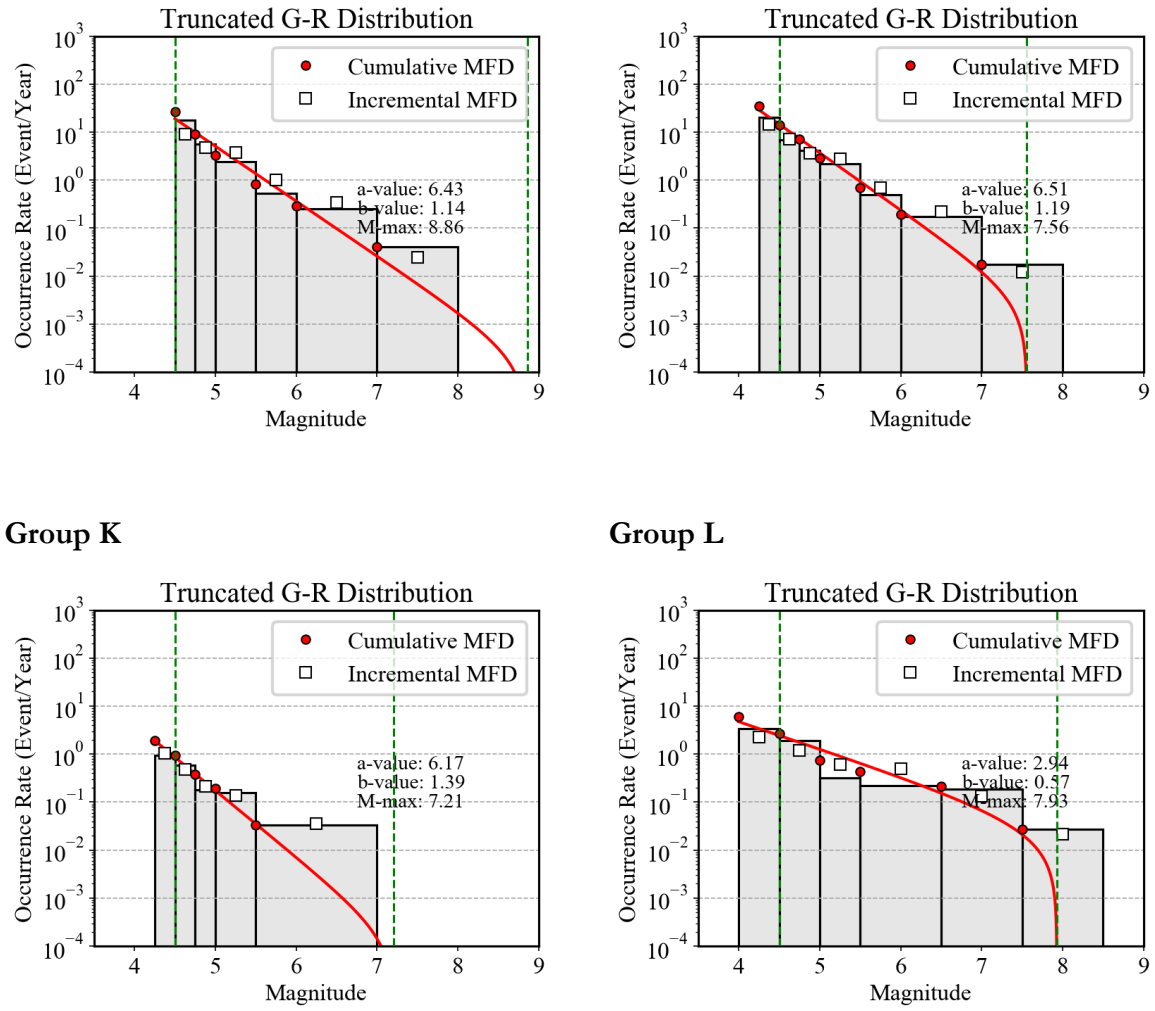

Figure 12. Gutenberg-Richter occurrence relations calibrated for the different source groups of the Central Asia model. White squares and red dots are respectively the observed incremental and cumulative occurrence rates, while the grey histogram and the red line represent the incremental and cumulative rates from the inverted Gutenberg–Richter relation. Minimum and maximum truncation magnitudes are indicated as grey dashed vertical bounds. Width of the incremental bins corresponds to that defined in the completeness matrixes of Table 10.

8.3 Rupture mechanism definition

A major feature of OpenQuake is the possibility to model the single earthquake events as ruptures of finite extension by simulating the spatial orientation and kinematics of each fault given a prescribed rupture mechanism. This is highly beneficial when using modern generation ground motion prediction models capable of using fault-dependent distance metric (e.g., Rjb, Rrup, see Douglas 2003 for a comprehensive discussion) and with mechanism-dependent calibration coefficients. The main drawback, however, is that the rupture mechanism probability distributions must be defined for each source (or source group), which is possible only if sufficient seismotectonic information is available for the region.

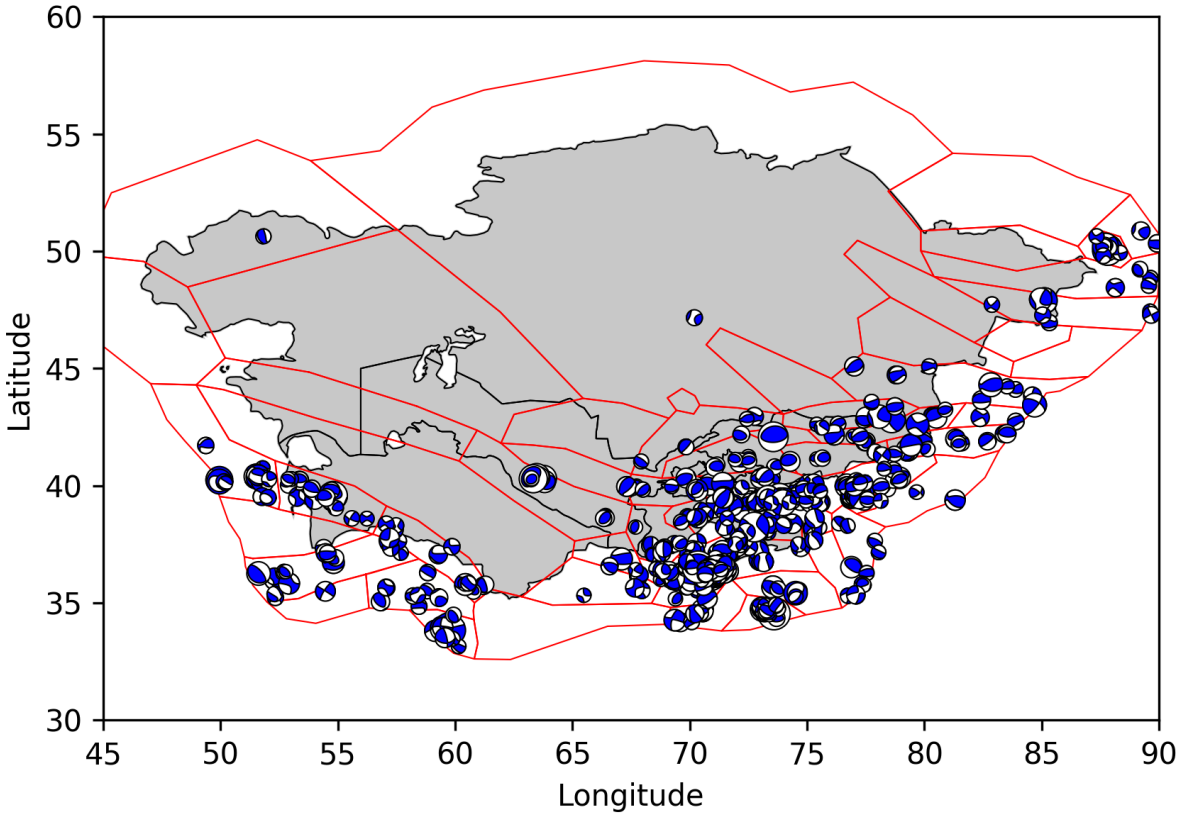

Figure 13. Distribution of "beachballs" of the 814 events available from the GCMT catalogue for the region. Traction axis is conventionally represented in blue. Plot was produced using the Obspy Python library. See Figure 14 for an interpretation of the rupture mechanisms illustrated by the beach balls.

To define the dominant rupture mechanism of each source zone of the Central Asian model we combine the available information from mapped surface faults (see fault database section), particularly for the strike direction, with moment tensor solutions from the GCMT bulletin. For the study region, 814 focal mechanisms are available for events in the range 4.64 < Mw < 7.61. Geometrical parameters (strike and dip orientation) of the different source zones were characterized by analyzing the geometry of the focal mechanism using the "beachball" representation (see Figure 13), while dominant faulting style was accessed by inspecting the distribution of the B-T axis orientations using Kaverina et al. (1996) classification diagrams (Figure 14, Figure 15), as implemented in the FMC code of Álvarez-Gómez (2019).

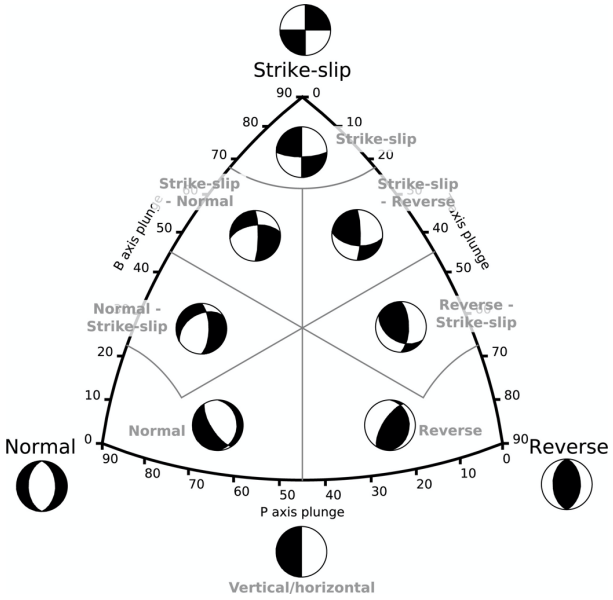

Figure 14. Correspondence between B-T axis classification and beachball representation of the moment tensor solutions in the Kaverina et al. (1996) plot (diagram from Álvarez-Gómez, 2019).

Group A

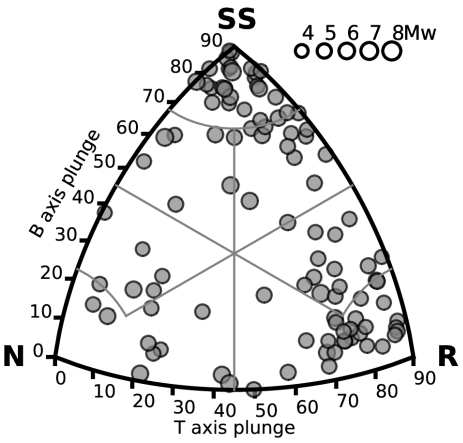

Group B

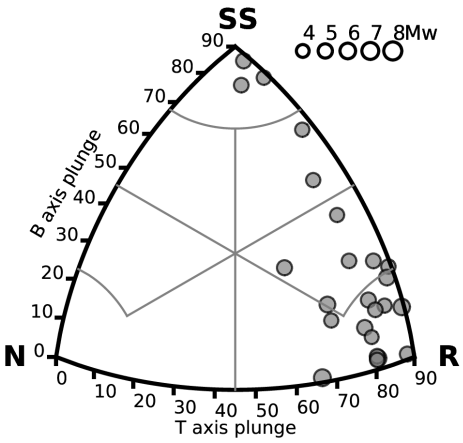

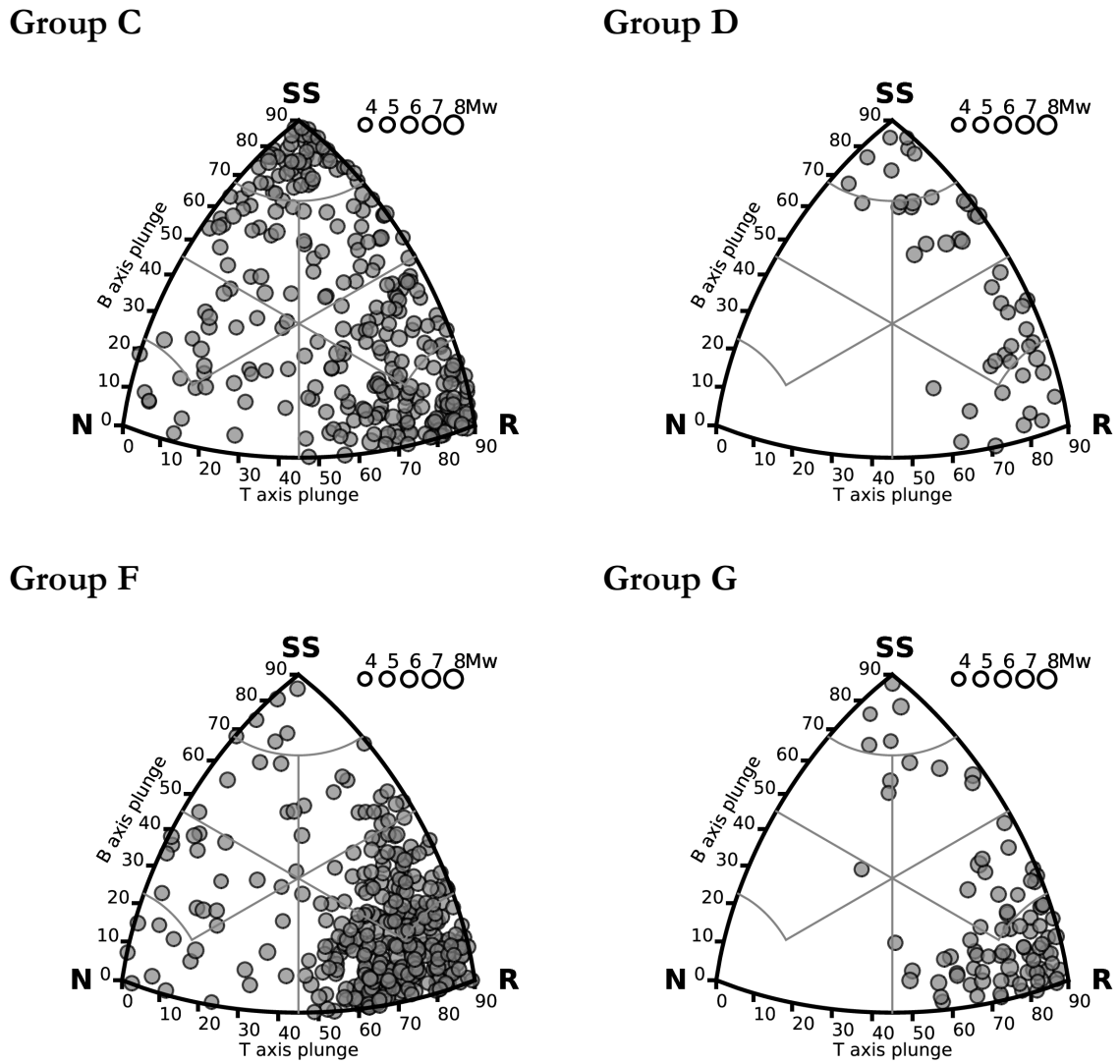

Figure 15. B-T axis classification of the GCMT moment tensor solutions available for each source group of the shallow seismicity model (due to lack of events, group E is not represented).

From the analysis, as expected, a major contribution of reverse style mechanisms is present over the whole area, with a minor although not negligible contribution of strike-slip events. A fraction of normal style mechanisms is also visible (e.g., group C and F) but less significant. For the rupture mechanism implementation in OpenQuake, dominant faulting style is represented using a combination of dip and rake angle (Table 11), according to the formalism described by Aki and Richards (1980). A summary of the rupture mechanisms associated to each zone group is given in Table 12.

Table 11. Conversion table between general faulting style and the geometrical fault parameters dip and rake as used in OpenQuake.

Fault style	Standard dip (deg)	Standard rake (deg)
Reverse	45°	90°
Normal	60°	-90°
Left-lateral strike slip	90°	0°
Right-lateral strike slip	90°	180°

Table 12. Summary of the rupture mechanisms assigned to each tectonic group with relative probability.

Group	Probability	Strike	Dip	Rake
A	0.4	60°	45°	90°
	0.2	120°	45°	90°
	0.4	120°	90°	180°
B	0.6	120°	45°	90°
	0.4	120°	90°	180°
C	0.5	70°	45°	90°
	0.4	120°	90°	180°
	0.1	30°	60°	-90°
D	0.25	70°	45°	90°
	0.25	120°	45°	90°
	0.5	120°	90°	180°
E	0.5	70°	45°	90°
	0.5	120°	90°	180°
F	0.7	70°	45°	90°
	0.3	30°	60°	-90°
G	0.8	80°	45°	90°
	0.2	120°	90°	180°
H	1.0	70°	45°	90°
K	1.0	120°	45°	90°
L	1.0	70°	45°	90°

8.4 Area source model

The source zones and the calibrated seismicity parameters have been used to create the homogenous areas source model in xml format using the Python utilities available from the Hazardlib of OpenQuake. Additional parameters required for the calculation were provided, such as:

- the magnitude scaling relation (Wells and Coppersmith, 1994), used to numerically constrain the subsurface length (L) and width (W) of the earthquake ruptures
- the rupture aspect ratio (1:2)
- the upper and lower seismogenic depths needed to limit the extension of the rupture plane (see Table 13)
- the distance interval used to discretize the area source model into a finite grid of sources (10km spacing)

Table 13. Lower and upper seismogenic depths adopted to constrain the rupture extension in the different source depth layers.

Depth layer	Lower seismogenic depth (LSG)	Upper seismogenic depth (USG)
Shallow depth sources	0km	65km
Intermediate depth sources	35km	200km
Deep sources	150km	350km

8.5 Smoothed seismicity model

Earthquake hazard computed using homogenous source zones assumes that the probability of occurrence is spatially uniform across each homogenous area. This assumption is particularly beneficial in regions of short and/or incomplete earthquake log, as it accounts for earthquakes occurring in potential locations not yet represented in the catalogue. The approach, however, may not be appropriate for regions where seismicity is known to be well localized along main tectonic structures and specific crustal domains. This is the case of the study region, particularly along the southern active collision margin, where the analysis earthquake catalogue confirms the existence of non-uniform spatial patterns of seismicity closely related to the development of specific seismotectonic features (e.g., thrusts). For example, the associated smearing effect might produce underestimation of the computed hazard at some locations close to the localized seismicity and overestimate the hazard at other locations farther from the localized seismicity. To overcome this limitation, the smoothed seismicity approach was introduced (e.g., Frankel, 1995), where computed occurrence rates are spatially reorganized to follow the observed earthquake pattern.

In this study, we use a variant of the smoothing procedure proposed by Poggi et al. (2020), which has the significant advantage of preserving the overall rate balance of each discrete zone. The level of smearing of the rates is controlled by smoothing length parameter (λ), which reflects the belief in the actual observed seismicity pattern. The larger is λ, the more uniform will be the occurrence rate pattern, ideally converging to the uniform zonation. Conversely, small value of λ will closely replicate the observed seismicity pattern.

Definition of an optimal smoothing length is however difficult, and a level of expert judgment is required. Being λ a loosely constrained parameter in the model and therefore contributing to its epistemic variability, different alternate values (a central value and two edge cases) were used in a logic-tree approach, with assigned triangular weight. Moreover, to avoid typical "bull eye" smearing effects on zones with too few observed events (e.g., the cratonic shield of Kazakhstan), a different combination of smoothing lengths was used for regions of high and low seismic productivity. High λ values were also used for the deep seismicity zones, where uncertainty on the location is high. See Table 14 for the smoothing length value combination associated to each group. Result of the smoothing procedure applied separately to the shallow, intermediate, and deep seismicity layers is presented in Figure 16, Figure 17 and Figure 18, respectively.

Table 14. Combination of smoothing length (λ) parameter adopted for regions of low and high seismicity of the Central Asia model, and associated weights.

	Smoothing length (λ)	Weight	Apply to region
Low seismicity zones + Deep sources	25	0.25	B, E, H, K, L
	50	0.50	
	100	0.25	
High seismicity zones	10	0.25	A, C, D, F, G
	20	0.50	
	40	0.25	

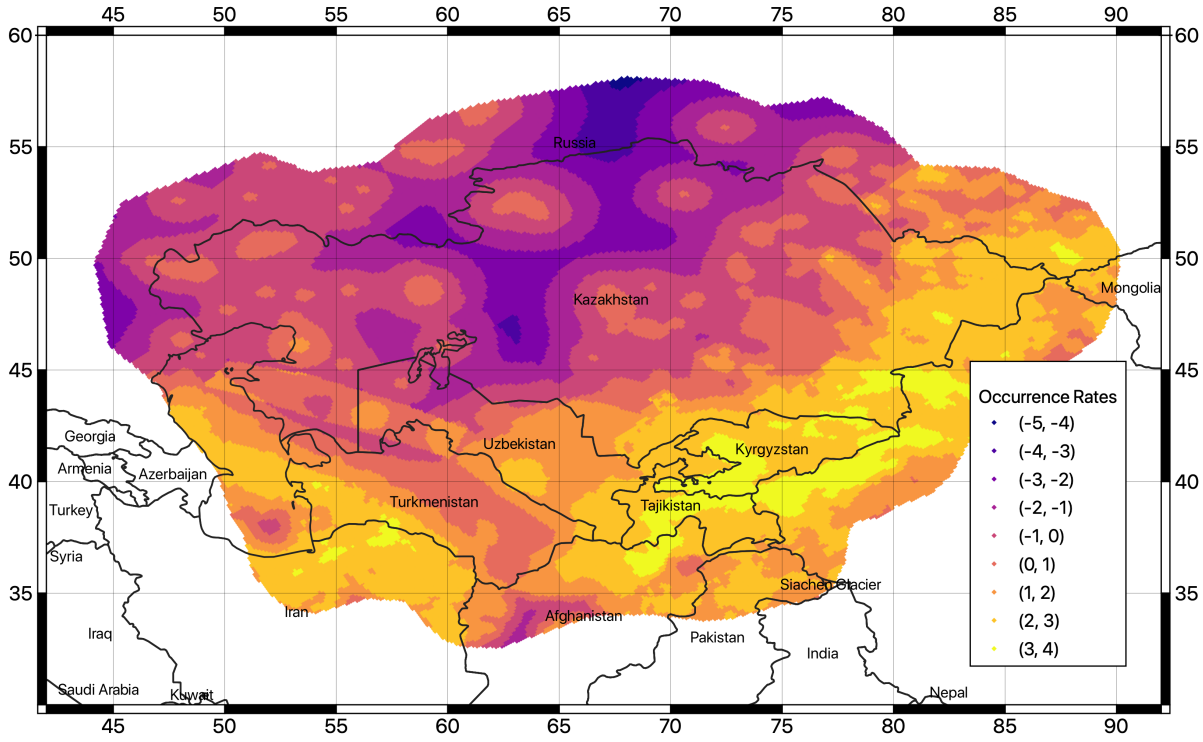

Figure 16. Spatially variable occurrence rates using the smoothing approach to the shallow-depth source layer. Presented rates are from a weighted average of the three smoothing length values in Table 14. Units are expressed as the logarithm of the annual occurrence rate (per grid cell) of events larger than zero.

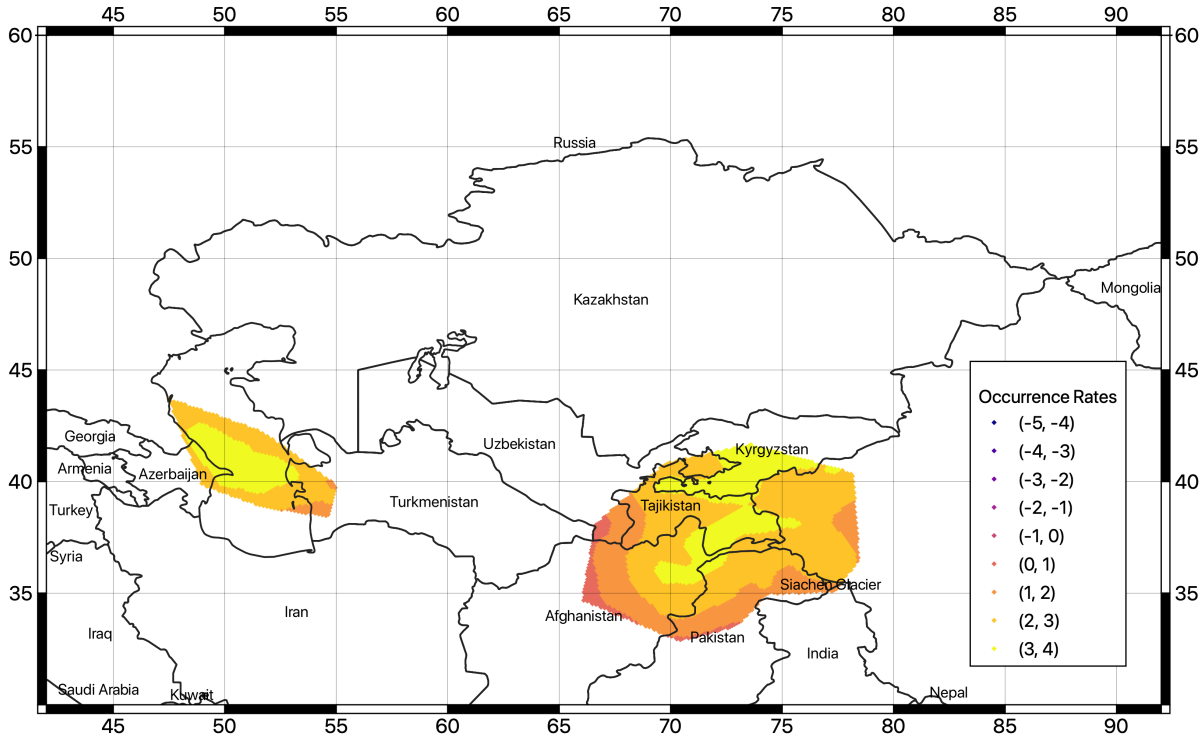

Figure 17. Spatially variable occurrence rates using the smoothing approach to the intermediate-depth source layer. Presented rates are from a weighted average of the three smoothing length values in Table 14. Units are expressed as the logarithm of the annual occurrence rate (per grid cell) of events larger than zero.

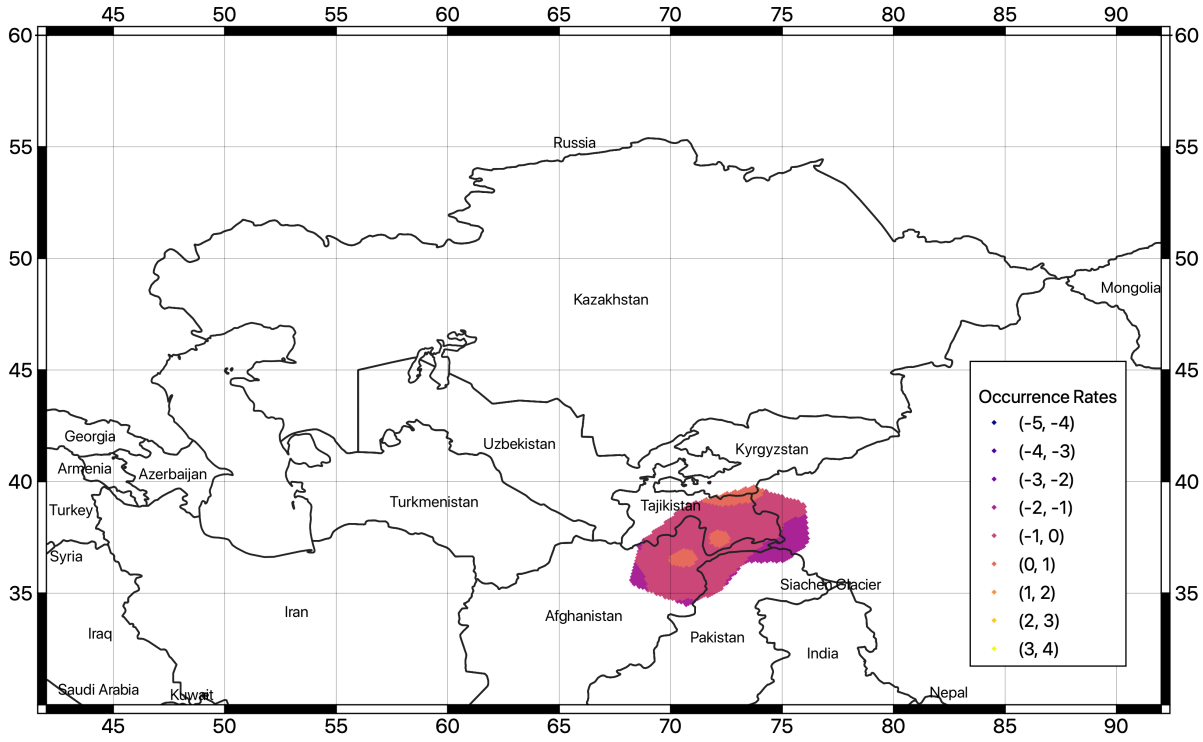

Figure 18. Spatially variable occurrence rates using the smoothing approach to the deep source layer. Presented rates are from a weighted average of the three smoothing length values in Table 14. Units are expressed as the logarithm of the annual occurrence rate (per grid cell) of events larger than zero.

9 Finite fault model

The use of standard distributed seismicity models has the advantage of integrating a wide set of possible earthquake scenarios in the calculation. Nonetheless, peculiarities of specific sources might be lost, which is particularly inconvenient when the near-field ground motion level is target. To partially overcome this limitation, a valid alternative is to include finite (3d) fault sources in the source model. However, this is only possible if enough information (fault geometry, kinematic parameters, displacement rates) is available for the investigated area with sufficient reliability (e.g., clear surface expression, known segmentation, well documented sign of quaternary activity or direct seismicity evidence, etc.), which is often not the case for all lineaments.

Starting from a regional dataset of potentially active faults, which incorporates information from geological studies, scientific literature and local databases, the fault source model is then built assuming an occurrence model and appropriate seismicity parameters (e.g., scaling relations, aseismic coefficient and seismogenic depths) using an ad-hoc Python tool developed within the *Model Building Toolkit* of GEM (https://github.com/GEMScienceTools/oq-mbtk).

9.1 Modelling strategy

Finite fault sources can be modelled in OpenQuake in different ways, depending on how accurate the fault representation is. In this study we use the "simple fault" approximation (see "OpenQuake

technical manual" for more details on the modeling), where the fault geometry is approximated by translating the fault trace from the Earth's surface to the lower seismogenic depth with an inclination equal to the dip angle (Figure 19, Pagani et al. 2014).

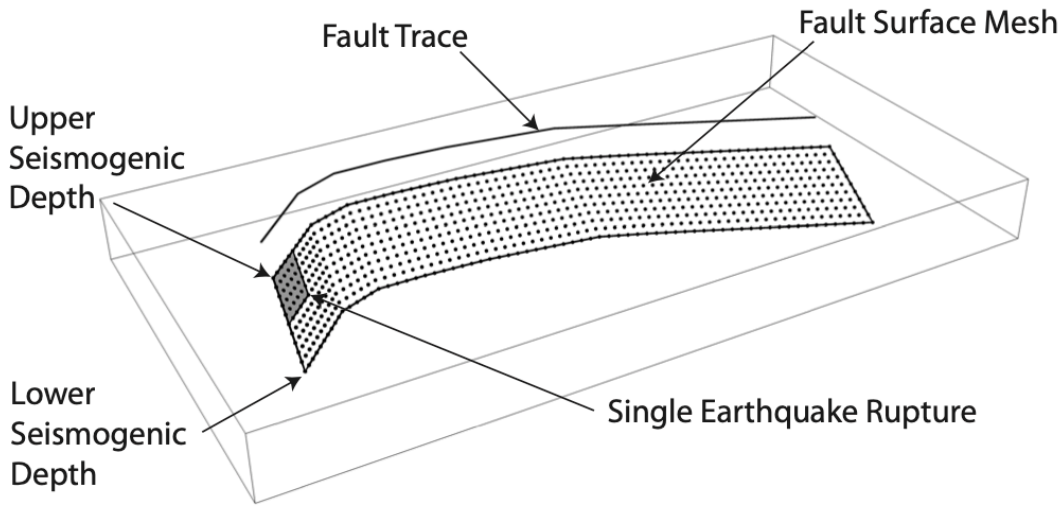

Figure 19. Simple Fault source in the OpenQuake engine (modified from "the OpenQuake-engine book: underlying hazard science").

As no clear evidence of "characteristic" model behavior is present, we use a simple double-truncated Gutenberg-Richter distribution to model earthquake occurrences on faults, in agreement with the occurrence model adopted for the distributed seismicity counterpart. Occurrence rates (a-values) of each fault are derived directly from slip rate estimates, by balancing the scalar seismic moment accumulation rate and the scalar moment release rate from the integral of the incremental MFD through a direct fitting procedure (Poggi et al. 2020). In this process we assume a default shear modulus of 30 GPa and an aseismic coefficient of 0.1 to account for accumulated seismic moment released aseismically by creep and plastic deformation. The b-value and maximum generated magnitude are imposed a priori as derived from seismicity analysis of the source zone enveloping the fault. However, if the fault has limited extension, the maximum magnitude is scaled accordingly by applying the Leonard (2014) scaling relation to avoid unrealistic large magnitudes. For the full list of modeling parameters and assumed values see Table 15.

Table 15. Summary of the essential parameters and the corresponding values used for the definition of a fault source model in Central Asia.

Parameter	Value
Fault trace	Taken from fault database (in geojson format)
Upper seismogenic depth (USD)	0 (surface rupture)

Lower seismogenic depth (LSD)	Defined by applying Leonard (2014), with the additional constraint of not exceeding the maximum seismogenic depth of the source group
Dip angle	Extrapolated from geometry description of the fault database (following the Aki-Richards convention, Aki and Richards, 1980)
Rake angle	Extrapolated from geometry description of the fault database (following the Aki-Richards convention, Aki and Richards, 1980)
Magnitude frequency distribution (MFD)	Double-truncated Gutenberg-Richter (GR) distribution, with lower-bound magnitude fixed to M6.0 and upper-bound magnitude defined by applying Leonard (2014), with the additional constraint of not exceeding the maximum magnitude of the source group
Magnitude-area scaling relationship	Leonard (2014)
Rupture aspect ratio (length/width)	Fixed to 2.0
Aseismic coefficient	Fixed to 0.1

9.2 Input fault datasets

At regional level, the most significant existing compilations are the GEM Global Active Fault Database (GEM GAF-DB, Styron and Pagani, 2020) and the Active Fault Database of Eurasia (hereinafter AFEAD, Bachmanov et al., 2017), which review and summarize most of the information available from published scientific studies for the target area.

In particular, the AFEAD database presently includes more than 20 thousand lineaments (faults, fault zones and associated structural forms) showing the signs of latest displacements in the late Pleistocene and Holocene. For each mapped fault, the database reports morphological and kinematic information, with quality indicators (four reliability classes A to D, from the most to the least reliable) and, where possible, an evaluation of the displacement rates (three ranks of late Quaternary movements). Conversely, only a limited set of faults from GEM GAF database have record sufficiently complete to be used for the creation of fault source models (e.g., because of missing slip rate estimates). By direct comparison, those faults are also represented in the AFEAD database, sharing most of the original source of information. For this reason, although the AFEAD database have shown some local discrepancies that require some attention (e.g., in fault segmentation), at present stage it represents the primary base of information for the creation of the finite fault source model for this study.

The database has also been exported in an open format compatible with GEM GAF (geojson, format, see following section) to facilitate the integration of any additional information eventually available from new local studies. Such compilation will be made openly accessible to promote further development on the area.

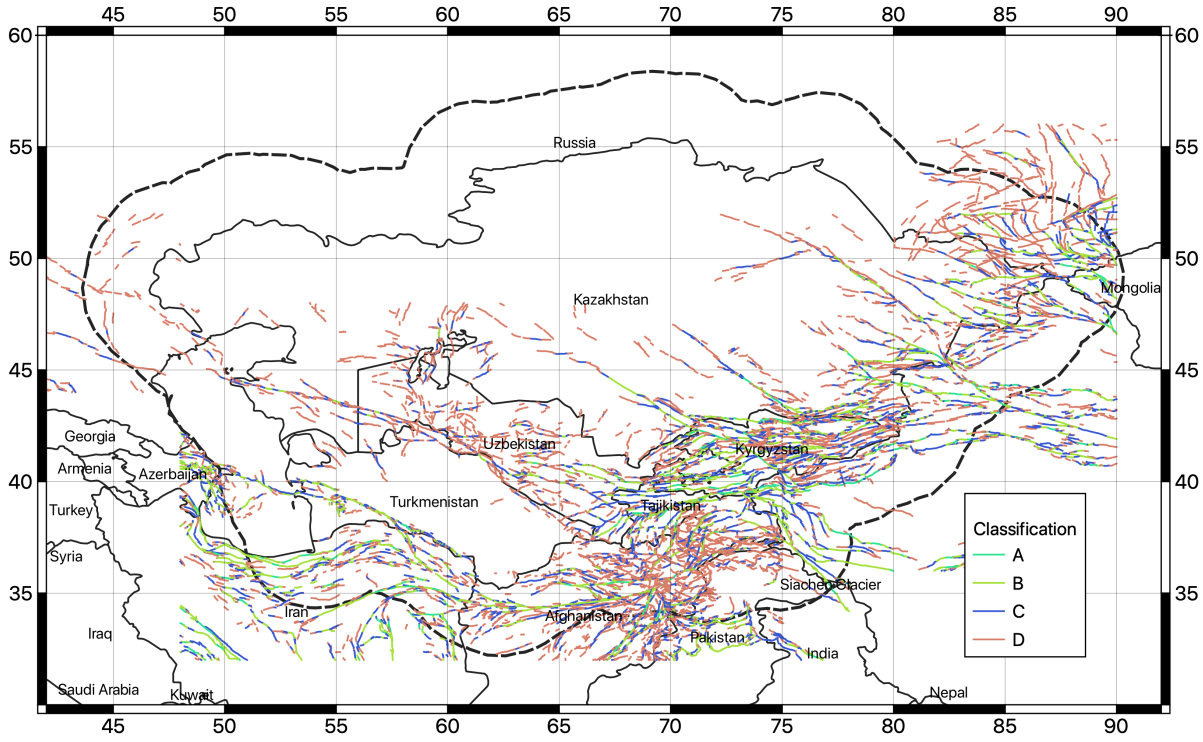

Figure 20. Traces of the faults available from the database of Active Fault for Eurasia and adjacent regions (AFEAD)

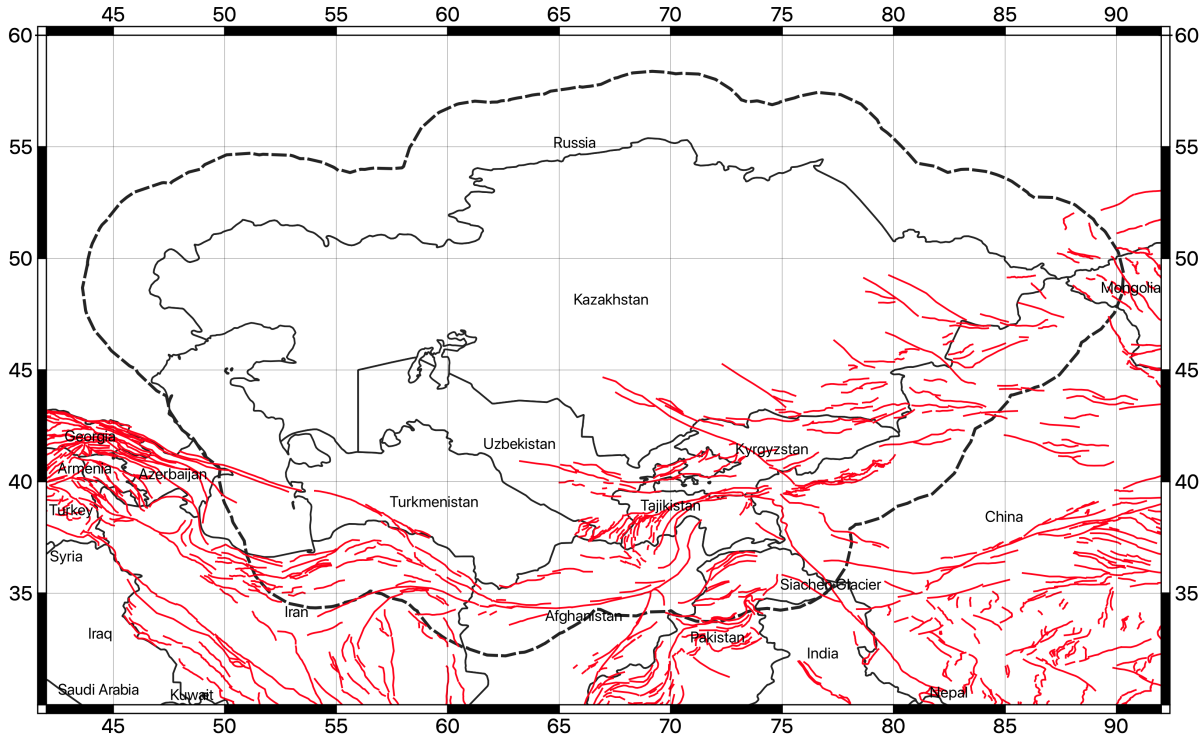

Figure 21. Traces of the faults available from the global active fault database of GEM (GEM GAF-DB).

9.3 Database conversion and selection

For the creation of the fault source model, the AFEAD database has been first converted into an intermediate format compatible with the GEM Global Active Fault Database. Such format is principally required for the creation of the OpenQuake source model using the Model Building Toolkit of GEM. However, being in plain text geojson format, it has the additional advantage of being of simple maintenance and extension using common versioning control tools (e.g., git) and GIS software (e.g., QGIS). The translation of the original AFEAD database into GEM format required a level of interpretation, as not all parameters have direct mapping. Moreover, only a subset of the GEM parameters is used (see https://github.com/GEMScienceTools/gem-global-active-faults for a description of the GEM GAF format).

Parameter conversion rules are described in Table 16. Note that all parameters not explicitly expressed in the conversion table have been discarded from the compilation. In addition, faults with missing required parametrization (e.g., unknown value for SIDE parameter) were not included and, thus, are not presently converted into the source model.

Table 16. Parameter conversion rules used to migrate the AFEAD database into the GEM GAF format.

GEM parameter	AFEAD parameter	Conversion convention
name	NAME	Same
slip_type	SENS1	D=Dextral, S=Sinistral, T=Thrust, R=Reverse, N=Normal
average_dip	SENS1	D=90°, S=90°, T=30° R=40°, N=60°
average_rake	SENS1	D=180°, S=0°, T=90° R=90°, N=-90°
dip_dir	SIDE	Same
net_slip_rate	RATE	3=(0.05, 0.1, 0.2), 2=(0.25, 0.5, 1.0), 1=(0.5, 1.0, 2.0) Values are (min, mean, max) slip rates in cm/y
reference	AUTH	Same
notes	TEXT	Same
--	CONF	Only quality class A and B have been considered

The most sensitive parameter of the conversion process is the net slip rate. The AFEAD database provides an approximate and rather broad range of slip rates for each RATE class (1,2,3), which we have converted into numerical values (in cm/y) by comparison with the slip rates reported from the GEM GAF database and from scientific literature. To account for the unavoidable uncertainty associated with the conversion, however, three alternative rate conversion models were implemented, including a mean estimate, an upper and a lower bound.

Only faults with reliability class A and B (independent signs of activity are available, in term of kinematics and clear evidence of strong earthquakes) have been explicitly considered, while class C and D have been rejected due to their unclear, incomplete, or inaccurate interpretation. Such

conservative choice might be relaxed in future analysis as soon as additional information becomes available for the lineaments in class C and D.

9.4 The fault source model

The fault source model presently contains 1444 individual fault segments (Figure 22), covering the most part of the active shallow crust presently interested by active seismicity.

Nonetheless, it must be stressed that the fault source model alone might not be sufficiently complete to fully represent the whole shallow seismicity, particularly at low magnitudes and large depths and, thus, it cannot be used as alternative to the distributed seismicity model. Therefore, to complement possible missing events, background source layers have been added to the fault model during calculation. The background model is taken from the homogenous zonation model (for shallow, intermediate, and deep sources), but limiting the maximum generated magnitude of the shallow zones to 6, under the assumption that ruptures above this threshold should have clear surface expression, and thus should be sufficiently represented in the fault database. Intermediate and deep sources remain unmodified.

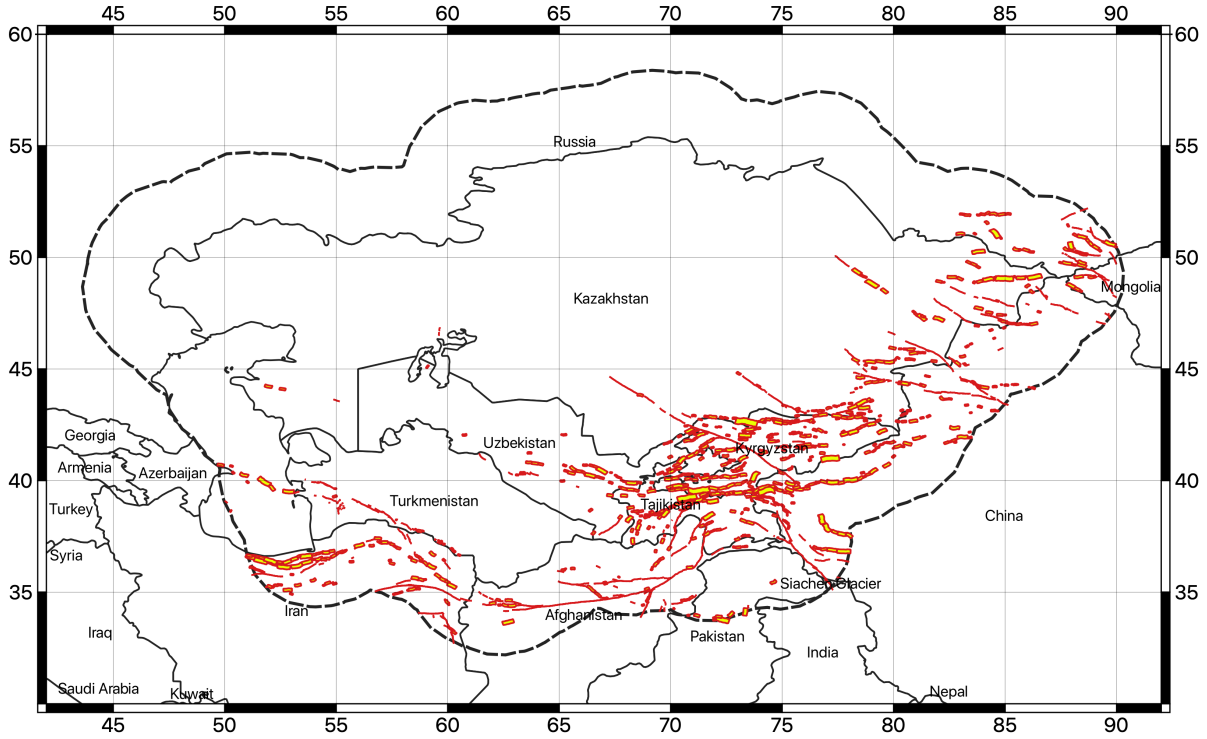

Figure 22. 3D geometry of the faults in the final source model. Surface traces are shown in red, while the surface projection of the fault plane is in yellow.

10 Ground motion model

The calibration of the ground motion prediction model represents an important issue in the development of the hazard analysis. Although few studies have been performed for the area, there is a general lack of usable models for the prediction of a complete set of the target response spectral accelerations. To overcome this limitation, a set of external ground motion prediction equations (GMPE) must be used.

Selection of best performing GMPEs should be preferentially performed by direct comparison against local earthquake recordings in a range of magnitude and distance that are meaningful for the analysis. If no or too few empirical earthquake observations are available, however, indirect selection criteria should be used, such as those described in Cotton et al. (2006). The criteria include:

- analysis of the performance of the ground motion model
- characteristics of the calibration dataset (type, quality, and coverage range of the data).
- compatibility of target tectonic setting with that of the model
- suitability of the functional form (availability of the information required for the predictor variables, consistency of the output with respect to hazard assessment requirements).

10.1 Regionalization

To account for the variability of the tectonic environments across the region, which is responsible for the different attenuation of the ground motion from source to site, a strategy for ground motion modelling regionalization was used. In a first step, sub regions of supposedly homogeneous attenuation behavior have been identified. For that, we rely on the classification proposed by Chen et al. (2018), which combines the analysis of seismological (seismic moment rates, attenuation of 1Hz Lg coda), geological (plate boundary models, digital geological mapping) and geophysical (crustal Vs velocities) data from worldwide datasets.

According to the classification, three seismotectonic domains are represented in Central Asia: the active shallow crust, the non-cratonic active stable crust and the cratonic stable continental crust (Figure 23). Based on that, with some adjustment due to local considerations, the different zones of the shallow seismicity source models have been classified accordingly into three main tectonic region types (TRT, see Figure 24):

- TRT 1 – Standard active shallow crust
- TRT 2 – Active stable crust
- TRT 3 – Cratonic crust

An additional fourth region (TRT4) was then added to represent the intermediate to large depth source zones. As a final step, one or more ground motion prediction models are selected for each TRT.

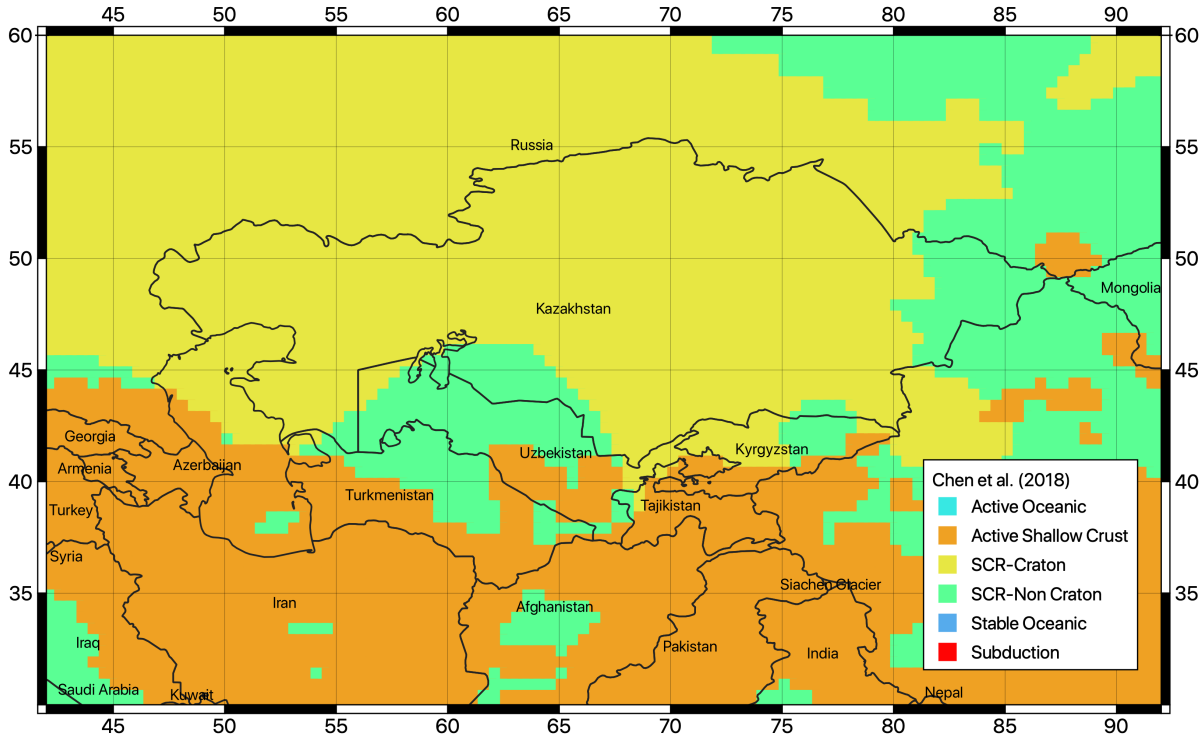

Figure 23. Tectonic classification proposed by Chen et al. (2018) used to guide the regionalization of the ground motion prediction model for Central Asia.

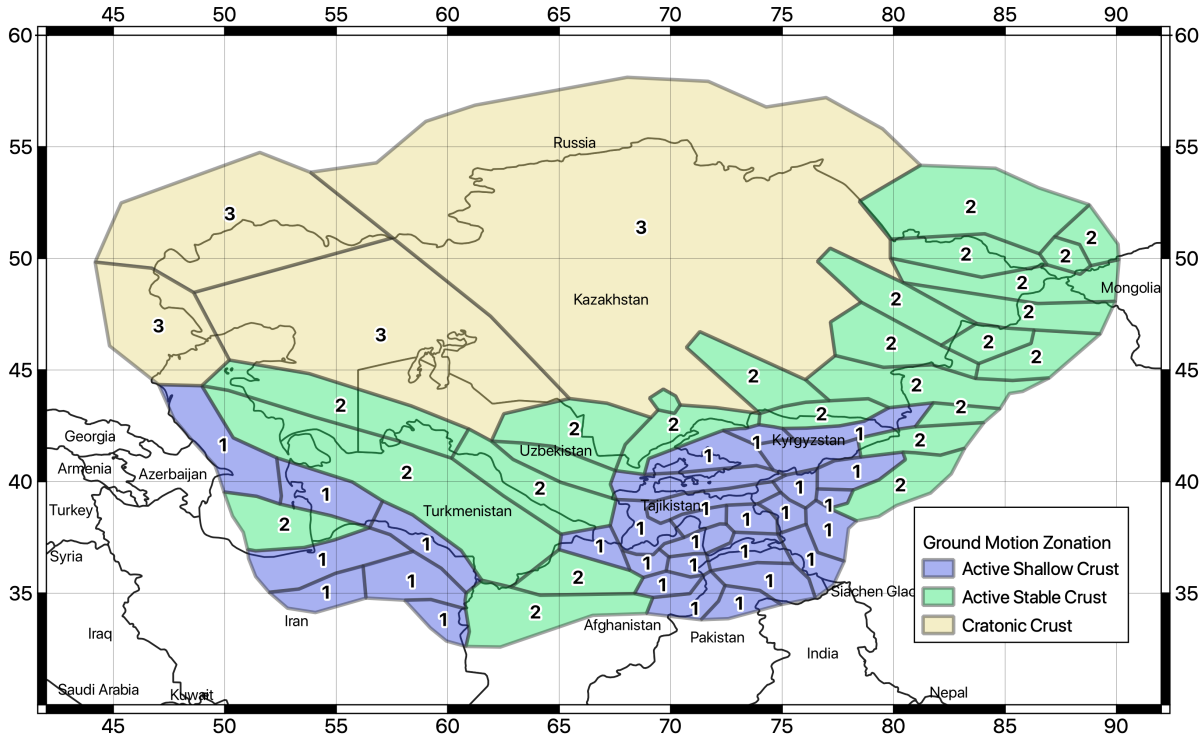

Figure 24. Tectonic region type (TRT) classification of the source zones of the Central Asia model.

10.2 GMPE selection

In a first step, ground motion models compatible with the identified TRT have been isolated from the ground motion model library of OpenQuake (the HazardLib). Following the selection criteria recommended by Cotton et al. (2006) and the studies recommended by the local experts of the consortium, the number of suitable models was restricted to the five most representative for the study region. The selected GMPEs and their corresponding relative weights are then summarized in Table 17. The performance of each ground motion model has been analyzed for a combination of magnitudes and distances, and for the different intensity measure types required for the study (see the Trellis plots in Figure 25).

It must be noted that ground motion models are defined for standard active shallow crust (AS), stable crust (SC) and deep seismicity (DS). Assuming that the SC models are compatible with purely stable cratonic crust (TRT3), we decided to represent the stable continental crust type (TRT2) as a combination of AS and SC model, as an intermediate attenuation behavior is expected. The relative weighting scheme for each tectonic group is presented in Table 18.

Table 17. Selected ground motion prediction models grouped by tectonic region applicability.

Tectonic Id	Ground Motion Model	Weight
AS	Campbell and Bozorgnia (2014)	0.5
	Chiou and Youngs (2014)	0.5
SC	Pezeshk et Al. (2011)	0.5
	Atkinson and Boore (2006) – Modified 2011	0.5
DS	Parker et Al. (2020) – for subduction interface	1

Table 18. Weight combination of the GMPE groups (Table 17) with respect to tectonic zonation of the Central Asia model.

	AS	SC	DS
TRT 1	1	0	0
TRT 2	0.5	0.5	0
TRT 3	0	1	0
TRT 4	0	0	1

The main advantage of such a two-step weighting procedure (for grounds motion models and tectonic groups) is that it yields smooth and regionally variable ground motion predictions, thus avoiding sharp variations between neighboring tectonic environments. Moreover, additional and/or different ground motion models or intermediate weighting (e.g., between AS and DS in TRT4) can be easily included by preserving the developed rationale for tectonic regionalization.

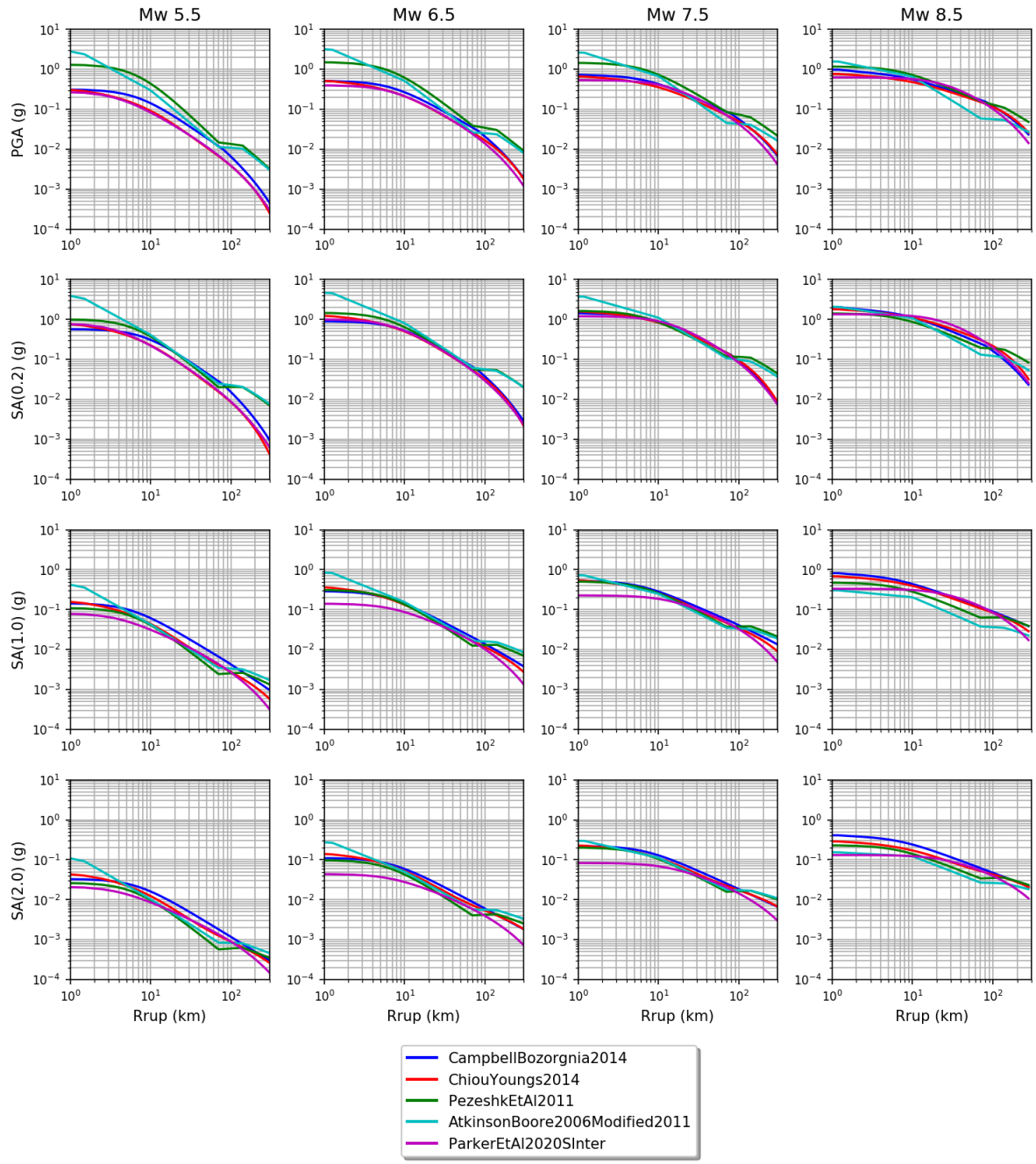

Figure 25. Comparison of ground motion distance attenuation for the view selected prediction models for different magnitudes (columns) and intensity measure types (rows). The typical ground motion deflection due Moho interface refraction is clearly visible at around 100km in the SC crust models.

10.3 Strong motion recordings

To validate the selection of ground motion models, a set of strong motion recordings from the ACROSS Central Asia Strong Motion Network has been analyzed. The ACROSS network (Parolai et al., 2017), which was developed and is currently maintained by *Helmholtz GeoForschungsZentrum* (GFZ, Potsdam) in cooperation with the Central Asian Institute for Applied Geosciences (CAIAG),

consists of 18 three-channel accelerometric stations deployed in Kyrgyzstan (Figure 26) and operating since 2005. Waveforms are publicly available through an EIDA node made available by the GEOFON program of the GFZ (https://geofon.gfz-potsdam.de; last access 18 August 2021), accessed using the FDSN service utilities of the ObsPy Python library (Beyreuther et al., 2010).

Of 708 identified regional events with magnitude larger than 5, 35 events (5<Mw<6.6) were recorded from the network within 300 km from the stations, for a total of 153 three-components waveforms. Each waveform consists of a 540s recording centered around the S-wave arrival (180s before and 360s after phase arrival) computed from the reported origin time of the event assuming a homogenous S-wave crustal model of 3.4km/s (see Figure 27 for an example event recorded at 6 stations). Each recording was corrected for instrumental response previous band-pass filtering in the range 0.02-45Hz.

Although the number of waveform recordings in a significant magnitude-distance range is not sufficient to perform objective GMPE ranking, the visual comparison with the predicted ground motion suggests that the selected models are reasonable in the intermediate to large distance range (see Figure 28 for an example at PGA) where data are available.

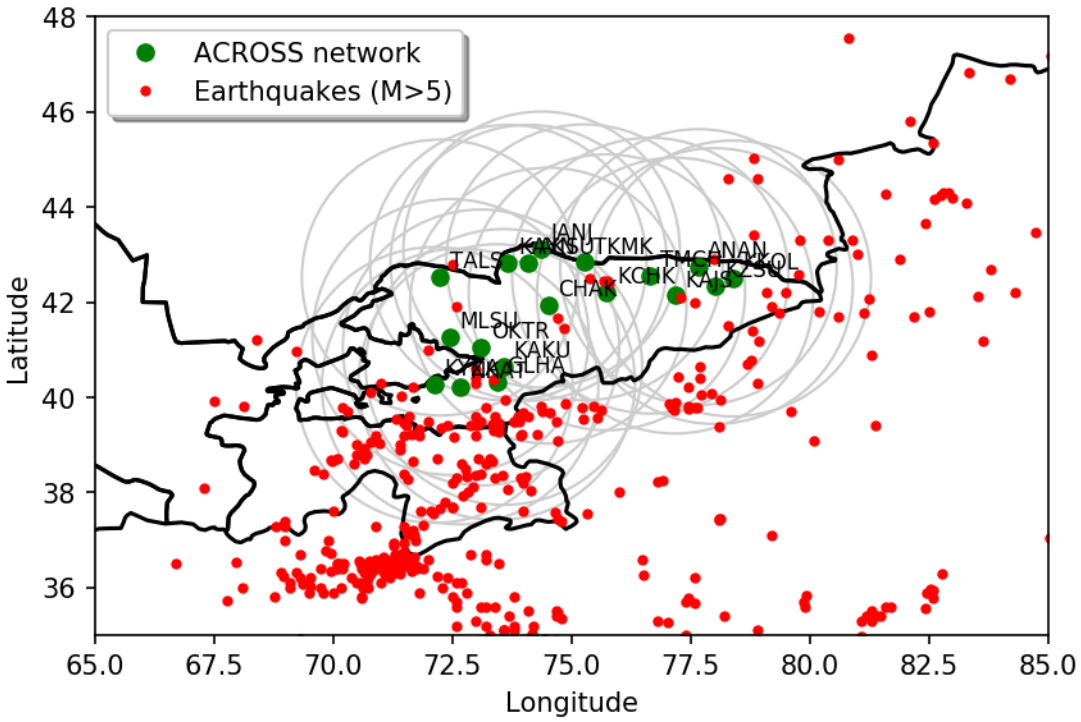

Figure 26. Distribution of accelerometric stations of the ACROSS network (in green) and of the surrounding earthquake events with Mw larger than 5.0. Gray circles represent the selection distance limit of 300 km from each station.

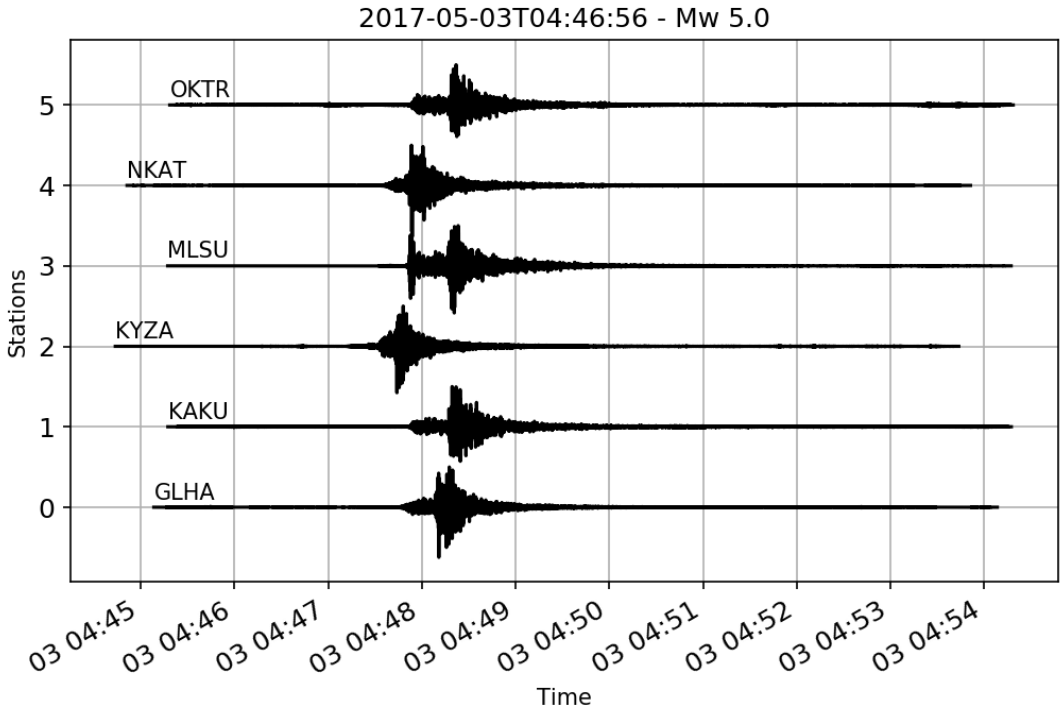

Figure 27. Example of strong motion waveforms (E-W components) from six stations of the ACROSS accelerometric network. Amplitudes are normalized to PGA for visualization purposes.

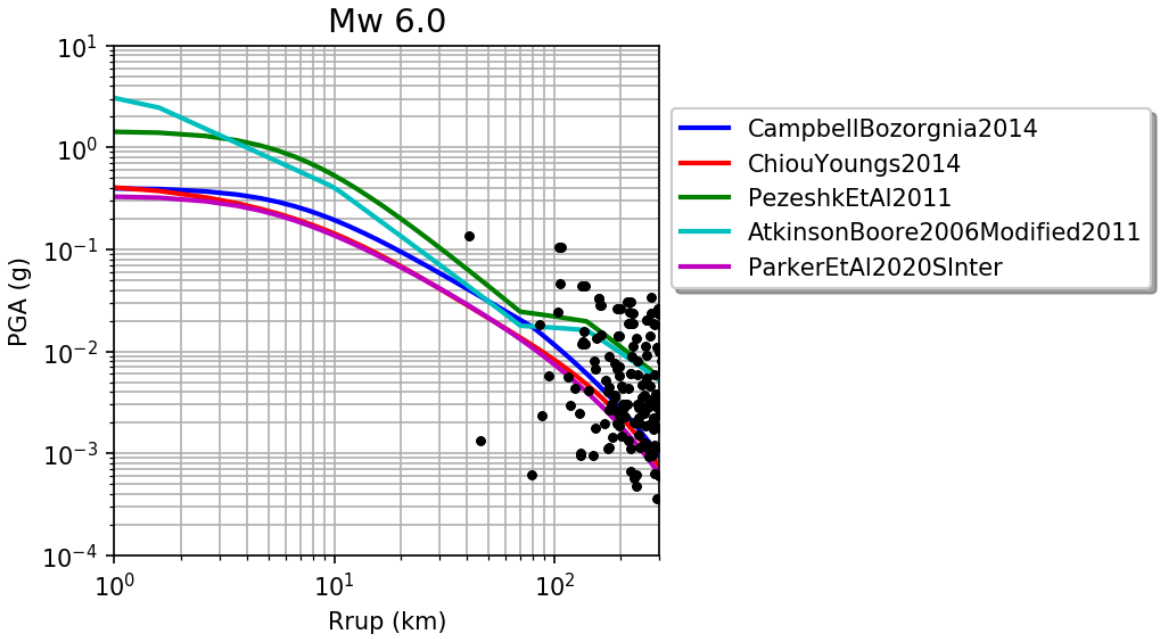

Figure 28. Example of comparison between observed peak ground acceleration from the 152 recordings of the ACROSS network and predicted value from the five selected ground motion prediction models.

11 Epistemic uncertainty and logic-tree

To account for epistemic variability of key model parameters, a logic-tree approach was used (Figure 29). From the technical point of view, the implemented logic-tree is split between the two main components of the model: source characterization and ground motion modeling characterization. Each component includes different branching levels, representing either an independent uncertainty type (as for the case of b-value and Mmax) or the permutation of alternate models applied in different regions (as for the case of GMPE regionalization).

The source model part of the logic tree includes both the developed distributed (smooth) seismicity model and the faults+background model, as independent branches. Equal weighting was used for the two. The main uncertainty associated with the fault model is about the definition of the slip rate conversion from rate classes (see section on fault model setup for details). Therefore, to represent the associated uncertainty, three alternative occurrence models were included. The model providing the middle estimate, considered the most reliable, has the largest weight (0.6) while the other two edge models have a lower one (0.2). Similarly, three independent distributed seismicity models were implemented using different smoothing length, which is presently still a highly subjective parameter. To decrease the complexity of the OpenQuake calculation, however, the alternate distributed models with different parametrization have been collapsed into a single weighted-average occurrence rate model, using weights as indicated in the logic-tree table. Therefore, smoothing length variability is not directly represented by independent branches, although formally accounted in the source model formulation. This simplification should be considered when the variability of hazard calculation (e.g., quantiles hazard curves) is to be examined.

The ground motion logic tree is composed of four branching levels, each representing a particular combination of ground motion prediction model groups (SA, SC and DS) applied to the different regions (TRT, see section on ground motion regionalization for details). It must be stressed that such a grouping approach, although it might appear complex at the first glance, allows a greater flexibility in the definition of regions with intermediate attenuation behavior, as heterogenous combination of different tectonic groups is allowed (see Figure 29).

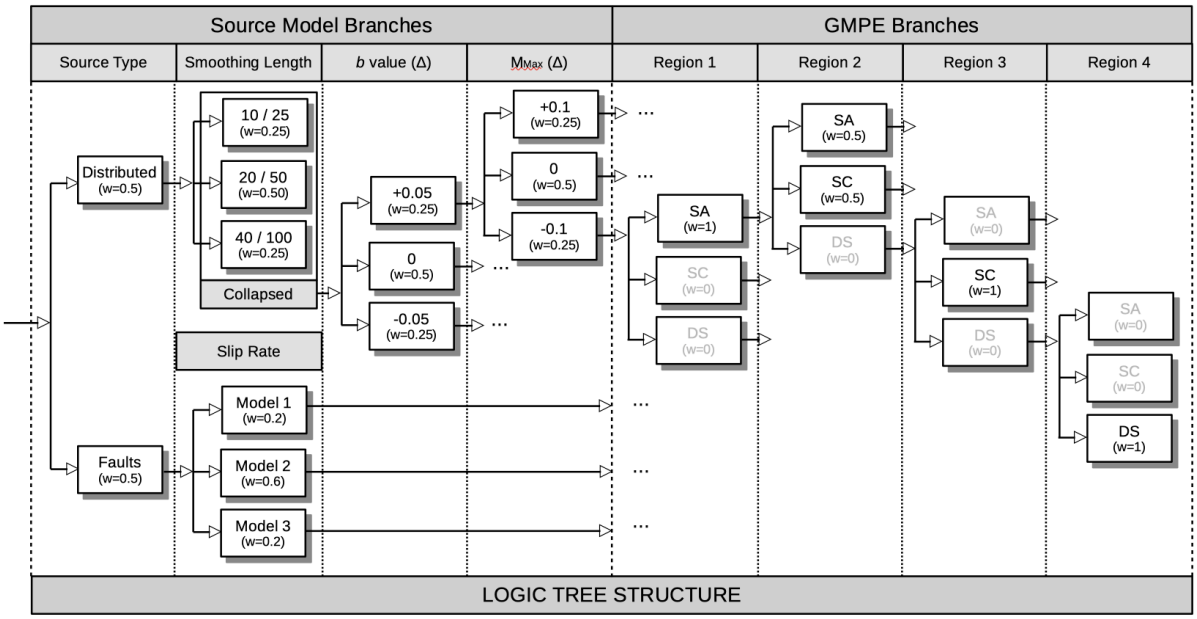

Figure 29. Diagram representation of the logic-tree structure of the Central Asia hazard model, which includes 4 branching levels to account for both the source model and ground motion model uncertainties.

12 PSHA Results

All calculations for this study were performed using Version 3.11 of the OpenQuake engine, which can be accessed at https://github.com/gem/oq-engine/tree/engine-3.11 (last access 16/08/2021).

The investigated area consists of a mesh of 8028 sites on a regular grid spaced at 0.2 degrees (approximately 20 km). For each site of the mesh, free rock conditions are assumed, with a fixed 30-metre averaged shear-wave velocity (Vs30) reference value of 800 m/s, corresponding to class A (standard rock) in Eurocode8 (CEN 2004) and NERHP (BSSC 2003) classification.

12.1 Hazard curves and derived products

Ground motion probability of exceedance (PoEs) for a given observation time are computed for PGA and for 5%-damped response spectral acceleration at 0.1s, 0.2s, 0.5s, 1s, 2s and 3s (vibration periods allowed by the selected ground motion models). As often done, ground motion integration has been truncated at 3 sigma of the prediction. Output of the calculation are a) mean and quantile (0.05, 0.15, 0.5, 0.85 and 0.95) hazard curves at each intensity measure type (Imt) and site (see Figure 30 and Figure 31 for example results computed at six sites selected as target for subsequent disaggregation analysis), b) Uniform Hazard Spectra (UHS, Figure 32) and c) hazard maps computed for return periods of 25, 50, 100, 250, 475, 500 and 1000 years, corresponding respectively to 86, 63, 39, 18, 10, 9 and 5% probability of exceedance in 50 years observation time. The calculations were carried out assuming a Poisson earthquake occurrence model. See Figure 33, Figure 34, Figure 35 and Figure 36 for example maps at PGA and selected return periods. It must be noted that shorter return periods could not be computed due to numerical limitations when approaching 100% PoE.

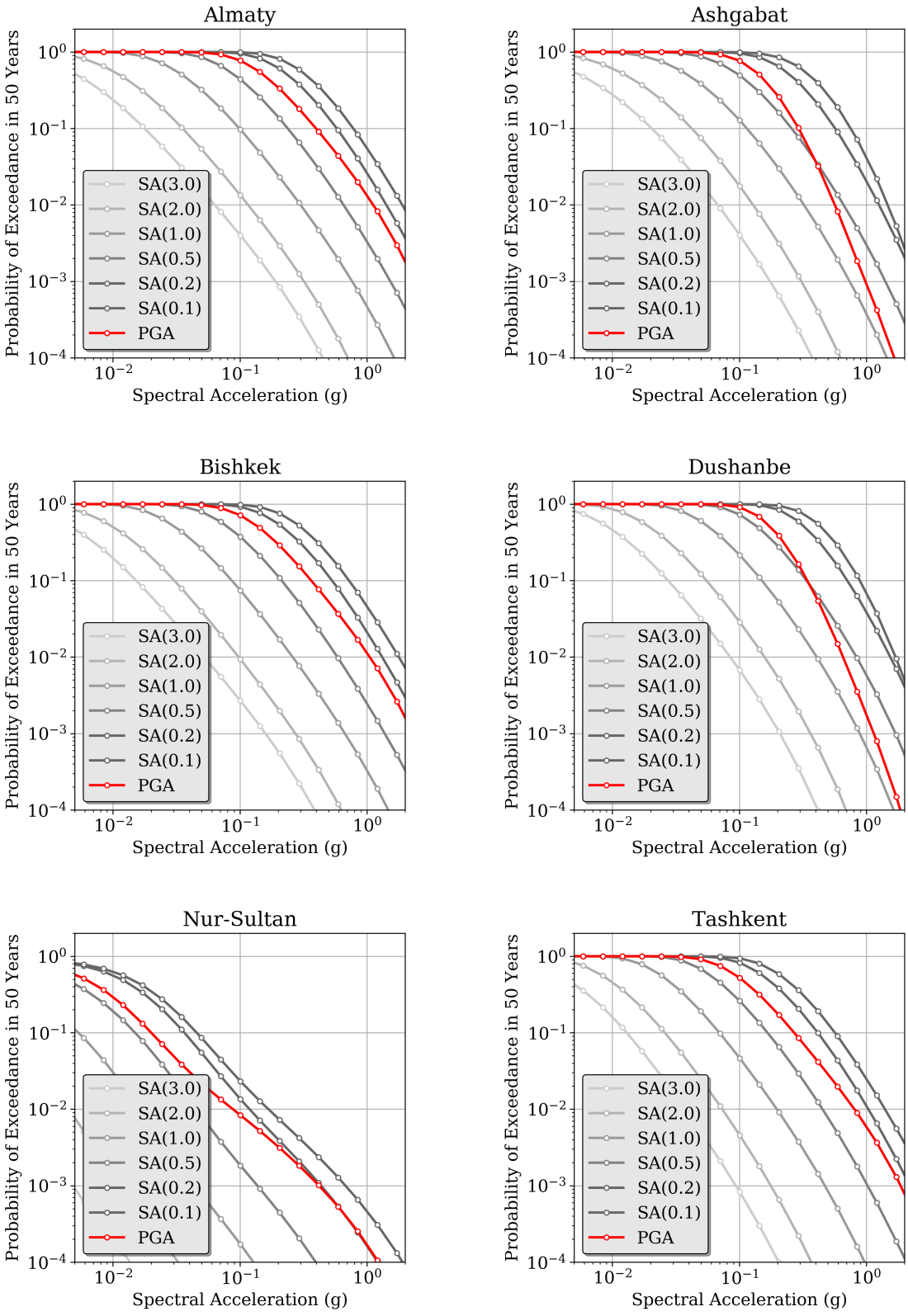

Figure 30. Example of mean hazard curves computed at six selected target sites (all country capitals plus Almaty, Kazakhstan. Note that Nur-Sultan was formerly known as Astana) for different intensity measure types (PGA and spectral accelerations for periods increasing from 0.2 s to 3 s) with 10% probability of exceedance in 50 years.

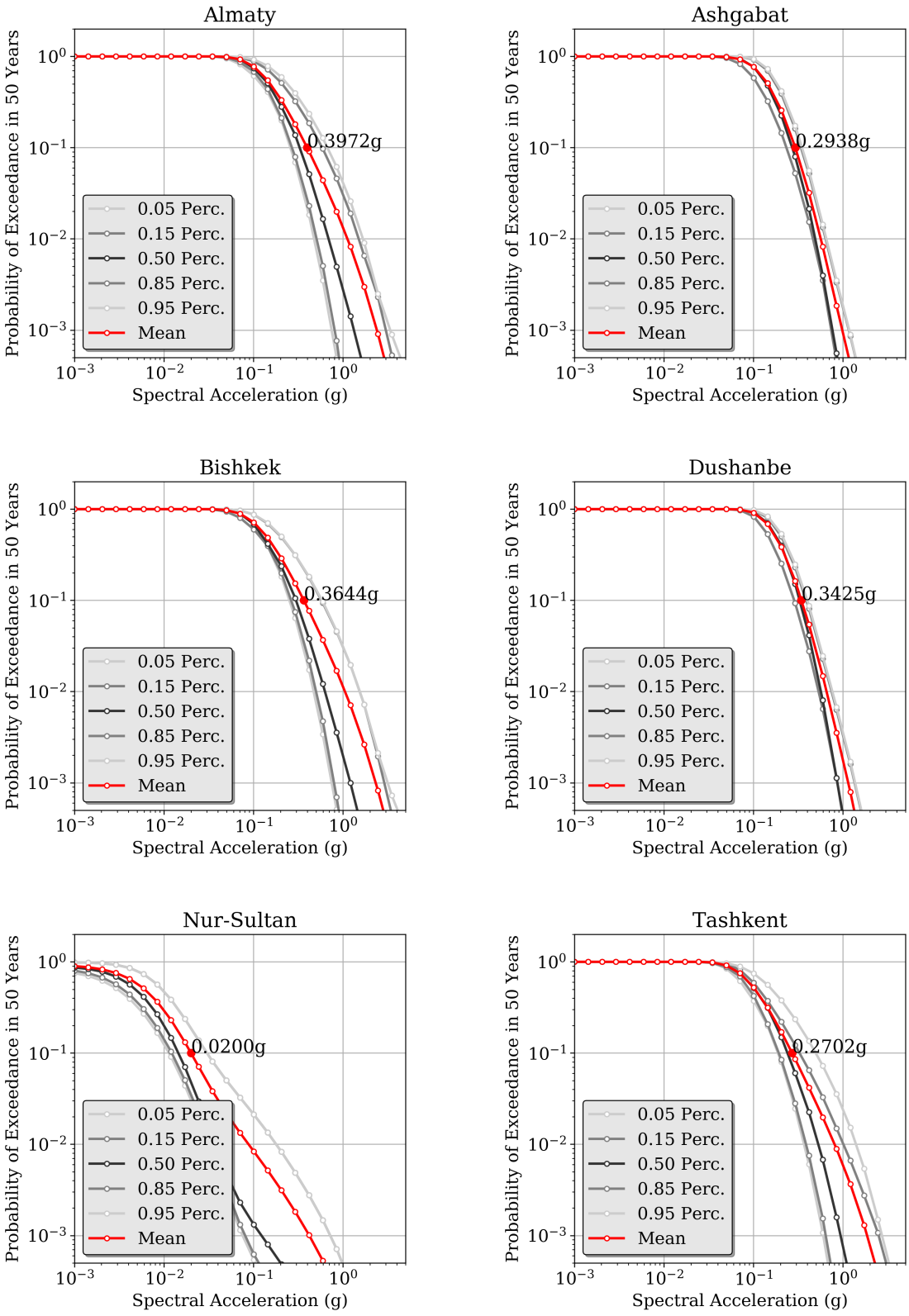

Figure 31. Example of mean hazard curve statistic (mean and quantiles) computed at six selected target sites (all country capitals plus Almaty, Kazakhstan) for PGA with 10% probability of exceedance in 50 years.

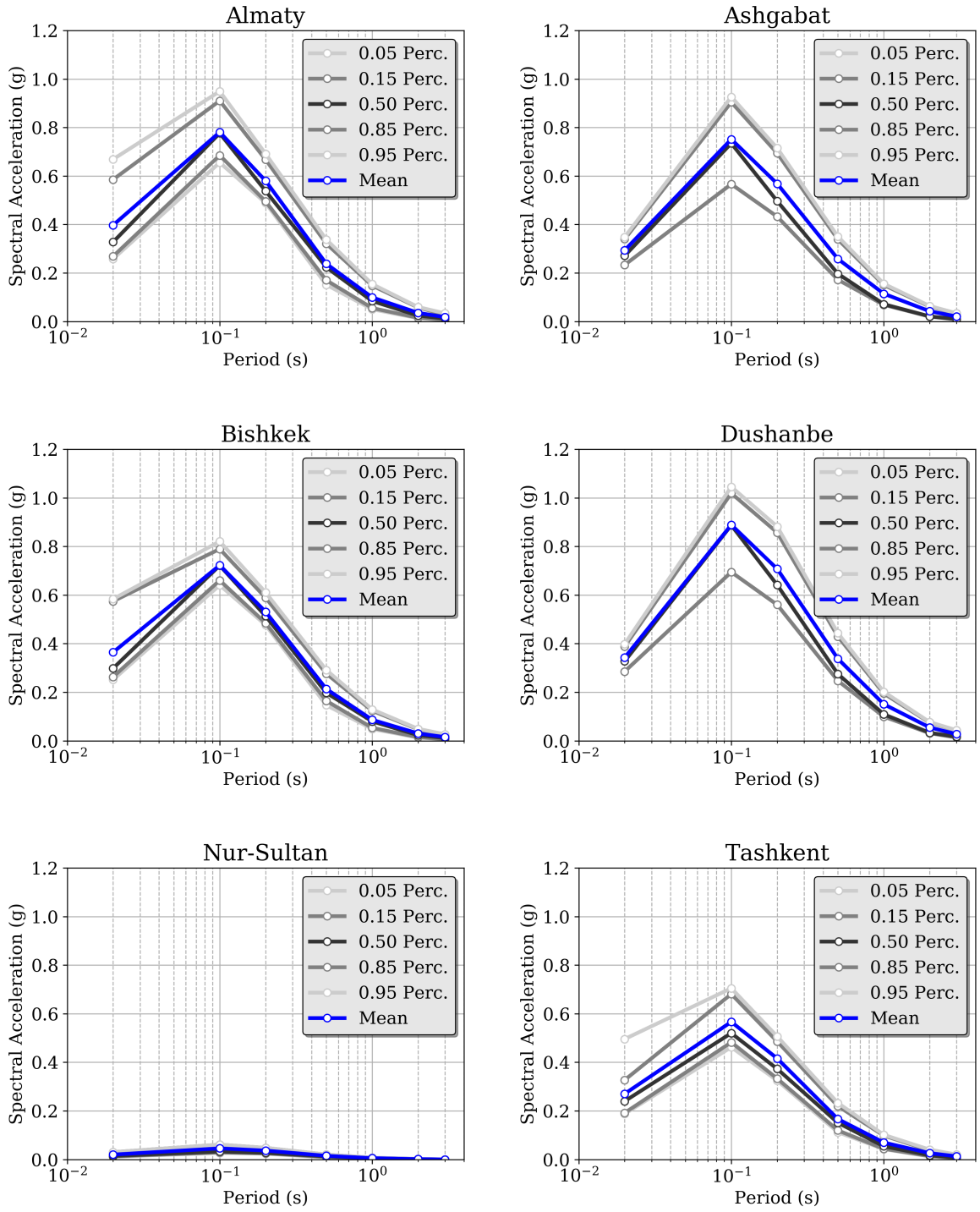

Figure 32. Example of uniform hazard spectra (UHS) computed at six selected target sites (all country capitals plus Almaty, Kazakhstan) for 10% probability of exceedance in 50 years. It must be noted that the sharp amplitude peak is due to lack of calculation periods below 0.1s and should be considered just as a graphical artifact. PGA is conventionally presented at period 0.02s (50Hz).

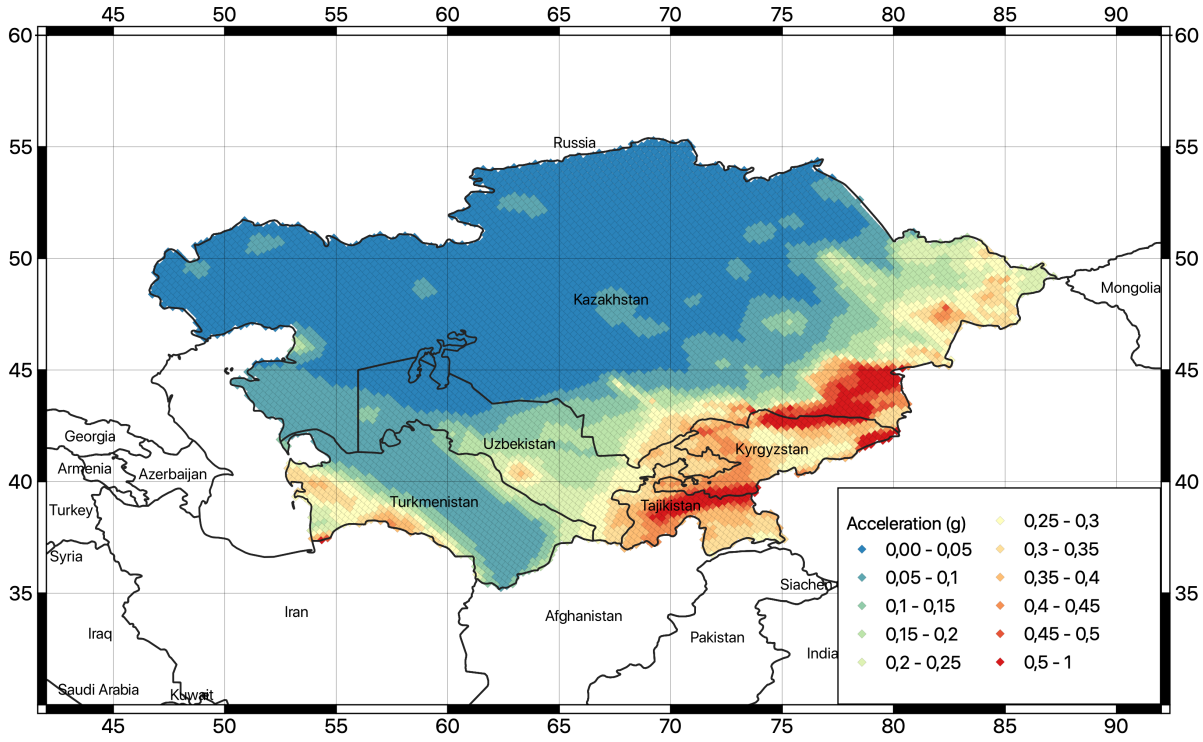

Figure 33. Map of the computed peak ground accelerations (PGA) with 5% probability of exceedance for 50 years investigation time (corresponding to about 1000 years return period) for rock conditions (Vs30 of 800m/s).

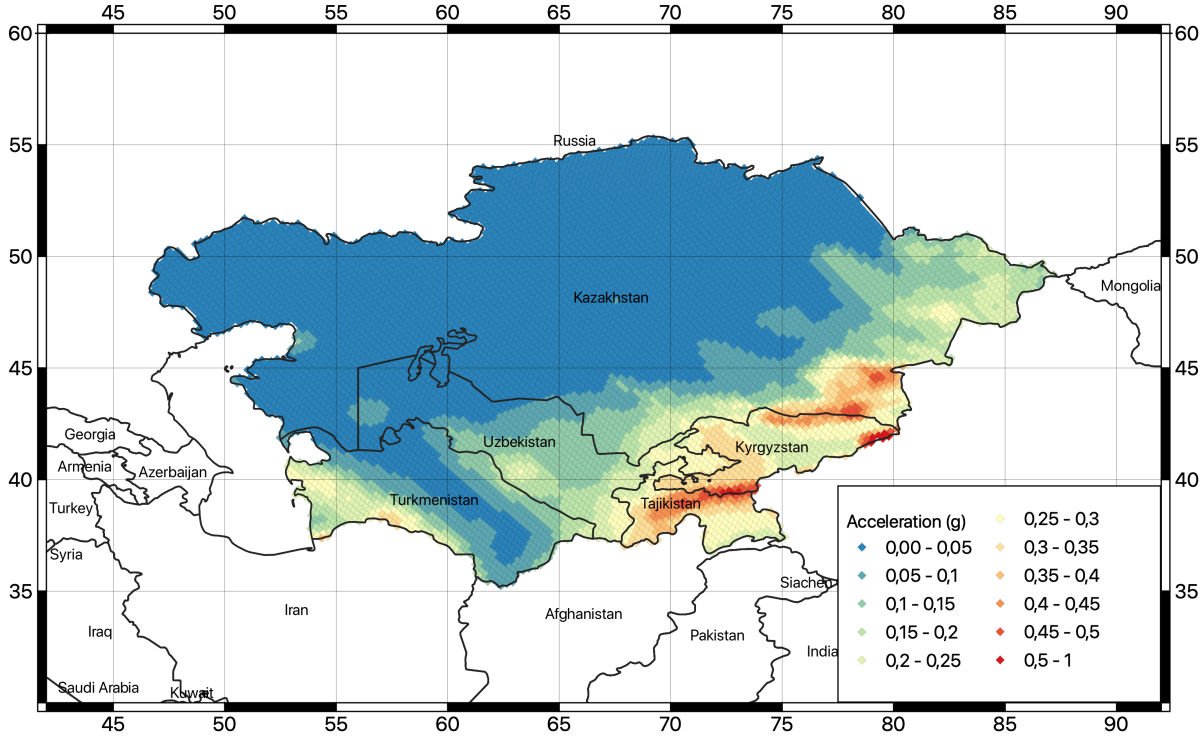

Figure 34. Map of the computed peak ground accelerations (PGA) with 10% probability of exceedance for 50 years investigation time (corresponding to about 475 years return period) for rock conditions (Vs30 of 800m/s).

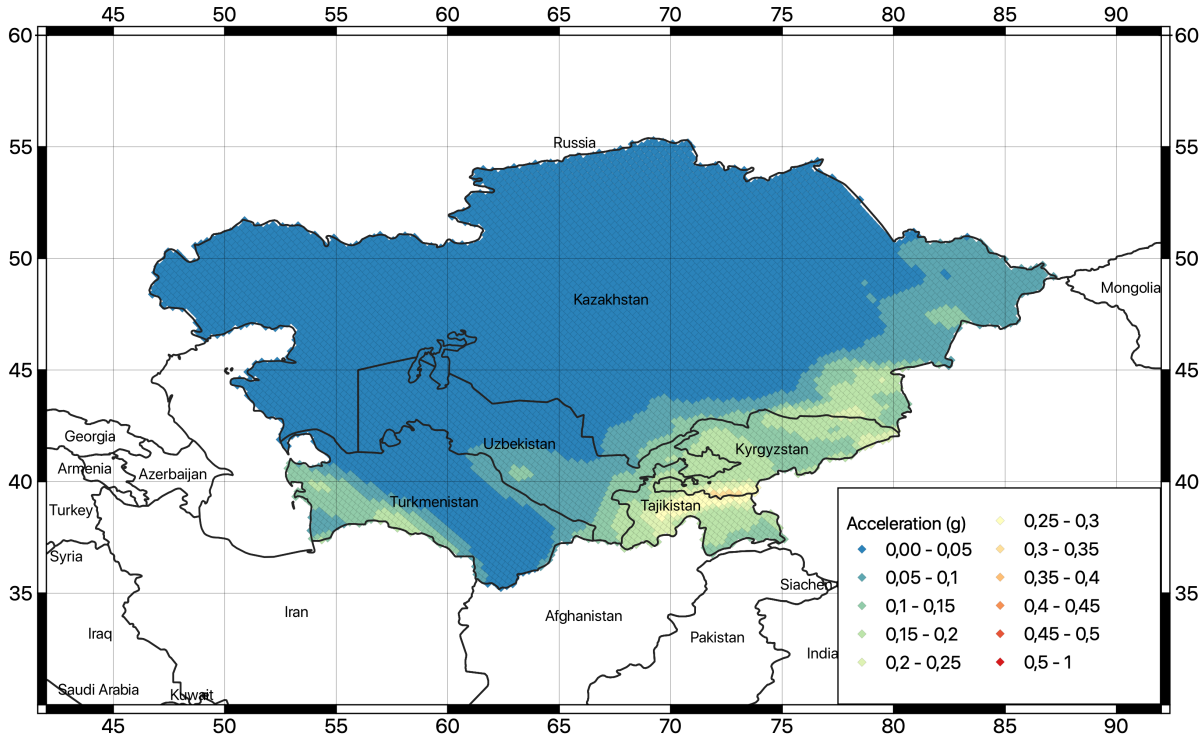

Figure 35. Map of the computed peak ground accelerations (PGA) with 39% probability of exceedance for 50 years investigation time (corresponding to about 100 years return period) for rock conditions (Vs30 of 800m/s).

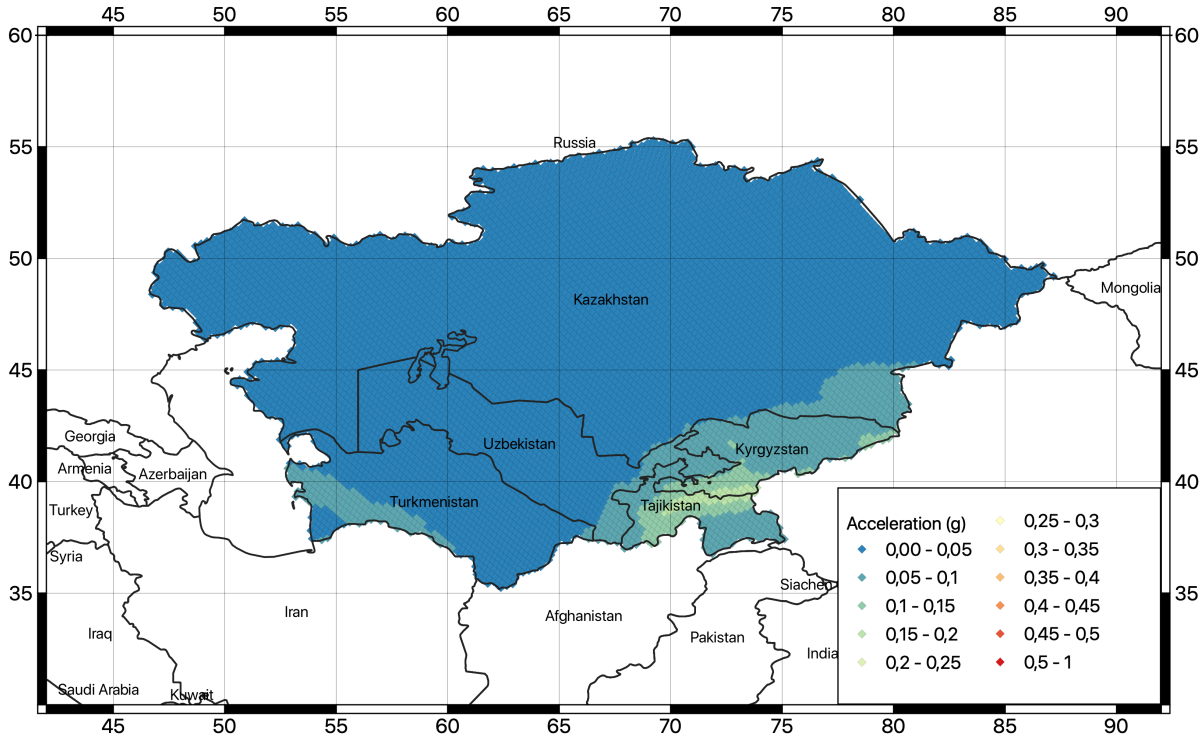

Figure 36. Map of the computed peak ground accelerations (PGA) with 89% probability of exceedance for 50 years investigation time (corresponding to about 25 years return period).

By comparison with previous PSHA studies, an overall agreement is found, although with some noticeable local difference. For instance, GSHAP predicts rather comparable PGA values at 10%PoE in the whole stable continental part, while overestimating peak accelerations in the more active southern seismic belt of Tajikistan and Turkmenistan, with PGA often exceeding 0.6g. In the current model, such threshold is exceeded only in few localized areas of Tajikistan, while in Turkmenistan accelerations are usually below 0.4g for this PoE. Consistent results were also found between the current model and the more recent calculations from Silacheva et al. (2018) for Kazakhstan and specifically for Almaty city, with PGA of around 0.38g. Peak accelerations in the range 0.2-0.4g are found Kyrgyzstan, close to the mean results from Abdrakhmatov et al. (2003). By comparing the hazard curves and uniform hazard spectra from Ischuk et al. (2018) for Almaty, Bishkek, Dushanbe, and Tashkent, slightly larger accelerations are found (with about 0.1g difference) at the different periods, although with an overall agreement of the relative response.

12.2 Conversion to macroseismic intensity

Although not strictly a requirement for risk assessment, to facilitate the comparison with previous hazard studies and to produce a representation of the hazard results more accessible also for non-experts, hazard maps at the different return periods have been converted to macroseismic intensity. In this study, conversion is done from PGA to MCS (Mercalli-Cancani-Sieberg) and the MSK (Medvedev–Sponheuer–Karnik) intensity scales using, respectively, the conversion relations developed by Faenza and Michelini (2011):

$$Imcs = 1.68 + 2.58\ log10(PGA(g) * 980.665)$$

and the regional relation from Aptikaev (2012):

$$Imsk = 1.89 + 2.50\ log10(PGA(g) * 980.665)$$

Identically, we tested the Mercalli Modified Intensity (MMI) equivalence as proposed by Worden et al. (2012) and currently implemented in the USGS ShakeMap software (Wald et al., 1999, Table 19). Conversion to other scales can be easily implemented if appropriate conversion relations become available.

Table 19. USGS ShakeMap Instrumental Intensity Scale, based upon Worden et al. (2012).

PERCEIVED SHAKING	Not felt	Weak	Light	Moderate	Strong	Very strong	Severe	Violent	Extreme
POTENTIAL DAMAGE	None	None	None	Very light	Light	Moderate	Mod./ Heavy	Heavy	Very heavy
PGA (%g)	<0.05	0.3	2.8	6.2	12	22	40	75	>139
PGV (cm/s)	<0.01	0.1	1.4	4.7	9.6	20	41	86	>178

INTENSITY	I	II-III	IV	V	VI	VII	VIII	IX	X+

It must be noted, however, that direct conversion of acceleration to intensity is a simplified approach that must be used carefully, mostly for first-order comparison with earlier hazard results (e.g., EMCA). A proper evaluation of the hazard using Intensity Prediction Equations (IPE), together with a granular site response information, would be better suited. This is not done here because it is not needed for risk assessment, which is the final objective of this study. Nonetheless, regionalized IPEs can be implemented and used for direct hazard evaluation in a possible follow up of this study.

Conversion from PGA to MCS and MSK intensities provided almost identical results (see Figure 37 for an example of MKS intensities computed for 10% percent probability of exceedance in 50 years). On the contrary, results converted in MMI using the relation by Worden et al. (2012) are systematically lower of about one intensity level (Figure 38). All intensity maps are consistent with a shear-wave rock reference velocity of 800m/s.

By comparison with the previous results of Ullah et al. (2015) for the EMCA project (Figure 39), the MSC/MSK converted intensities of the current study are overall larger of about one intensity unit. Such differences, however, are likely to be attributed to the conversion relation, which conservatively predicts too large damage also for relatively small PGA values (see Figure 34). Moreover, it must note that Ullah et al. (2015) performed the intensity calculations directly using IPEs, thus avoiding the uncertainty associated to the additional conversion step. Nonetheless, considering the large uncertainties related to macroseismic intensity assessment, the results are nonetheless very comparable, with a rather consistent spatial pattern between models. More similar results are then found by comparison with the MMI conversion of Worden et al. (2012), confirming the rather large variability associated with the direct macroseismic intensity conversion.

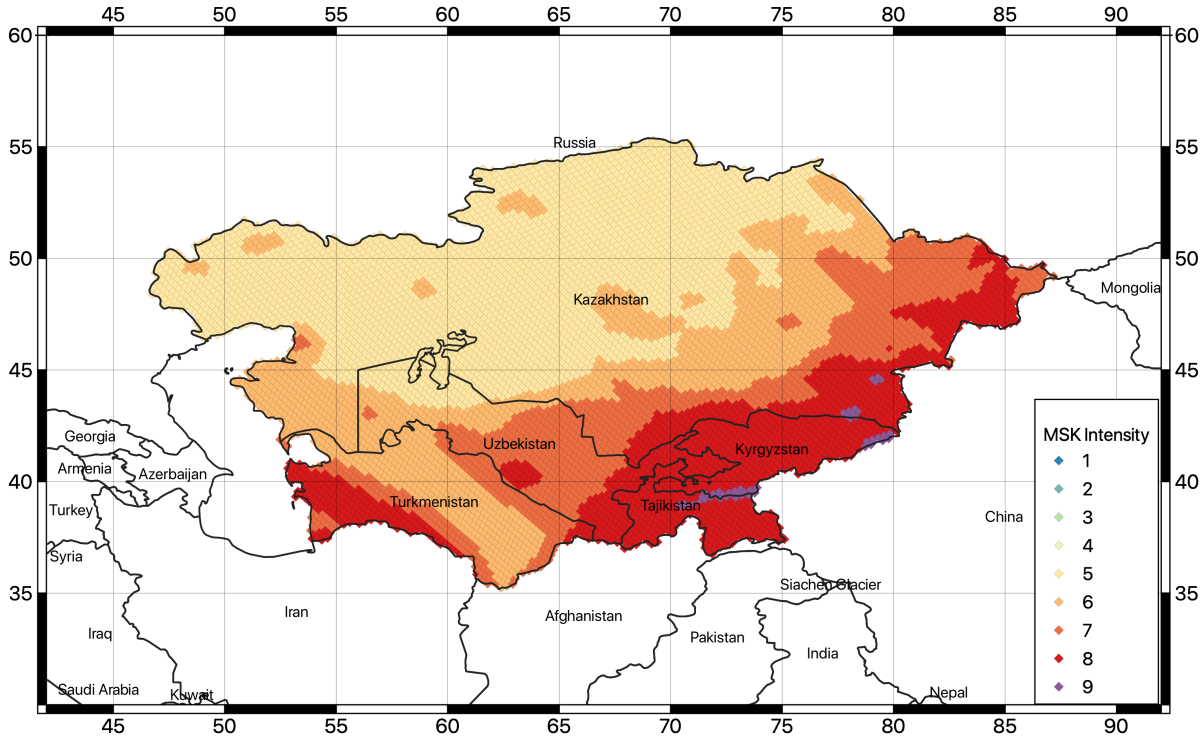

Figure 37. Map of the PGA converted macroseismic intensity (MSK) with 10% probability of exceedance for 50 years investigation time (corresponding to about 475 year return period) computed for this study.

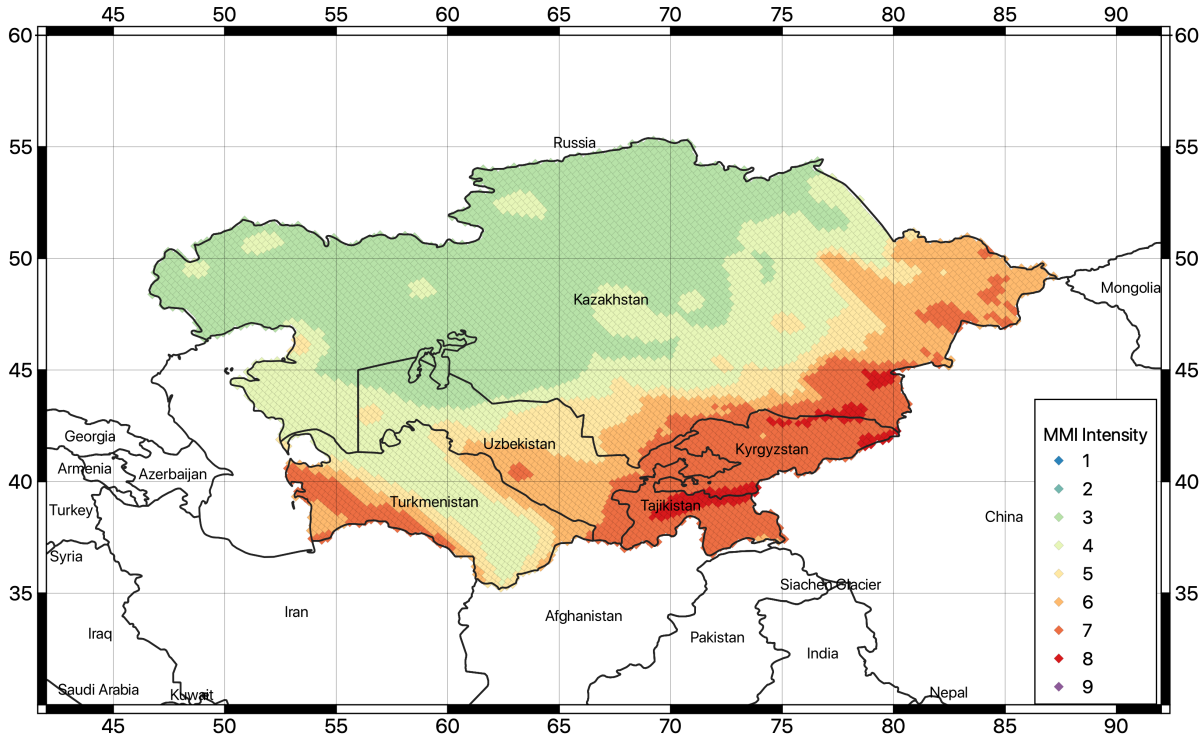

Figure 38. Map of the PGA converted macroseismic intensity (MMI) with 10% probability of exceedance for 50 years investigation time (corresponding to about 475 year return period) computed for this study.

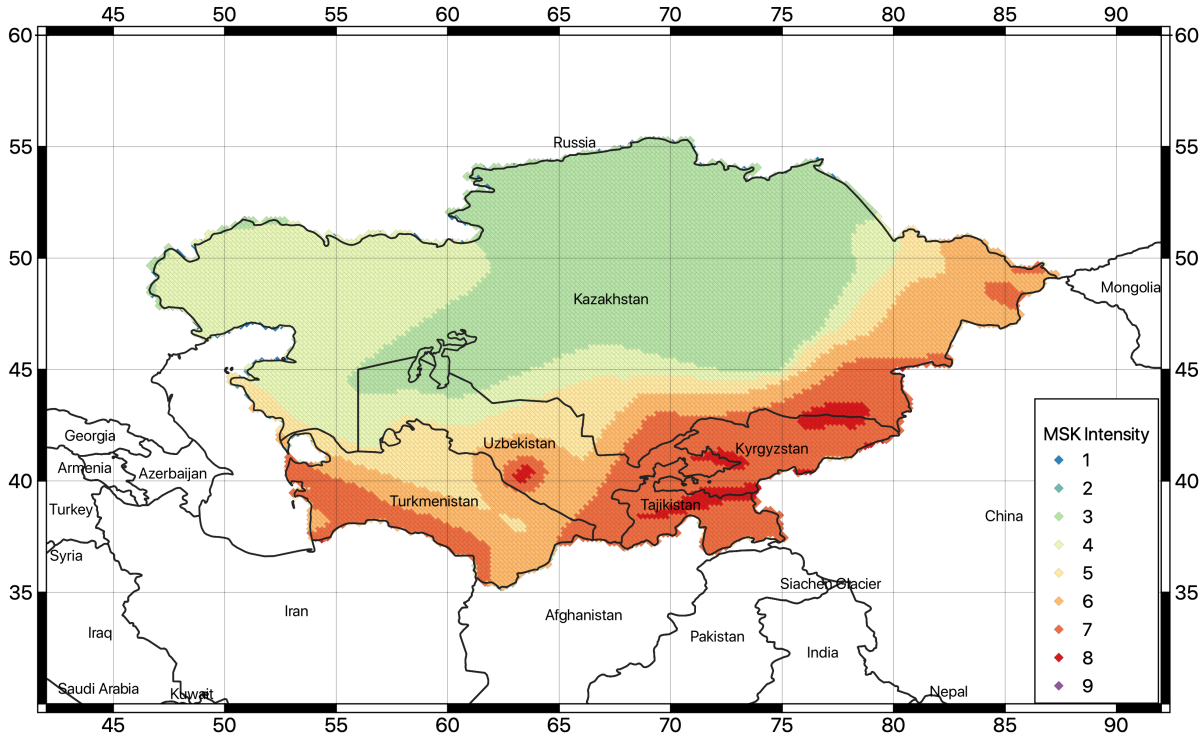

Figure 39. Map of the macroseismic intensity (MSK) with 10% probability of exceedance for 50 years investigation time computed by Ullah et al. (2015) within the EMCA project.

12.3 Disaggregation and stochastic event set

To identify the controlling scenario for the stochastic event set calculation, seismic disaggregation was performed for all considered intensity measure types (PGA, SA(0.1), SA(0.2), SA(0.5), SA(1.0), SA(2.0), SA(3.0) and return periods (25, 50, 100, 250, 475, 500 and 1000 years) at six selected target sites, corresponding to the capitals of the five Central Asian countries (Ashgabat, Bishkek, Dushanbe, Nur-Sultan – formerly known as Astana -- and Tashkent) plus the city of Almaty (Kazakhstan) due to its exposure to earthquake hazard. In total, 294 disaggregation calculations were carried out. Results are for magnitude-distance-epsilon (MDE) and geographical (Lat-Lon) disaggregation. An example of the magnitude-distance-epsilon disaggregation matrix at the six sites is presented in Figure 40 for 0.2 second spectral acceleration, while the example of controlling scenarios identified for probability of exceedance of 10% in 50 years is provided in Table 20 (results for all other PoEs are provided as calculation output).

A) Almaty

B) Ashgabat

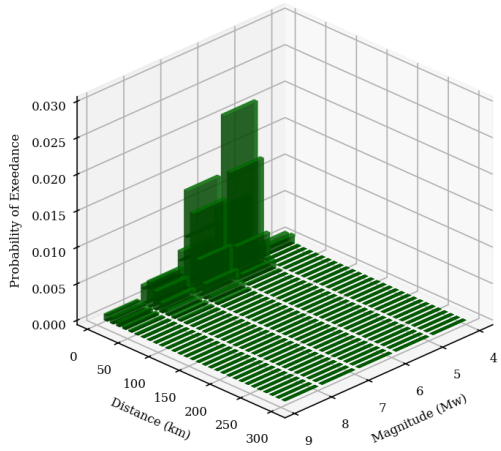

C) Bishkek

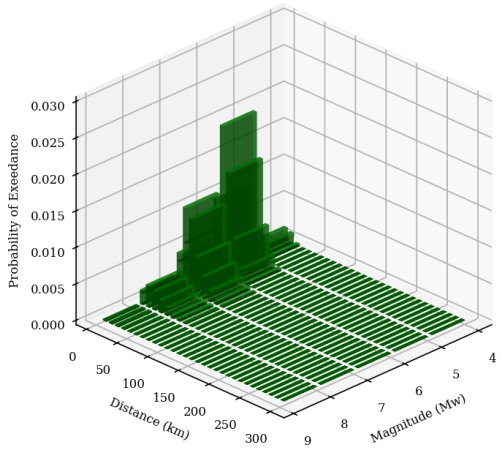

D) Dushanbe

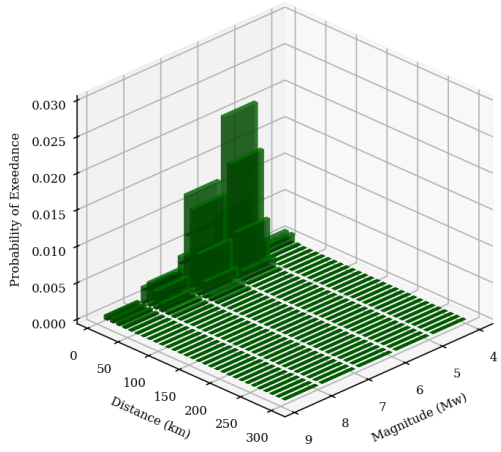

E) Nur-Sultan

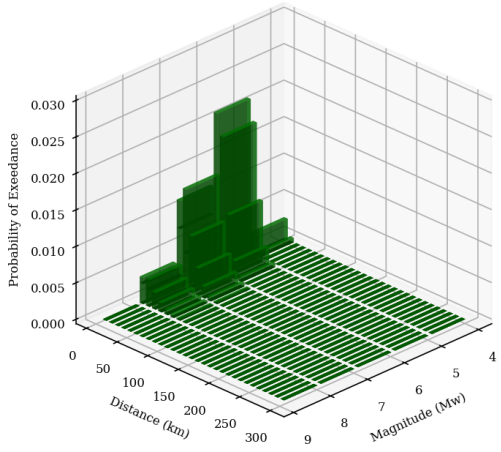

F) Tashkent

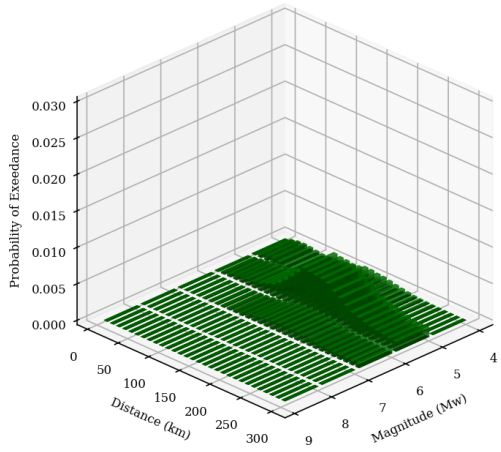

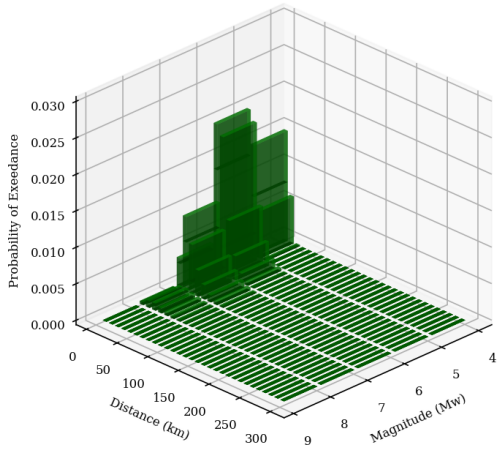

Figure 40. Contribution by magnitude-distance bins at the six target sites for the exceedance of 0.2 second spectral acceleration and return period of 475 years (10% PoEs in 50 years investigation time).

Table 20. Example of controlling earthquake scenarios identified from magnitude-distance disaggregation of the 6 target sites at 10% PoE in 50 years.

Site	IMT	Dist. (Km)	Mag. (Mw)
Almaty	PGA	15.0	5.5
	SA(0.1)	15.0	5.5
	SA(0.2)	15.0	5.5
	SA(0.5)	15.0	6.5
	SA(1.0)	15.0	6.5
	SA(2.0)	15.0	6.5
	SA(3.0)	15.0	6.5
Nur-Sultan	PGA	145.0	5.5
	SA(0.1)	145.0	5.5
	SA(0.2)	145.0	5.5
	SA(0.5)	185.0	5.5
	SA(1.0)	185.0	5.5
	SA(2.0)	185.0	5.5
	SA(3.0)	--	--
Bishkek	PGA	15.0	5.5
	SA(0.1)	15.0	5.5
	SA(0.2)	15.0	5.5
	SA(0.5)	15.0	6.5
	SA(1.0)	25.0	6.5
	SA(2.0)	25.0	6.5
	SA(3.0)	25.0	6.5
Tashkent	PGA	5.0	5.5
	SA(0.1)	5.0	5.5
	SA(0.2)	5.0	5.5
	SA(0.5)	5.0	5.5
	SA(1.0)	15.0	6.5
	SA(2.0)	15.0	6.5
	SA(3.0)	25.0	6.5
Ashgabat	PGA	15.0	5.5

	SA(0.1)	25.0	5.5
	SA(0.2)	15.0	5.5
	SA(0.5)	15.0	5.5
	SA(1.0)	25.0	6.5
	SA(2.0)	15.0	6.5
	SA(3.0)	15.0	6.5
Dushanbe	PGA	5.0	5.5
	SA(0.1)	15.0	5.5
	SA(0.2)	5.0	5.5
	SA(0.5)	5.0	5.5
	SA(1.0)	5.0	5.5
	SA(2.0)	15.0	6.5
	SA(3.0)	15.0	6.5

After performing disaggregation, a stochastic earthquake event set was computed for a 10,000-year simulation period and using a minimum magnitude threshold of 5. For each simulated event, the earthquake size (in Mw), geographical coordinates and rupture mechanism are provided as calculation output. Given the complexity of the model, logic-tree sampling was however necessary. In this analysis, a set of 1000 randomly selected end branches was sampled.

To perform subsequent risk analysis, then, the ground motion field associated to each event of the stochastic set is then computed at each investigated target site for PGA and the different spectral acceleration periods (0.1s, 0.2s, 0.5s, 1s, 2s and 3s). It must be noted that risk calculation will be computed using site specific ground motion, by using the local slope-based Vs30 value obtained from the global USGS Vs30 Map Server (Worden et al., 2015). Vs30 values for the six investigated cities is presented in Table 21, while the regional Vs30 map is shown in Figure 41.

Table 21. Vs30 from topographic slope correlation obtained for the six investigated cities from the USGS Vs30 Map Server (Worden et al., 2015).

City	State	Longitude	Latitude	Vs30 (m/s)
Almaty	Kazakhstan	76.889709	43.238949	536
Nur-Sultan	Kazakhstan	71.445980	51.180100	308
Bishkek	Kyrgyzstan	74.582748	42.882004	433
Tashkent	Uzbekistan	69.240562	41.311081	270
Ashgabat	Turkmenistan	58.238.056	37.862499	466
Dushanbe	Tajikistan	68.780000	38.536670	297

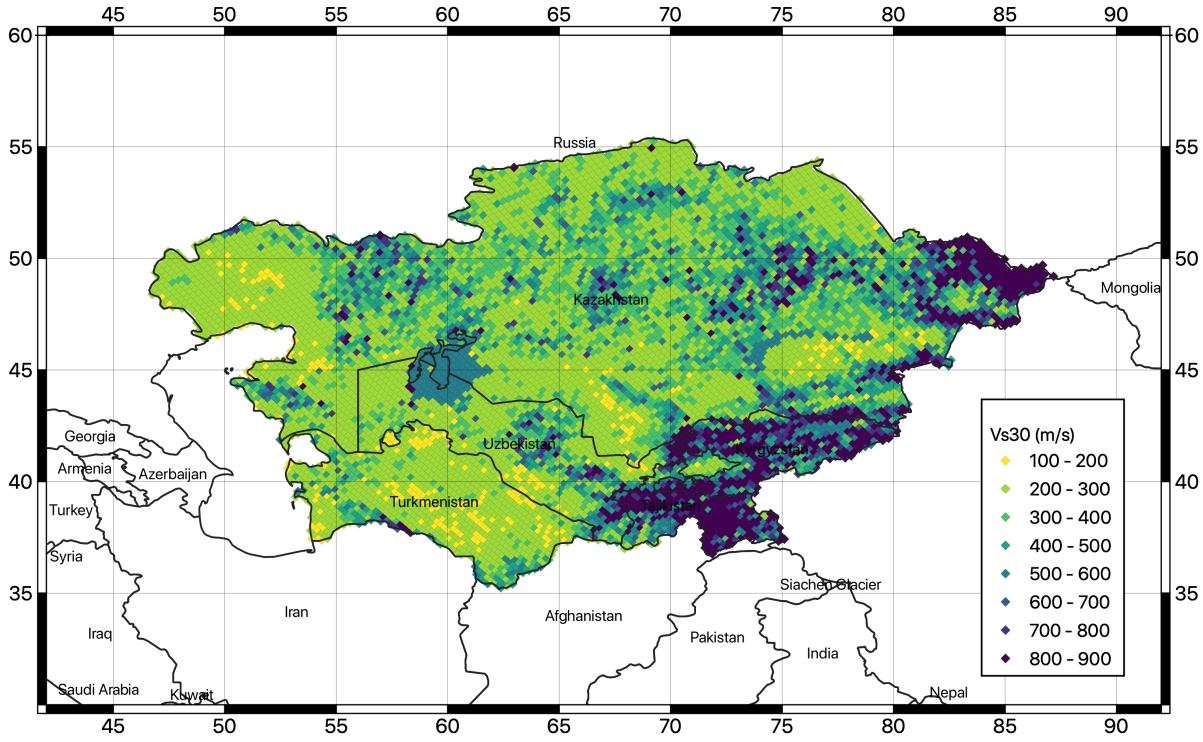

Figure 41. Vs30 map from topographic slope correlation computed for the whole study area.

13 Challenges and limitations faced

The major issue affecting the presented model is the shortage of strong-motion recordings within a rupture-to-site distance shorter than 80km to be used for selection and validation of existing ground motion prediction models. In this study, decision on suitable GMPEs is done mostly using indirect information that relies on a set of tenable assumptions from seismotectonic considerations but, strictly speaking, lacks an empirical validation. Future implementation of new strong-motion stations at potentially hazardous sites and the strengthening of existing seismic networks will be an essential advancement to verify the applicability of existing ground motion prediction models at short distances and to promote the development of new locally calibrated ones. Moreover, the availability of strong-motion recordings will support site-specific hazard studies, which require empirical data for the calibration and verification of numerical seismic-response models. This might be a possible second-phase extension of this project.

14 Recommendations on users and applications

The current model does not cover – yet - a level of detail usually required to develop national hazard models, such as those utilized for underpinning national building codes, although it provides the essential information needed for such an application. Nevertheless, until superior studies are carried out, the findings of this study can be used, albeit with caution, to estimate seismic hazard and to stimulate awareness of seismic hazard in local governmental institutions. Extending the

present model to national level and for city scenario clearly represents a natural follow-up, as soon as new local information (e.g., studies on nearby faults and site response analyses, weak, and strong ground motion recordings) are available. Of course, the hazard estimates computed herein are appropriate for regional calculation of losses, which is the final objective of this study.

References

Abdrakhmatov, K., 2009. ISTC Project No. KR 1176, Establishment of the Central Asia Seismic Risk Initiative (CASRI). Final Proj. Tech. Rep. Work Performed from 02.01. 2006 to 04.30. 2009.

Abdrakhmatov, K., Havenith, H.B., Delvaux, D., Jongmans, D., Trefois, P., 2003. Probabilistic PGA and Arias Intensity maps of Kyrgyzstan (Central Asia). J. Seismol. 7, 203–220. https://doi.org/10.1023/A:1023559932255

Abdrakhmatov, K., Parolai, S., others, 2015. Probabilistic seismic hazard assessment for Central Asia. Ann. Geophys. 58.

Abdrakhmatov, K.Y., Aldazhanov, S.A., Hager, B.H., Hamburger, M.W., Herring, T.A., Kalabaev, K.B., Makarov, V.I., Molnar, P., Panasyuk, S. V, Prilepin, M.T., others, 1996. Relatively recent construction of the Tien Shan inferred from GPS measurements of present-day crustal deformation rates. Nature 384, 450–453.

Abdullabekov, K.N., Artikov, T.U., Ibragimov, R.S., 2002. Seismic hazard and seismic zoning technology of Uzbekistan. Miner. Resour. Geol.

Abdullabekov, K.N., Artikov, T.U., Ibragimov, R.S., Ziyaudinov, F.F., 2012. Seismic hazard of Uzbekistan territory., in: Geosciences in Uzbekistan. GP '93NIIMR,'94 Tashkent, pp. 195–202.

Aki K., Richards P., 1980. Quantitative seismology, theory and methods, vols. I and II. W.H. Freeman, San Francisco

Albini P., Musson R.M.W., Rovida A., Locati M., Gomez Capera A.A., Viganò D., 2014. The global earthquake history. Earthq Spectra 30(2):607–624

Álvarez-Gómez J., 2019. FMC—earthquake focal mechanisms data management, cluster and classification. SoftwareX 9:299–307

Artikov, T.U., Ibragimov, R.S., Ibragimova, T.L., Kuchkarov, K., Mirzaev, M.A., 2018. Quantitative assessment of seismic hazard for the territory of Uzbekistan according to the estimated maximum ground oscillation rates and their spectral amplitudes. Geodyn. Tectonophys. 9, 1173–1188.

Bachmanov, D.M., Kozhurin, A.I., Trifonov, V.G., 2017. The active faults of Eurasia database. Geodyn. Tectonophys. 8, 711–736.

Beyreuther, M., Barsch, R., Krischer, L., Megies, T., Behr, Y., and Wassermann, J., 2010, ObsPy: A Python Toolbox for Seismology, Seismological Research Letters, 81 (3), 530-533.

Bindi, D., Abdrakhmatov, K., Parolai, S., Mucciarelli, M., Grünthal, G., Ischuk, A., Mikhailova, N., Zschau, J., 2012. Seismic hazard assessment in Central Asia: Outcomes from a site approach. Soil Dyn. Earthq. Eng. 37, 84–91.

Bindi, D., Parolai, S., Gómez-Capera, A., Locati, M., Kalmetyeva, Z., Mikhailova, N., 2014. Locations and magnitudes of earthquakes in Central Asia from seismic intensity data. J. Seismol. 18, 1–21. https://doi.org/10.1007/s10950-013-9392-1

Bindi, D., Parolai, S., Oth, A., Abdrakhmatov, K., Muraliev, A., Zschau, J., 2011. Intensity prediction equations for Central Asia. Geophys. J. Int. 187, 327–337.

BSSC, 2003. The 2003 NEHRP recommended provisions for new buildings and other structures. Part 1: provisions (FEMA 450), Building Seismic Safety Council. www.bssconline.org

CEN, 2004. Eurocode 8: design of structures for earthquake resistance—part 1: general rules, seismic actions and rules for buildings. European Committee for Standardization, British Standard BS EN 1998-1:2004: E, 219

Chen Y-S., Weatherill G., Pagani M., Cotton F., 2018. A transparent and data-driven global tectonic regionalization model for seismic hazard assessment. Geophys J Int 213(22):1263–1280

Cotton, F., Scherbaum, F., Bommer, J.J., Bungum, H., 2006. Criteria for Selecting and Adjusting Ground-Motion Models for Specific Target Regions: Application to Central Europe and Rock Sites. J. Seismol. 10, 137–156. https://doi.org/10.1007/s10950-005-9006-7

Di Giacomo D., Bondár I., Storchak D., Engdahl E.R., Bormann P., Harris J., 2015. ISC-GEM: global instrumental earthquake catalogue (1900–2009), III. Re-computed MS and mb, proxy MW, final magnitude composition and completeness assessment. Phys Earth Planet Inter 239:33–47

Di Giacomo D., Engdahl E.R., Storchak D.A., 2018. The ISC-GEM earthquake catalogue (1904–2014): status after the extension project. Earth Syst Sci Data 10:1877–1899

Douglas J., 2003. Earthquake ground motion estimation using strong-motion records: a review of equations for the estimation of peak ground acceleration and response spectral ordinates. Earth Sci Rev 61:43–104

Edwards B., Allmann B., Fäh D. et al., 2010. Automatic computation of moment magnitudes for small earthquakes and the scaling of local to moment magnitude. Geophys J Int 183:407–420

Ekstrom G., Nettles M., Dziewonski A.M, 2012. The global CMT project 2004–2010: centroid-moment tensors for 13,017 earthquakes. Phys Earth Planet Int 200–201:1–9

Faenza L. and A. Michelini, 2011. Regression analysis of MCS intensity and ground motion spectral accelerations (SAs) in Italy. Geophysical Journal International, vol. 186, pp. 1415-1439.

Frankel A., 1995 Mapping seismic hazard in the Central and Eastern United States. Seismol Res Lett 66(4):8–21

Free, M., Coates, K., Grant, D., Fourniadis, Y., Ader, T., Sousa, L., Fleming, K., Pittore, M., Moldobekov, B., Ormukov, C., 2018. Seismic Risk in the Kyrgyz Republic, Central Asia, in: 16th European Conference on Earthquake Engineering.

Gardner J.K., Knopoff L., 1974. Is the sequence of earthquakes in Southern California, with aftershocks removed, Poissonian? Bull Seismol Soc Am 64:1363–1367

Giardini D (ed) 1999. The global seismic hazard assessment program 1992–1999. Annali Geofis 42(6):248

Grünthal G. 1985. The up-dated earthquake catalogue for the German Democratic Republic and adjacent areas—Statistical data characteristics and conclusions for hazard assessment. In Proceedings of the 3rd International Symposium on the Analysis of Seismicity and Seismic Risk, Liblice Castle, Czechoslovakia, June 17-22, 19-25. Geophysical Institute of the Czechoslovak Academy of Sciences, Prague, Czech Republic.

Hanks T.C., Kanamori H., 1979. A moment magnitude scale. J Geophys Res 84(5):2348–2350

Kaverina A.N., Lander A.V., Prozorov A.G., 1996. Global creepex distribution and its relation to earthquake- source geometry and tectonic origin. Geophys J Int 125(1):249–265

Ischuk, A., Bjerrum, L.W., Kamchybekov, M., Abdrakhmatov, K., Lindholm, C., 2018. Probabilistic Seismic Hazard Assessment for the Area of Kyrgyzstan, Tajikistan, and Eastern

Uzbekistan, Central AsiaProbabilistic Seismic Hazard Assessment for the Area of Kyrgyzstan, Tajikistan, and Eastern Uzbekistan. Bull. Seismol. Soc. Am. 108, 130–144.

Ischuk, A.R., Mamadjanov, Y., 2014. Seismicity and seismic hazard of the Territory of Tajikistan , in: Özyazıcıoğlu, M. (Ed.), EARTH REALITY ALONG THE SILK ROAD AND SCIENTIFIC COOPERATION. Bishkek, Kyrgyzstan.

King, S.A., Khalturin, V.I., Tucker, B.E., 1999. Seismic Hazard and Building Vulnerability in Post-Soviet Central Asian Republics, in: '94 Proceedings of the NATO Advanced Research Workshop on Earthquake Risk Management Strategies for Post-Soviet Central Asian Republics: Avoiding Repetition of 1988 a Shakhalin Disasters. Almaty, Kazakhstan, 22-25 October 1996.

Leonard M., 2014. Self-consistent earthquake fault-scaling relations: update and extension to stable conti- nental strike-slip faults. Bull Seismol Soc Am 104:1971–1988

Mikhailova, N. N., A. S. Mukambayev, I. L. Aristova, G. Kulikova, S. Ullah, M. Pilz, and D. Bindi, 2015. Central Asia earthquake catalogue from ancient time to 2009, Ann. Geophys. 58, no. 1, S0102, doi: 10.4401/ag-6681.

Mosca, I., Baptie, B., Sargeant, S., Walker, R.T., 2019. Integrating Outcomes from Probabilistic and Deterministic Seismic Hazard Analysis in the Tien ShanIntegrating Outcomes from Probabilistic and Deterministic Seismic Hazard Analysis in the Tien Shan. Bull. Seismol. Soc. Am. 109, 688–715.

Parolai, S., Boxberger, T., Pilz, M., Fleming, K., Haas, M., Pittore, M., Petrovic, B., Moldobekov, B., Zubovich, A., Lauterjung, J., 2017. Assessing earthquake early warning using sparse networks in developing countries: case study of the Kyrgyz Republic. Front. Earth Sci. 5, 74.

Rautian,T., Khalturin, K., Fujita, K., Mackey, G. & Kendall, A. D., 2007. Origins and methodology of the Russian Energy K-Class Sys- tem and its relationship to magnitude scales, Seismol. Res. Lett., 78, 579– 590.

Silacheva, N. V, Kulbayeva, U.K., Kravchenko, N.A., 2018. Probabilistic seismic hazard assessment of Kazakhstan and Almaty city in peak ground accelerations. Geod. Geodyn. 9, 131–141.

Storchak D.A., Di Giacomo D., Bondár I., Engdahl E.R., Harris J., Lee W.H.K., Villaseñor A., Bormann P., 2013. Public Release of the ISC-GEM Global Instrumental Earthquake Catalogue (1900–2009). Seismol Res Lett 84:810–815

Storchak D.A., Di Giacomo D., Engdahl E.R., Harris J., Bondár I., Lee W.H.K., Bormann P., Villaseñor A.,2015. The ISC-GEM global instrumental earthquake catalogue (1900–2009). Introd Phys Earth Planet Int 239:48–63

Storchak D.A., Harris J., Brown L., Lieser K., Shumba B., Verney R., Di Giacomo D., Korger E.I. M., 2017. Rebuild of the Bulletin of the International Seismological Centre (ISC), part 1: 1964–1979. Geosci Lett (2017) 4:32. https://doi.org/10.1186/s40562-017-0098-z

Styron, Richard, and Marco Pagani, 2020. "The GEM Global Active Faults Database." Earthquake Spectra, vol. 36, no. 1_suppl, pp. 160–180, doi:10.1177/8755293020944182.

Tunini, L., Jimenez-Munt, I., Fernandez, M., Verges, J. & Bird, P., 2017. Neo-tectonic deformation in central Eurasia: a geodynamic model approach, J. geophys. Res., 122(11), 9461–9484.

Uhrhammer R., 1986. Characteristics of Northern and Central California seismicity. Earthq Notes 57:21

Ullah, S., Bindi, D., Pilz, M., Danciu, L., Weatherill, G., Zuccolo, E., Ischuk, A., Mikhailova, N.N., Abdrakhmatov, K., Parolai, S., others, 2015. Probabilistic seismic hazard assessment for Central Asia. Ann. Geophys. 58.

Ulomov, V.I., Group, G.R. 7 W., others, 1999. Seismic hazard of northern Eurasia.

Vilanova S.P., Nemser E.S., Besana-Ostman G.M., Bezzeghoud M., Borges J.F., Da Silveira A.B., Cabral J., Car- valho J., Cunha P.P., Dias R.P., Madeira J., Lopes F.C., Oliveira C.S., Perea H., García-Mayordomo J., Wong I., Arvidsson R., Fonseca J.F.B.D., 2014. Incorporating descriptive metadata into seismic source zone models for seismic-hazard assessment: a case study of the Azores-West Iberian region. Bull Seismol Soc Am 104:1212–1229

Wald, D.J., V. Quitoriano, T.H. Heaton, H. Kanamori, C.W. Scrivner, and C.B. Worden, 1999. TriNet "ShakeMaps": Rapid Generation of Peak Ground-motion and Intensity Maps for Earthquakes in Southern California, Earthquake Spectra 15(3), 537-556.

Weatherill G.A., Pagani M., Garcia J., 2016. Exploring earthquake databases for the creation of magni- tude-homogeneous catalogues: tools for application on a regional and global scale. Geophys J Int 206(3):1652–1676

Wells, D. L. and Coppersmith, K. J., 1994. New empirical relationships among magnitude, rupture length, rupture width, rupture area, and surface displacement, BSSA, 84, 974–1002.

Worden, C.B., M.C. Gerstenberger, D.A. Rhoades, D.J. and Wald, 2012. Probabilistic relationships between ground-motion parameters and Modified Mercalli intensity in California Bull. Seism. Soc. Am. 102(1), 204-221.

Worden, C. B., D. J. Wald, J. Sanborn, and E. M. Thompson, 2015, Development of an open-source hybrid global Vs30 model, Seismological Society of America Annual Meeting, 21-23 April, Pasadena, California.

Zubovich, A. V., Wang, X., Scherba, Y.G., Schelochkov, G.G., Reilinger, R., Reigber, C., Mosienko, O.I., Molnar, P., Michajljow, W., Makarov, V.I., Li, J., Kuzikov, S.I., Herring, T.A., Hamburger, M.W., Hager, B.H., Dang, Y., Bragin, V.D., Beisenbaev, R.T., 2010. GPS velocity field for the Tien Shan and surrounding regions. Tectonics 29, n/a-n/a. https://doi.org/10.1029/2010TC002772